TAMPEREEN TEKNILLINEN YLIOPISTO
TAMPERE UNIVERSITY OF TECHNOLOGY
Julkaisu 682 • Publication 682

Antti Isomäki

Ultrafast Fiber Lasers Using Novel Semiconductor Saturable Absorbers and Photonic-Crystal Dispersion Compensators

Tampere 2007

Tampereen teknillinen yliopisto. Julkaisu 682
Tampere University of Technology. Publication 682

Antti Isomäki

Ultrafast Fiber Lasers Using Novel Semiconductor Saturable Absorbers and Photonic-Crystal Dispersion Compensators

Thesis for the degree of Doctor of Technology to be presented with due permission for public examination and criticism in Tietotalo Building, Auditorium TB104, at Tampere University of Technology, on the 26th of October 2007, at 12 noon.

Tampereen teknillinen yliopisto - Tampere University of Technology
Tampere 2007

ISBN 978-952-15-1852-2 (printed)
ISBN 978-952-15-1915-4 (PDF)
ISSN 1459-2045

ABSTRACT

This thesis is concerned with development and demonstration of new techniques for mode-locked fiber lasers using semiconductor saturable absorbers and advanced dispersion compensators.

Semiconductor saturable absorber mirrors have been widely used for controlling a large variety of mode-locked lasers since the beginning of 1990s. Several absorber designs have been proposed during these years aiming at optimizing the dynamic properties to achieve reliable start-up and to sustain mode-locking in different types of lasers. In this thesis I present two approaches for semiconductor absorbers – a reverse-biased saturable absorber reflector and a saturable absorber used in transmission. While the first, mirror-type absorber was suitable for linear cavity fiber lasers, the transmission-type absorber was conveniently implemented in a ring cavity. The performance of the absorbers in starting the pulse operation and in shaping ultra-short pulses was tested in Er- and Yb-fiber lasers, respectively.

Traditionally, the dispersion has been tackled by inserting prisms and diffraction gratings in the laser cavity. However, finding alternatives to these conventional bulk optical components has been of substantial interest in fiber systems. In this thesis I consider two very dissimilar solutions for dispersion management in fiber lasers. A semiconductor Gires-Tournois interferometer can be used to generate a tunable delay within a limited optical bandwidth. The saturable absorption in this structure provides means for controlling the dispersion of the device. Secondly, a method based on solid-core photonic bandgap fibers offers an all-fiber solution. The high anomalous dispersion of this new class of optical fibers can compensate for the normal dispersion of other cavity components at 1 μm wavelength range. This unique property makes these fibers attractive candidates when looking for methods to produce ultra-short laser pulses at this spectral range.

ACKNOWLEDGEMENTS

The research work presented in this Thesis has been carried out in the Optoelectronics Research Centre (ORC) at Tampere University of Technology during the years 2002-2006. This Thesis was financially supported by the Graduate school in Electronics, Telecommunications, and Automation (GETA), the Academy of Finland, the Finnish Funding Agency for Technology and Innovation (Tekes), the Jenny and Antti Wihuri Foundation, and European Union, which are gratefully acknowledged. I am also grateful to the Ulla Tuominen Foundation and TTY:n tukisäätiö for supporting my work with personal grants.

I would like to thank my supervisor, Professor Oleg Okhotnikov for his professional guidance and encouragement. Without his devotion to laser research I would not have made it this far. I am also grateful to Professor Markus Pessa, Director of ORC. His ability to make things happen is something exceptional.

I would like to thank all my coworkers at ORC for their help and inspiring atmosphere. I am most indepted to Dr. Matei Rusu, who is not only a consummate engineer, but first and foremost a great friend. Special thanks go to Dr. Robert Herda for providing the numerical simulations. Dr. Mircea Guina, Lasse Orsila, and Antti Härkönen are thanked for valuable discussions and their help in numerous issues that made my life a lot easier. I also thank Tommi Hakulinen, Samuli Kivistö, Dr. Luis Gomes, Dionisio Pereira, Kaj Torrkulla, and Dr. Claudio Porzi for all the help during these years. My co-authors Soile Suomalainen, Jari Lyytikäinen, Anne Vainionpää, and Pietari Tuomisto are thanked for their professional work with MBE. My work has greatly benefited from the cooperation with Dr. Claus Friis Pedersen from NKT Research, Denmark. I would like to express my gratitude also to Anne Viherkoski for taking care of the administrative issues.

I warmly thank my parents for encouraging and supporting me in all my choices. Special thanks go to my brother Petri for leading my way to the world of physics.

My dear wife Heini, you truly gave me heart in the dark days. And our son Toivo – thanks for bringing joy and hope in my life.

Tampere, September 2007

Antti Isomäki

TABLE OF CONTENTS

LIST OF PUBLICATIONS

This Thesis is a compendium, which contains some unpublished material, but is mainly based on the following papers published in open international literature. In the text, these publications are referred to as P1–P5.

[P1] A. Isomäki, A. Vainionpää, J. Lyytikäinen, and O. G. Okhotnikov, "Semiconductor mirror for dynamic dispersion compensation", *Appl. Phys. Lett.*, Vol. 82, No. 17, pp. 2773–2774 (2003)

[P2] A. Isomäki, A. Vainionpää, S. Suomalainen, and O. G. Okhotnikov, "Self-starting mode-locked fiber laser using biased semiconductor absorber mirror", in *Congress on Optics and Optoelectronics*, Warsaw, Poland, 28 August – 2 September (2005) Lasers and Applications, edited by Krzysztof M. Abramski, Antonio Lapucci, Edward F. Plinski, *Proc. SPIE* Vol. 5958, 59580R (2005)

[P3] A. Isomäki, M. D. Guina, P. Tuomisto, and O. G. Okhotnikov, "Fiber laser mode-locked with a semiconductor saturable absorber etalon operating in transmission", *IEEE Photon. Tech. Lett.*, Vol. 18, No. 20, pp. 2150–2152 (2006)

[P4] A. Isomäki and O. G. Okhotnikov, "All-fiber ytterbium soliton mode-locked laser with dispersion control by solid-core photonic bandgap fiber", *Opt. Express*, Vol. 14, No. 10, pp. 4368–4372 (2006)

[P5] A. Isomäki and O. G. Okhotnikov, "Femtosecond soliton mode-locked laser based on ytterbium-doped photonic bandgap fiber", *Opt. Express*, Vol. 14, No. 20, pp. 9238–9243 (2006)

Author's contribution

The work presented in this dissertation is a part of teamwork. My main responsibilities were to characterize the semiconductor and fiber components, to design and build up the fiber laser setups, and to collect the final data. I have also conducted computational modeling [P1, P3] and taken part in designing the semiconductor saturable absorber etalon [P3]. In addition, I have been directly involved in building and testing of four different systems for dispersion measurements needed in this work. A list of my contribution on the research work and preparing the scientific papers is given in the table below.

Table 1. *Author's contribution. Measurement: Practical efforts in preparing the experiment and acquisition of data. Reporting: Writing the article draft and refining the final manuscript.*

Paper #	Measurement	Reporting
P1	80 %	30 %
P2	80 %	40 %
P3	80 %	50 %
P4	100 %	70 %
P5	100 %	80 %

Related publications

Other publications related to this work but not included in the Thesis:

[RP1] A. Isomäki, A. Vainionpää, J. Lyytikäinen, and O. G. Okhotnikov, "Semiconductor mirror for optical noise suppression and dynamic dispersion compensation", *IEEE J. of Quantum Electron.*, Vol. 39, No. 11, pp. 1481–1485 (2003)

[RP2] A. Isomäki, M. Rusu, L. Orsila, M. Guina, and O. G. Okhotnikov, "Properties and applications of resonant nonlinear semiconductor reflectors", Presentation at the 20th Nordic Semiconductor Meeting, Tampere, Finland, 25 – 27 August, 2003. *Physica Scripta* T114, pp. 145–151 (2004)

[RP3] A. Vainionpää, S. Suomalainen, A. Isomäki, O. Tengvall, M. Pessa, and O. G. Okhotnikov, "Semiconductor saturable absorber mirror with wavelength tailored distributed Bragg reflector", *J. Grystal Growth*, Vol. 278, pp. 751–755 (2005)

[RP4] R. Herda, A. Isomäki, and O. G. Okhotnikov, "Soliton sidebands in photonic bandgap fibre lasers", *Electron. Lett.*, Vol. 42, pp. 19–20 (2006)

[RP5] A. Isomäki, A. Vainionpää, J. Lyytikäinen, O. G. Okhotnikov, and M. Pessa, "Amplified spontaneous noise suppression using non-linear vertical cavity semiconductor gate", *OSA Trends in Optics and Photonics*, Vol. 79, Nonlinear Optics, OSA Technical Digest, Postconference Edition, pp. 31–33. Maui, Hawaii, USA, 29 July – 2 August (2002)

[RP6] A. Isomäki, A. Vainionpää, J. Lyytikäinen, and O. G. Okhotnikov, "Vertical-cavity semiconductor discriminator for amplified spontaneous emission", *LEOS 2002*, Glasgow, U.K., 11 – 12 November, 2002. Conference Proceedings Vol. 1, IEEE Catalog Number:02CH37369, pp. 147–148 (2002)

[RP7] A. Isomäki, A. Vainionpää, J. Lyytikäinen, and O. G. Okhotnikov, "Optically tunable dispersion compensators based on semiconductor Gires-Tournois interferometer", *CLEO Europe 2003*, Europhysics Conference Abstracts Vo. 27E CE5-6-Thu, Munich, Germany, 23 – 27 June (2003)

[RP8] A. Isomäki, B. Ryvkin, and O. G. Okhotnikov, "Optical limiting semiconductor saturable absorber mirror", *CLEO Europe 2003*, Europhysics Conference Abstracts Vo. 27E CD4-5-Thu, Munich, Germany, 23 – 27 June (2003)

[RP9] A. Vainionpää, S. Suomalainen, A. Isomäki, O. Tengvall, and O. G. Okhotnikov, "Semiconductor saturable absorber mirror with wavelength tailored distributed Bragg reflector", *MBE 2004 Conference*, Edinburgh, U.K., 22 – 27 August (2004)

[RP10] C. Porzi, A. Isomäki, M. Guina, and O. G. Okhotnikov,"Impedance-detuned high-contrast vertical cavity semiconductor switch", *OFC 2005*, Anaheim, California, USA, 8 – 10 March (2005)

[RP11] M. Guina, C. Porzi, A. Isomäki, O. G. Okhotnikov, and K. Arstila, "Design and performance of an impedance-detuned high-contrast vertical cavity semiconductor switch", *CLEO Europe 2005*, Conference Digest on CD-Rom, Vol. 29B, Munich, Germany, 12 – 17 June (2005)

[RP12] A. Isomäki, M. Guina, P. Tuomisto, and O. G. Okhotnikov, "Fiber laser mode-locked with a semiconductor saturable absorber etalon operating in transmission", *CLEO 2006*, Technical Digest on CD-Rom, ISBN: 1-55752-813-6, CThC1, Long Beach, California, USA, 21 – 26 May (2006)

[RP13] A. Isomäki and O. G. Okhotnikov, "Femtosecond soliton mode-locked laser based on ytterbium-doped photonic bandgap fiber", *LEOS 2006*, Conference Proc. on CD-Rom, ISBN: 0-7803-9556-5, pp. 394–395, Montreal, Canada, 29 October – 2 November (2006)

LIST OF ABBREVIATIONS

APM	Additive pulse mode-locking
AR	Anti-reflection
ARROW	Anti-resonant optical waveguiding
ASE	Amplified spontaneous emission
ATE	Absorbing transmission etalon
CFBG	Chirped fiber Bragg grating
cw	Continuous wave
DBR	Distributed Bragg reflector
DCF	Dispersion compensating fiber
DCM	Double chirped mirror
DFF	Dispersion-flattened fiber
DSF	Dispersion-shifted fiber
D-SAM	Dispersive saturable absorber mirror
FP	Fabry-Pérot
FWHM	Full width at half maximum
GTI	Gires-Tournois Interferometer
GDD	Group delay dispersion
GVD	Group velocity dispersion
HC-PBGF	Hollow-core photonic bandgap fiber
HOM	Higher order mode
HR	High reflectivity
LMA	Large mode area
LT	Low temperature
MBE	Molecular beam epitaxy
MFD	Mode field diameter

ML	Mode-locked
MQW	Multiple quantum wells
NLSE	Nonlinear Schrödinger equation
NPE	Nonlinear polarization evolution
NZ-DSF	Non-zero dispersion-shifted fiber
PBGF	Photonic bandgap fiber
PCF	Photonic crystal fiber
pin-SESAM	p-i-n-structured SESAM
p-i-n	p-type–intrinsic–n-type
PM	Polarization maintaining
QCSE	Quantum confined Stark effect
QW	Quantum well
RSAM	Resonant saturable absorber mirror
RTA	Rapid thermal annealing
SBR	Saturable Bragg reflector
SC-PBGF	Solid-core photonic bandgap fiber
SESAM	Semiconductor saturable absorber mirror
SMF	Single-mode fiber
SPM	Self-phase modulation
SS	Solid-state
SS-MBE	Solid-source molecular beam epitaxy
TBP	Time-bandwidth product
TOD	Third order dispersion
UV	Ultraviolet
WDM	Wavelength division multiplexing
Yb-PBGF	Ytterbium-doped photonic bandgap fiber

1. INTRODUCTION

The ever-increasing demand for high-capacity data transfer has been – and still is – one of the main driving forces behind the optoelectronics research. The efficient generation of short laser pulses is the key enabling technology in optical communication systems. Typically, this is done by directly modulating semiconductor lasers or using specific optical modulators. However, the shortest possible pulses are generated using mode-locking technique. High-speed transmission over thousands of kilometers has been demonstrated using soliton pulses [1]. In future, a mode-locked laser could, for example, replace multiple continuous wave (cw) lasers as the source for a very densily wavelength-division multiplexed system, thus allowing for extremely high bandwidth transmission. Despite the importance and the fast progress of the optical communication techniques, the main use for mode-locked lasers is still in the fields of science and material technology.

Mode-locked lasers have several interesting applications in bio-detection and imaging. These include two-photon microscopy [2], Raman spectroscopy [3], optical coherence tomography [4], and terahertz imaging [5]. Measurements of absolute optical frequencies in optical clocks and high precision optical metrology [6, 7] have gained lots of attention recently. The Nobel Prize in physics was awarded to John Hall and Theodor Hänsch in 2005 for achievements in this area.

While ultrashort pulse mode-locked lasers are still mainly used in laboratories for scientific research, they are gaining more and more commercial interest. High-precision material processing is an increasingly important field exploiting these lasers. Current systems are useful for marking, micromachining, and soldering applications [8]. With power levels scaled up to several watts, such systems become applicable to industrial welding and cutting applications. In medicine, ultrashort pulses can be used in eye and dental surgery [9, 10], cell and tissue cutting or welding [11], and even in nano-scale dissection of subcellular organelles [12].

Fiber lasers are available in a spectral range from UV to near-infrared with average powers ranging from few mW to several kW. With these parameters, they are expected to become attractive alternatives to a number of other types of lasers. In comparison with conventional gas lasers (e.g. Argon-laser) and solid-state lasers (e.g. Nd:YAG), the advantages of fiber lasers lie in their ruggedness (especially in all-fiber construction), low power consumption, high gain bandwidth and flexibility

in pumping wavelengths. In addition, fiber lasers have no critical issues with cooling of the gain medium and are also potentially cheaper than the bulk crystal solid-state lasers in high volume production due to fewer mechanical components. However, when it comes to producing ultrashort high-energy pulses needed in many existing and emerging applications, fiber sources still lack behind their bulk crystalline competitors. In particular, Ti:Sapphire laser systems can deliver a few femtosecond long pulses with mJ-level energy and peak power of several TW [13] – something not conceivable in current fiber systems.

Large group delay dispersion (GDD) and relatively high nonlinearities are the main obstacles to sub-picosecond pulse generation from fiber lasers. Typically, the dispersion has been tackled by inserting dispersive dielectric mirrors, prisms or diffraction gratings in the laser cavity. However, finding alternatives to these conventional bulk optical components has been of continuous interest. While many solutions have been proposed, the problem still remains, especially in case of fiber lasers operating with λ<1.3 μm, i.e., in the normal dispersion region of optical fiber. No practical all-fiber solutions have been available until recently.

Photonic crystal technology has been one of the most promising fields of optics research over the past few years. Several unforeseen optical properties have been demonstrated based on the inherently large design flexibility of the photonic crystal fibers (PCFs) [14]. These include endlessly single-moded guiding [15], extremely high or low nonlinearity [16, 17], and anomalous dispersion in the short-wavelength region [18]. Among the possible applications, efficient supercontinuum generation [19] and dispersion management [20] using PCFs are two convincing examples of the usefulness of the technique.

1.1 Objective and scope of research

The purpose of my research work is to improve the general understanding and to explore new methods for ultra-short pulse generation in fiber lasers. In particular, the research aims at the development of practical techniques for mode-locking and optical pulse shaping by using semiconductor saturable absorbers and novel dispersion management methods.

The work presented in this Thesis concentrates on fiber lasers that use either an erbium- or an ytterbium-doped fiber as the gain medium. Therefore, certain results may not be applicable directly to other types of laser sources as such. Some of the results are more general and should be useful in other fields of photonics and laser technology. These perspectives will be discussed in the following chapters.

The studies of pulse shaping concentrate on the effects of chromatic dispersion in the laser cavity. Although the nonlinear phenomena in optical fibers are also important,

these effects are dealt very briefly here. In this matter, the reader is referred to [21].

The experiments reported here are characteristically proof-of-concept by their nature. This work is important in testing new ideas but leaves room for technical improvements. The author's humble wish is that these results will help others avoid at least some pitfalls along the way to a brighter future.

1.2 Main results

The main achievements of each included journal article are summarized here.

[P1] *Semiconductor mirror for dynamic dispersion compensation*

In this paper we report on group delay tuning in a semiconductor Gires-Tournois interferometer (GTI). The effect of optical pumping on the phase evolution in a nonlinearly behaving GTI mirror is demonstrated for the first time. The analytical model supports the observations. This concept may find applications in adaptive dispersion compensation. The intensity dependence of group delay in resonant structures is important also when dispersive saturable absorber mirrors (D-SAMs) or optical delay lines for slow light applications are considered.

[P2] *Self-starting mode-locked fiber laser using biased semiconductor absorber mirror*

In this paper we describe a reverse-biased saturable absorber mirror for mode-locking an erbium-doped fiber laser. This device, implemented in a fiber laser cavity for the first time, is shown to offer a practical way to control the mode-locking start-up capability and the pulse duration. It can also be used to suppress the Q-switching instability in a fiber laser.

[P3] *Fiber laser mode-locked with a semiconductor saturable absorber etalon operating in transmission*

In this study a semiconductor saturable absorber etalon is used for mode-locking a ring-cavity ytterbium fiber laser. The novelty of the approach is to exploit the resonant structure to enhance the modulation depth while simultaneously taking advantage of the low-loss transmission state. The device ensures a robust self-starting mode-locking mechanism, which is also highly tolerant to the total cavity dispersion.

[P4] *All-fiber ytterbium soliton mode-locked laser with dispersion control by solid-core photonic bandgap fiber*

In recent theoretical studies, photonic bandgap fibers (PBGFs) have been considered as one of the most promising candidates for dispersion compensation. In this paper we report on the first experimental realization of an ytterbium fiber laser using a

solid-core photonic bandgap fiber for dispersion compensation. The benefits and the challenges of the technique are discussed as well.

[P5] *Femtosecond soliton mode-locked laser based on ytterbium-doped photonic bandgap fiber*

As a further development to the study reported in [P4], we demonstrated a mode-locked laser using a solid-core ytterbium-doped photonic bandgap fiber. Again, this is the first demonstration of using such a fiber that provides both the gain and the anomalous dispersion needed for a compact sub-picosecond soliton laser at 1 μm wavelength regime.

1.3 Thesis outline

This Thesis is organized as follows. Chapter 2 gives a short review of the mode-locking theory, concentrating on passive mode-locking using semiconductor saturable absorbers. Chapter 3 deals with the theory of ultra-short pulse formation in fiber lasers. In particular, the influence of intracavity dispersion on pulse shaping is discussed.

Chapters 4 and 5 sum up my research results regarding semiconductor saturable absorbers and dispersion compensation techniques, respectively. In this disquisition, I also present some unpublished material about the experiments and cover the details of the theory behind them.

The final conclusions are presented in Chapter 6.

2. MODE-LOCKED FIBER LASERS

The theory of mode-locking has been described in great detail in several articles and books [22, 23, 24]. Therefore, the purpose of this chapter is to present only the basic principles of the technique with emphasis on fiber lasers. The theoretical background is discussed briefly, and the most common methods used for mode-locking are presented in Section 2.1. From these methods, semiconductor-based saturable absorbers are used in all fiber lasers studied in this thesis. For this reason, these devices are discussed extensively in Section 2.2.

2.1 Basic principles of mode-locking

A standing-wave resonator supports modes that satisfy the condition that an integer number of half-wavelengths are contained between the cavity mirrors. Similarly, a ring-cavity (i.e. travelling-wave) resonator supports modes with an integer number of full-wavelengths. These modes usually oscillate with random phases and irregular amplitudes leading effectively to continuous-wave operation. In a mode-locked laser, a fixed phase relationship is established amongst these longitudinal modes allowing for their constructive interference and leading to the generation of ultrashort optical pulses.

To obtain the shortest pulses, the largest possible number of modes should be locked together. As the number of modes with fixed phase relationship increases, two effects take place: the pulse becomes shorter and the amplitude of the pulse increases. At the steady-state condition a discreate pulse circulates in the laser cavity with a high peak power and ultrashort duration. A large spectral bandwidth of the laser gain medium is needed for supporting the large number of modes and, consequently, short pulse formation. The cavity dispersion over the pulse bandwidth has to be managed carefully to achieve sufficient pulse shortening. The different shaping mechanisms of ultrashort pulses will be discussed in more detail in Chapter 3.

An alternative way to understand the build-up of modelocking is to consider the loss evolution in a laser cavity. Since a laser always operates in a regime with minimum losses, one should design the laser cavity with low-loss state corresponding to the ultrashort pulses formation. In practise, mode-locked operation can be reached by

the use of different kinds of active or passive modulation elements inside the laser cavity.

Active mode-locking is obtained using an electrically driven amplitude or phase modulator, typically an electro-optic Mach-Zehnder modulator or a semiconductor electroabsorption modulator. When the modulation is synchronized with the cavity round-trip frequency, only the modes with the desired phase remain in the cavity. Driving the modulator at a multiple of the fundamental frequency can generate higher repetition rates up to several gigahertzes [25, 26]. This operation regime, referred to as harmonic mode-locking, is typical for long cavity fiber lasers that have sufficient pump power to support many pulses in the cavity.

An important advantage of active mode-locking is that the output pulse train matches to an external electrical signal. This is particularly important in telecommunication where the transmitted data and a clock signal need to be synchronized. On the downside, ultrashort pulses with duration shorter than a few picoseconds are difficult to achieve using active methods.

Passive mode-locking is accomplished by inserting a saturable absorbing medium into the laser cavity. Different semiconductor materials in the forms of quantum wells or quantum dots are particularly suited for this purpose [27, 28]. More recently, carbon nanotube mode-lockers have been introduced for lasers using both erbium [29] and ytterbium [30] fiber as the gain medium. Other methods based on fast *artificial saturable absorption* include Kerr-lens mode-locking [31, 32], additive pulse mode-locking (APM) [33], nonlinear polarization evolution (NPE) [34], and self-phase modulation (SPM) in loop mirrors [35]. Out of all these possible approaches, semiconductor saturable absorbers and NPE are the most widely adopted for mode-locking fiber lasers.

Generally, a saturable absorber has a higher transmission for an intense pulse than for low-intensity cw radiation. The loss is reduced for pulsed operation, so the laser tends to operate in a mode-locked regime. The peak of a pulse becomes less attenuated than the low-intensity edges leading to effective shortening of the pulse duration with every pass through the absorber. Eventually, the cavity-induced pulse broadening balances the pulse narrowing effect, and a steady-state pulsed operation is reached. In general, passively mode-locked lasers can produce shorter pulses than actively driven systems.

One of the great advantages of mode-locking based on saturable absorption is that pulsed operation is self-starting for properly designed laser cavities. The technique is regarded as self-starting when no external trigger is needed to begin the mode-locked operation. This is often not the case in other mode-locking schemes, where start-up is achieved e.g. by using a separate amplitude modulator or by vibrating one of the cavity mirrors.

Passively mode-locked systems may suffer from instabilities in pulse amplitude and timing, which limit their usability in telecommunication applications requiring long-term stability and low timing jitter. Reduced damping of relaxation oscillations may also lead to very large periodic variations in pulse energy known as Q-switched mode-locking. Q-switched ML can be utilized in applications requiring very high pulse peak intensities. In many cases, however, it is the most probable damage mechanism of the saturable absorber.

2.2 Semiconductor saturable absorbers

The sophisticated semiconductor growth techniques, molecular beam epitaxy (MBE) in particular, have enabled the development of highly controlled saturable absorbers. Devices that combine the absorption effects in quantum wells (QWs) with the high reflectivity semiconductor distributed Bragg reflector (DBR) mirrors were initially demonstrated by Tsuda et. al. [36] with further developments being made by Keller et. al. [27]. These mode-locking elements are known as saturable Bragg reflectors (SBRs) or semiconductor saturable absorber mirrors (SESAMs). They can be conveniently integrated into different laser cavities as a cavity end mirror. Similar structures can be used in transmission, for example in a form of an absorbing transmission etalon (ATE) that I have used in [P3]. Transmission absorbers are naturally employed in ring-cavity lasers. The general structure of both a reflecting and a transmitting type semiconductor saturable absorber are shown schematically in Fig. 2.1. Typically, the absorbing QW region is monolithically integrated within a Fabry-Pérot (FP) cavity formed by DBR mirrors and the semiconductor-air interface or a dielectric coating.

The performance of a semiconductor saturable absorber depends primarily on the nonlinear intensity response and the absorption recovery time. Other important parameters are the operation wavelength and the spectral bandwidth, which ultimately set the limit to the shortening of the pulse duration. These parameters should be optimized for specific laser system to be mode-locked with the saturable absorber.

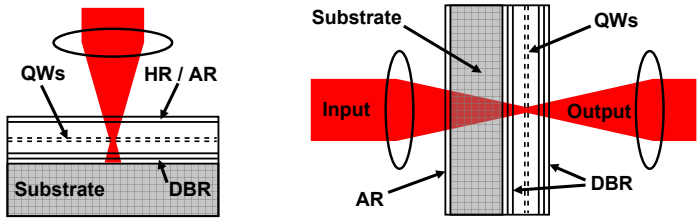

(a) (b)

Fig. 2.1. *Schematic structures of (a) a SESAM and (b) an ATE. The laser beam is focused in the absorbing QW layer. HR – high reflectivity coating, AR – anti-reflection coating.*

2.2.1 Nonlinear intensity response

Semiconductor material absorbs photons through band-to-band transition when the photon energy is sufficient to excite electrons from the valence band to the conduction band. At a high level of excitation, the absorption saturates because all ground states are depleted while upper states of the transition are strongly populated. This gives rise to the nonlinear intensity response characteristic to semiconductor absorbers. The advantage of using QW layers instead of bulk semiconductor absorbers is the precise control over the absorbed wavelength by adjusting the QW depth and width. In addition, QW structures may have lower saturation energy and a higher nonlinear modulation depth [37]. Increasing the number of QWs, i.e. the volume of the absorbing layer, yields higher nonlinearity, but the non-saturable losses may increase as well [38], [RP1].

The intensity-dependent, time-averaged loss of a slowly recovering saturable absorber can be modeled theoretically using equation [39]

$$q_p(F) = \alpha_0 + q_0 \frac{1 - exp(-F/F_{sat})}{F/F_{sat}}. \tag{2.1}$$

Here F is the incident photon fluence, F_{sat} is the saturation fluence, q_0 is the modulation depth, and α_0 includes the non-saturable losses. Figure 2.2 shows a typical reflectivity change as a function of the incident pulse fluence of a semiconductor saturable absorber mirror. An absorber used in transmission has similar characteristics.

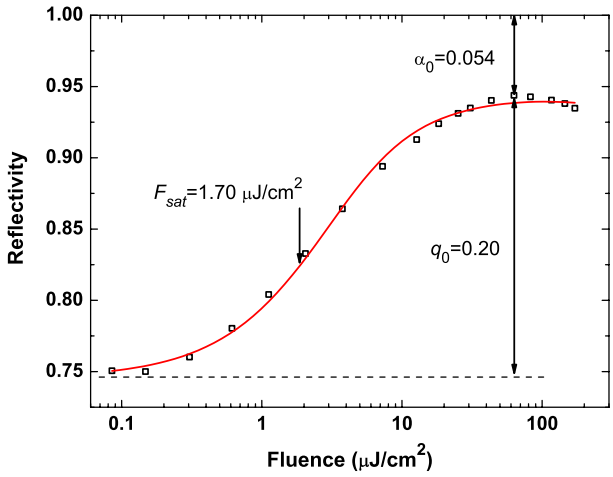

Fig. 2.2. *Nonlinear reflectivity of a typical resonant semiconductor saturable absorber mirror.*

Depending on the FP cavity length the absorber may exhibit either resonant or antiresonant behavior at the operation wavelength. Antiresonant designs provide constant saturation characteristics and low dispersion over a relatively broad wavelength range. Resonant designs, on their side, produce a higher modulation depth and lower saturation fluence beneficial to easy self-starting and to preventing Q-switched mode-locking [40]. The saturation and dispersion characteristics are, however, wavelength dependent around the resonance, which may limit the pulse quality and duration.

Antiresonant absorbers are particularly suited for passively mode-locked solid-state lasers. Fiber lasers, however, typically require a higher modulation depth for reliable start-up of mode-locking, in particular for high value of cavity dispersion [40]. In addition, fiber lasers can tolerate relatively high unsaturable losses, thanks to the large gain available. For these reasons, resonant-type semiconductor saturable absorbers are often used with fiber lasers.

In addition to be a convenient method for mode-locking different kinds of lasers, the nonlinear response of a semiconductor MQW structure can be used for other purposes. These include all-optical amplified spontaneous noise suppression in cascaded fiber amplifier systems [RP1], fast optical switching [RP10], synchronization of mode-locked lasers [41], and wavelength conversion [42]. Moreover, the nonlinear phase response in such a structure allows for devices like a nonlinear optical phase shifter [43] and a tunable dispersion compensator [P1]. A closer look at the latter application will be taken in Section 5.2.

2.2.2 Absorption recovery time

The high-speed functions of semiconductor optoelectronic devices rely on the short transport and recovery times of carriers in the active area of the structure. For quantum-well-based devices, the most important parameters are (1) the transport of carriers in the barrier material surrounding the QWs followed by their capture into the wells, and (2) the interband recombination of these carriers. The first parameter limits the upper modulation frequency in devices such as semiconductor lasers. The fast response time of saturable absorbers, in contrast, is mainly determined by the recombination time of carriers.

Both long and short absorption recovery times have their advantages. In general, slow recovery results in a reduced saturation intensity of absorption, which facilitates self-starting mode-locking. In fiber lasers, however, too long recovery time may provoke a decrease in the modulation depth, thus giving a negative impact on the mode-locking startup and stability. Fast recovering absorbers, in turn, are more effective in sub-picosecond pulse shaping. In fact, without pulse shaping by soliton formation (see Chapter 3), an absorber with the temporal response as fast as possible is always desirable for efficient pulse shortening [44]. In addition, fast absorbers are

more stable against multiple-pulse break-up if the absorber is oversaturated [45]. For a mode-locked fiber laser, the optimal value of the absorption recovery time is in the range of a few picoseconds to 25 ps [46]. However, in a high-quality crystalline semiconductor, the recombination of the carriers takes much longer, typically of an order of nanoseconds. Fortunately, there are several techniques to reduce the recovery time.

At room temperature, the absorption recovery time of III-V semiconductors depends primarily on the non-radiative recombination rate of carriers [47, 48, 49]. The non-radiative decay of carriers from QWs usually occurs via trap states. Thus, a certain number of crystal defects are desired to achieve short carrier lifetimes. The techniques used to introduce defects include low-temperature (LT) epitaxial growth [50], LT-growth in conjunction with beryllium doping [51], metamorphic growth [52], and post-growth irradiation using protons [53] or heavy-ions [54, 55]. Yet another way to affect the absorber recovery time – without introducing crystal defects – is to apply an electric field across the absorbing semiconductor region [P2]. The basic principles of these techniques are introduced next.

Low-temperature growth is an efficient way to reduce the recovery time [50]. In order to get high crystalline quality, the substrate temperature during the MBE growth should be $\sim 600\,^{\circ}\mathrm{C}$. Growth at lower temperatures, typically from 150 to 400 °C, yields various defects in the structure. However, it usually produces a non-uniform distribution of defects over the sample. Also the modulation depth may reduce due to the optical transitions to the deep levels. This problem has been alleviated recently by using Be-doping, which seems to preserve the nonlinear response from degradation during the LT-growth [51].

Metamorphic growth forms defects and dislocations through the relaxation of the high strain between the lattice mismatched materials. This occurs when the difference between the lattice constants of adjacent material layers is large and the thickness of the grown film exceeds the critical value. For example, the metamorphic growth of InP on GaAs induces high density of dislocations near the interface. Since GaAs and InP have remarkably different lattice constants (5.6533 Å and 5.8688 Å, respectively), the critical thickness is small, only about 6.8 Å, which is close to the thickness of one atomic layer. These materials have been used to decrease the recovery time of 1.55 μm SESAMs used in erbium-doped fiber lasers [52]. Similarly, growth of lattice mismatched InGaP on GaAs has been used to fabricate a fast SESAM operating at the 1 μm wavelength range [56].

Post-growth irradiation using protons or heavy ions has significant advantages over LT-growth. Once the epi-wafer has been grown, the physical properties of QWs can be tailored by choosing the type, the energy, and the dose of implanted particle and possible rapid thermal annealing (RTA) conditions. Proton bombardment is a rather simple technique to use. However, the created recombination centers are mainly point defects with low activation energies. This may lead to long-term instabilities

and strong variations in decay times owing to annealing that may occur during the exposure to high intensity radiation. Implantation using heavy ions, such as O^+, Au^+, Ni^+, or Ne^+, is technically more challenging, but it creates defects and traps inside the heterostructure in a more reproducible manner. Ion-implantation is particularly attractive due to the accurate control over the amount of ions and their location in the structure. Heavy-ion-formed recombination centers have high activation energies and are, therefore, rather stable [57], especially after proper RTA treatment [58]. The carrier lifetime can by shortened precisely from nanoseconds (as-grown) to picoseconds or even femtosecond levels [54].

As mentioned above, there is yet another way to affect the absorber properties without introducing defects in the structure. An external electric field applied across the absorbing semiconductor region may reduce the recovery time. In brief, the field sweeps the carriers out of the quantum wells partially, which effectively reduces the level of saturation. This is realized by incorporating the QWs in the intrinsic region of a p-i-n diode, and reverse biasing the diode. I will present a detailed description of the carrier sweep-out process together with some experimental results in Section 4.1.

3. ULTRASHORT PULSE SHAPING MECHANISMS

Important for setting up the passive mode-locked operation, the saturable absorber has a limited effect on the steady-state pulse duration. In fact, in certain laser types (e.g. soliton mode-locked lasers) the absorber may only start-up and stabilize the pulsed operation, while other mechanisms are dominant for pulse shaping. The aim of this chapter is to provide an overview of these effects.

3.1 Nonlinear Ginzburg-Landau equation

The performance of any mode-locked laser – a fiber laser in particular – is largely determined by the overall dispersion and the optical Kerr nonlinearity present in the laser cavity. In addition, the finite gain bandwidth and the gain saturation contribute to the laser dynamics. For ultrashort-pulse generation, these mechanisms act together with pulse shaping by the saturable absorber described in the previous chapter.

Traditionally, the Haus master equation [59] has been used to analytically study the dynamics of mode-locking. However, in case of passively mode-locked fiber lasers, a more comprehensive pulse propagation model is often needed in order to get reliable results without over-simplifying assumptions. The nonlinear Ginzburg-Landau equation [60] describes the propagation of ultrashort pulses in single-mode fibers. It is also known as the generalized (or extended) nonlinear Schrödinger equation (NLSE), and can be written in the form

$$\frac{\partial E}{\partial z} = -\beta_1 \frac{\partial E}{\partial t} - i\frac{\beta_2}{2}\frac{\partial^2 E}{\partial t^2} + \frac{\beta_3}{6}\frac{\partial^3 E}{\partial t^3} + i\gamma|E|^2 E - \Gamma E + g(z)\left(1+\tau_g^2\frac{\partial^2}{\partial t^2}\right)E, \quad (3.1)$$

where $E(z,t)$ is the slowly-varying pulse amplitude, z is the distance along the fiber, t is the pulse local time, β_1 is the inverse group velocity, β_2 is the group-velocity dispersion (GVD), β_3 is the third order dispersion (TOD), γ is the nonlinear parameter, and Γ is the linear loss. The gain g has the characteristic recovery time $\tau_g = 2\pi c/(\omega_0^2 \Delta\lambda_g)$, where c is the velocity of light, ω_0 is the carrier frequency, and $\Delta\lambda_g$ is the gain bandwidth. The pulse amplitude is assumed to be normalized such that $|E|^2$ represents the optical power.

The significance of different terms in Eq. 3.1 depends on the construction of the laser cavity. The GVD plays the most critical role in propagation of ultrashort optical pulses in single-mode fiber. The dispersion-induced pulse broadening is always present in optical fibers, even at low intensities when the nonlinear effects are insignificant. Therefore, special attention has to be paid to GVD management as it will be discussed in Chapter 5. The effect of the third order dispersion term in Eq. 3.1 is typically very small for pulses longer than 100 fs. It may set an ultimate limit to the pulse width if the net cavity GVD is close to zero. Furthermore, exceptionally high TOD values, for example in photonic bandgap fibers, affect the pulse formation [P4, RP4].

The linear loss is usually small for practical lengths of standard single-mode fiber needed in fiber lasers. It may still become an important parameter if intra-cavity bulk optical elements such as diffracion gratings or special fibers, photonic crystal fiber for instance, are used.

The Kerr nonlinearity is typically significant in fibers, except for the air-core PCF and large mode area (LMA) fibers. The nonlinear parameter γ is defined as

$$\gamma = \frac{n_2 \omega_0}{c A_{eff}}, \tag{3.2}$$

where n_2 is the nonlinear-index coefficient and A_{eff} is the effective mode area. It is evident that the nonlinearity becomes more predominant as the fiber core size decreases. This has a significant effect in small-core PCFs and in fiber tapers. The higher order nonlinear terms, e.g. self-steepening, Raman shifting, and two photon absorption, are typically negligible in fiber lasers and, thus, usually omitted in Eq. 3.1.

For undoped fibers the gain $g = 0$, whereas for doped fibers the gain saturation depends on the local pulse energy $\mathscr{E}_{pulse}(z)$. It is described as

$$g(z) = \frac{g_0}{1 + \mathscr{E}_{pulse}(z)/\mathscr{E}_{sat}}, \tag{3.3}$$

where g_0 is the small-signal gain and $\mathscr{E}_{sat}$ is the gain saturation energy, both determined by the pump power level.

Typically, the Eq. 3.1 is solved by the split-step Fourier method [21]. Among the solutions, it is possible to distinguish three steady-state mode-locked operation regimes that depend on the dominant pulse shaping mechanisms in the laser cavity:

(1) *soliton pulse regime* determined by the balance between anomalous dispersion and self-phase modulation resulting from Kerr nonlinearity,

(2) *stretched-pulse regime* determined by dispersion-managed solitons, and

(3) *self-similar pulse regime* determined by the interrelation of normal dispersion and finite-bandwidth gain.

Next, I will describe the characteristics of each of these regimes in more detail. As it will be seen, the classification is still somewhat debatable.

3.2 Soliton pulse regime

The interplay between self-phase modulation and group-velocity dispersion can result in an overall pulse spreading or pulse compression, depending on the magnitudes and signs of these two effects. When the GVD fully compensates the effect of SPM, the pulse of certain shape can travel in a nonlinear dispersive medium without changes, similar to the pulse propagation in an ideal linear nondispersive medium. This is called solitary-wave propagation, and it is possible only if $\beta_2 < 0$ (i.e., the medium exhibits anomalous GVD) and $\gamma > 0$ (i.e., the SPM coefficient $n_2 > 0$). [61]

Equation 3.1 has so-called "true" soliton solutions in the limit in which the real parts of the coefficients vanish. In that limit, only dispersion and nonlinearity affect the pulse propagation, and the cubic form of the equation reduces to

$$\frac{\partial E}{\partial z} = -i\frac{\beta_2}{2}\frac{\partial^2 E}{\partial t^2} + i\gamma|E|^2 E, \tag{3.4}$$

which is recognized as the nonlinear Schrödinger equation [61]. The simplest solitary-wave solution of the Eq. 3.4 is called a *fundamental soliton*. The fundamental soliton pulse envelope corresponds to a hyperbolic-secant function

$$E(z,t) = E_0 \,\mathrm{sech}\left(\frac{t - z/v_g}{\tau_0}\right)\exp\left(\frac{iz}{4z_0}\right), \tag{3.5}$$

where E_0 is the peak amplitude and v_g is the group velocity. The width of the amplitude envelope τ_0 is related to the full-width at half-maximum (FWHM) pulse width by $\tau_{FWHM} = 1.76\tau_0$. As it can be seen, the accumulated phase shift is constant over time or frequency; in other words, the soliton remains unchirped during propagation. Thus, a pulse of this shape travels in a fiber without altering its shape. It should be noted, however, that if the the pulse amplitude changes due to the gain or losses, the pulse width has to change accordingly such that the relation

$$E_0\tau_0 = \sqrt{|\beta_2|/\gamma} \tag{3.6}$$

is preserved. The peak amplitude is inversely proportional to τ_0, and the peak power is inversely proportional to τ_0^2. The pulse energy $\mathscr{E}_{pulse}(z) = \int_{-T_R/2}^{T_R/2} |E(z,t')|^2 dt'$ (integration over the cavity round-trip time T_R) is directly proportional to E_0, and therefore inversely proportional to τ_0. Thus, a soliton of shorter duration must carry greater energy.

Soliton-like pulses can be generated in laser cavities with net anomalous round-trip dispersion [33, 62]. These pulses are sometimes referred to as *quasi-solitons*, since the balance between the dispersion and nonlinearity is not fully preserved along the propagation path. For instance, different fibers have substantially dissimilar dispersion properties. Also the pulse energy varies during a cavity round trip. Nevertheless, the pulses may behave like solitons if the periodic deviations from the balance are not too large during one round trip.

In soliton mode-locked lasers, the pulse duration is nearly independent of the absorber recovery time. Indeed, soliton pulses with duration much shorter than the absorber recovery time have been demonstrated [63]. The shortest soliton pulses extracted from fiber lasers have sub-500 fs durations [64]. Such short pulses are obtained with small values of anomalous dispersion as depicted in Fig. 3.1(a).

The Kelly sidebands visible in the two traces corresponding to net anomalous dispersion in Fig. 3.1(b) are characteristic to the output spectrum of a soliton mode-locked fiber laser [65]. The sidebands arise from the interaction between the soliton field and the non-solitonic dispersive waves. The dispersive wave is made up of the energy periodically lost from the soliton wave due to the cavity perturbations such as output couplers, intracavity filters, and gain/loss elements. For certain frequencies, the two waves become phase matched, which results in the formation of narrow peaks superimposed on the otherwise smooth soliton spectrum. The sidebands are useful in determining the net cavity GVD [66]. Generally they are still an undesired effect that is a signature of soliton pulse losses.

The pulse energy achievable in soliton fiber laser systems is limited to some tens of picojoules [67]. At higher pump powers, nonlinear effects cause wave breaking [68], which leads to multiple-pulse operation. Despite the rather small pulse energies, soliton operation is often desired because of the high pulse quality (i.e., a small value of the time-bandwidth product as seen in Fig. 3.1(c)). It is possible to construct soliton lasers that emit nearly transform-limited pulses directly from the cavity. Low chirp minimizes dispersive temporal broadening, which is very desirable e.g. in optical fiber communications. Efficient supercontinuum generation and frequency conversion in periodically-poled nonlinear crystals require the use of transform-limited pulses as well [22].

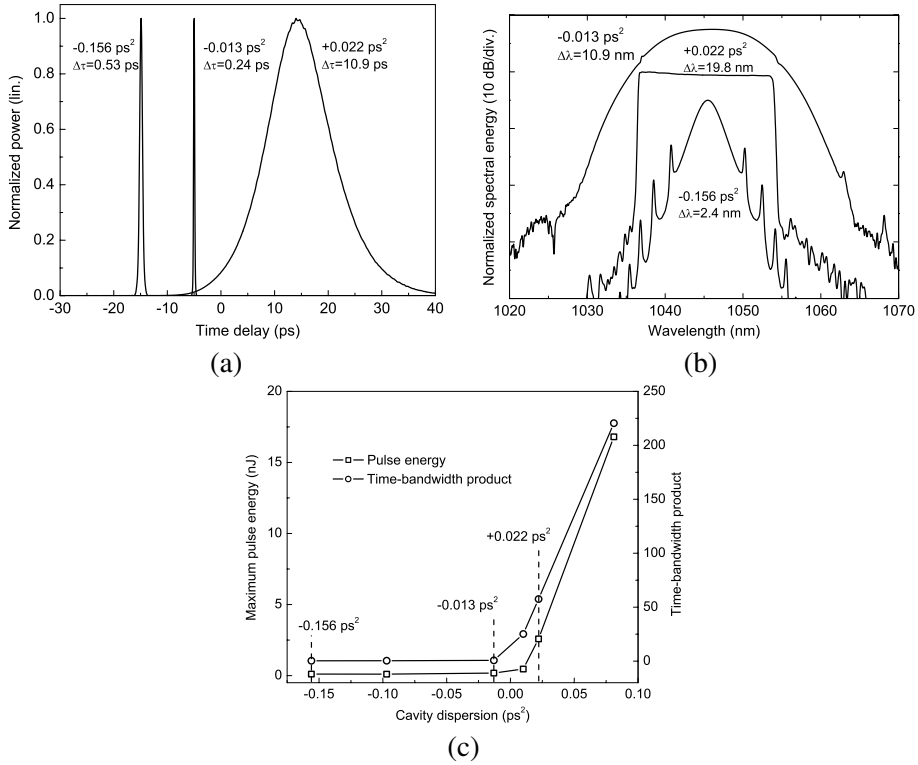

Fig. 3.1. *Simulated temporal (a) and spectral (b) profiles for pulses from cavities with various net dispersion values. The spectra have been shifted vertically for clarity. (c) Pulse energy and time-bandwidth product (TBP) as a function of net cavity dispersion. The highest pulse energies are obtained with large net normal dispersion, but only in conjunction with strong chirp (high TBP). (Courtesy of R. Herda.)*

3.3 Stretched-pulse regime

A stretched-pulse laser cavity consists of sections with normal and anomalous dispersion causing the chirp to change from positive to negative and back during one round trip [69, 70]. The large periodic variations in GVD need to be taken into account when solving the Eq. 3.1. The solutions are referred to as *dispersion-managed solitons* [71, 72]. The temporal shape of such pulses is close to being Gaussian rather than the hyperbolic-secant shape of true solitons.

For stretched-pulse generation, the net round-trip GVD can have either a low anomalous or normal value. For anomalous regime, in contrast to solitons, the phase modulation is only partially compensated resulting in relatively large local chirp within the cavity. With net normal dispersion, the output pulses are chirped much stronger than with net anomalous dispersion resulting in large spectral widths that may exceed 50

nm. Figure 3.1(b) shows the shape of the pulse spectrum in a cavity with dispersion of 0.022 ps^2. The steep spectral edges are typical characteristics of a mode-locked

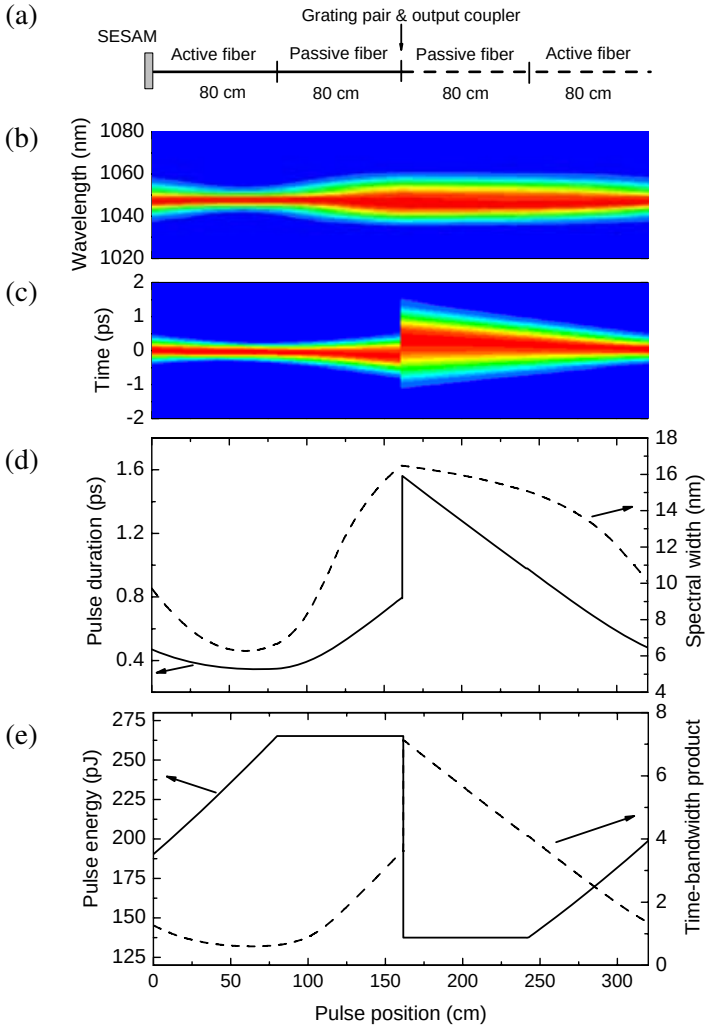

Fig. 3.2. *Simulated pulse evolution within a round-trip in a stretched-pulse laser. (a) Cavity consists of a SESAM, 80 cm of gain fiber (γ=5.9/Wkm, gain bandwidth 20 nm), and 80 cm of passive fiber both having normal dispersion (β_2=26 ps^2/km) at 1 μm regime. Grating pair dispersion compensator and the output coupler are modeled as an abrupt change in the dispersion and loss. The cavity has a low total value of anomalous dispersion. (b-d) Evolution of the spectral and temporal pulse profiles. The pulse is unchirped and has the minimum duration at ∼60 cm from the SESAM. The sign of the chirp is positive from this point up to the output coupler. (e) Evolution of the pulse energy and the TBP. The pulse energy at the output is high, but the pulses are strongly chirped (TBP≈7). (Courtesy of R. Herda.)*

laser with net normal cavity GVD. Analytical evaluation of the functional form for the normal dispersion regime indicates that the spectrum tends to a sharp top-hat shape with increasingly large chirp parameter [73].

The shortest and cleanest pulses can be generated with low net normal GVD. In this dispersion regime, pulses of 50-fs duration after external chirp compensation have been demonstrated [74]. In contrast, the high-energy pulses are obtained with increased amount of normal dispersion as can be seen in Fig. 3.1(c). At the high degree of pulse stretching, nonlinear saturation can be avoided and the pulse energies become significantly higher than for less stretching. The stretched pulses can also tolerate nonlinear phase shifts an order of magnitude higher than ordinary solitons without breaking into multiple pulses. Consequently, the pulse energy can exceed the maximum soliton energy by the same factor [75]. Stretched-pulse lasers with output energies from tens of picojoules to a few nanojoules have been reported [76, 77, 78, 74]. However, with large net normal dispersion mode-locking is difficult to initiate, and operation suffers from instability. To certain extent such problems can be tolerated by simultaneous use of slow and fast saturable absorbers in the cavity [79]. To take the full advantage of very high net normal dispersion, self-similar pulse regime should be used (see Section 3.4).

In a stretched-pulse configuration, the pulses' spectral and temporal widths undergo large variations during a round-trip through the cavity. This kind of behavior is sometimes referred to as "breathing" [80], and can be clearly seen in the simulation shown in Fig. 3.2. The ultrashort pulses experience large amount of stretching in the cavity section with positive chirp. This is desired because the highly chirped long pulses can acquire an increased energy from the gain material [81]. After chirped pulse amplification, the cavity section with anomalous GVD (e.g. a grating pair) compensates for the high positive chirp. The complete chirp compensation, and the shortest pulse, is obtained at a certain position in the cavity defined by the laser parameters. While it is not always convenient to place the output coupler at this position, the dechirping can be accomplished with an external dispersive delay-line as well [69], [P3].

3.4 Self-similar pulse regime

Solitary propagation of short optical pulses in amplified dispersive medium was first considered theoretically in 1989 [82]. The theoretical analysis of propagation of short parabolic optical pulses in fibers with normal GVD and strong gain was presented in 1993 [83]. Several years later, it was demonstrated that pulses with linear chirp and parabolic intensity profile can be generated in high gain amplifiers [84, 85]. Recently, this new type of pulse shaping was applied to mode-locked fiber lasers [75, 86, 87]. The pulses generated in the regime with net normal dispersion and high gain as the dominant shaping mechanisms are referred to as self-similar pulses, or

similaritons [88]. Self-similar pulse is always a scaled version of itself. Due to their shape-preserving nature, the pulses are also called *gain-guided solitons* [87]. As the unestablished terminology suggests, all the pulse shaping mechanisms are not yet fully understood. In fact, the self-similar pulse regime has recently been shown to be embedded in a more general regime of *wave-breaking free* operation [89].

Self-similar pulses are asymptotic solutions to the nonlinear Schrödinger equation in the high-intensity limit. The chirp of the pulse increases monotonically as it propagates inside the fiber, thus causing an exponential increase in the temporal and spectral widths. The solution cannot be stable in a system with optical feedback such a laser cavity. Therefore, a restricting mechanism that limits the progressive pulse broadening is needed. In practice, the pulses evolve until the available gain bandwidth is filled.

The characteristic spectrum profile of self-similar pulses has a parabolic-like top and steep edges. This results from the parabolic gain profile and net normal intra-cavity dispersion [75]. The edge-to-edge width is determined by the gain bandwidth and the nominal value of net dispersion. The pulses have also an approximately parabolic temporal profile.

The pulse evolution in a self-similar oscillator differs from pulse evolution in the other regimes. In contrast to static solitons and dispersion-managed solitons, the self-similar pulses are positively chirped throughout the cavity round-trip. In order to exploit the full gain bandwidth, the pulses should be extracted from the cavity at the point corresponding to the maximum chirp. Thanks to the linear chirp, the pulses can be dechirped to nearly transform-limited duration external to the laser cavity. Ultrashort self-similar pulses with $\sim$100 fs duration have been demonstrated using this scheme [75, 90].

It was found that parabolic self-similar pulses can tolerate a strong nonlinear phase shift without wave breaking [83]. This makes self-similar regime very attractive for high energy applications. Recently, pulse energies above 10 nJ have been demonstrated, thus exceeding the energy ever achieved from stretched-pulse fiber lasers [91].

Finally, it should be noted that the transition from the stretched-pulse regime to the self-similar regime is not abrupt. For instance, the square-shaped spectrum of stretched pulses changes gradually to parabolic-like self-similar spectrum with an increase in the net normal cavity dispersion [92, 93]. Similar transition can be seen for fixed dispersion value when the amount of gain is increased [94, 87]. This parameter regime in which the pulses are always positively chirped due to purely normal GVD inside the cavity and the gain bandwidth and saturation do not influence the propagation much, possesses some distinct characteristics. Therefore, it is often separated from the stretched-pulse and self-similar regimes, and termed as *all-normal dispersion regime* [95, 96] or *dispersion compensation-free regime* [40, 97]. As an

example, the ring-cavity laser I have described in [P3] was operated in the soliton and streched-pulse regimes as well as the all-normal dispersion regime by changing the net cavity dispersion (see Section 4.2.2).

4. SEMICONDUCTOR SATURABLE ABSORBERS FOR MODE-LOCKING FIBER LASERS

In this chapter I will describe two alternative semiconductor saturable absorber components. First in Section 4.1 I present the results published in [P2], where we demonstrated that absorbers based on a p-type–intrinsic–n-type (p-i-n) structure can be efficiently used for controlling mode-locked operation in fiber lasers. Another approach, presented in Section 4.2, deals with a semiconductor saturable absorber etalon, i.e., an absorber component operating in transmission instead of usually used reflection mode. We demonstrated a mode-locked ring-cavity fiber laser using this mode-locker in [P3].

4.1 Reverse-biased semiconductor saturable absorber mirror

The absorption recovery time is one of the key parameters that determine the start-up and stability of mode-locking in saturable-absorber-based systems. As discussed in section 2.2, low-temperature epitaxial growth or post-growth heavy-ion irradiation are the most popular methods of reducing the recovery time of semiconductor absorbers. Another approach is based on MQWs placed into a p-i-n structure that allows for exploiting the reverse-voltage induced carrier sweep-out. [98, 99, 100]. These devices provide an attractive flexibility in controlling both the amount of absorption and its response time.

Reverse-biased absorbers are used in monolithic edge-emitting mode-locked semiconductor lasers and in electroabsorption modulators [101, 102, 103, 104, 105]. More recently, biased saturable absorber mirrors have been used for active control of mode-locking in the vertical cavity surface emitting lasers [106, 107] and in solid-state lasers [108, 109]. In [P2], we demonstrated that a p-i-n-structured SESAM (pin-SESAM) can also efficiently control the mode-locking start-up capability and the pulse width of a fiber laser.

4.1.1 Carrier sweep-out process

The pin-SESAM has an undoped zone of an intrinsic semiconductor separating the p- and n-doped regions as shown in Fig. 4.1(a). Since no space charges exist in the intrinsic zone, where the QWs are located, the bias voltage applied to the diode will cause a constant electric field which affects the band shapes and the distribution of photo-generated carriers. In general, the presence of an electric field in semiconductor leads to splitting and shift of degenerated absorption lines into several components. This feature is known as the Stark effect. The quantum-confined Stark effect (QCSE) [110], i.e. an electro-absorption mechanism seen in semiconductor QW structures, further enhances the shifts in band-edge absorption by bound excitons. This is due to the fact that the electric field applied perpendicular to the surface pulls the photo-generated electrons and holes in opposite directions, but they remain confined in the smaller bandgap QW layer.

Figure 4.1(b) shows schematically the reverse bias induced tilt in the valence and conduction bands and the corresponding reduction in the effective height of the QW barriers. The lower barriers combined with the influence of the QCSE lead to a significant decrease in both the thermal and tunneling lifetimes of photocarriers. As the result, the absorption recovery time experiences an exponential decay with increasing reverse bias [99, 107]. In high purity semiconductor material (i.e., material with low number of trap states) the carrier recombination may become negligible in comparison to the faster tunneling and thermionic emission rates [98]. Recombination becomes more dominant only with low fields in samples with high or thick QW barriers.

After escaping the QWs, the electrons and holes are swept to the n- and p-contacts, respectively. The transit time across the intrinsic region depends on the layer thickness and the reverse-bias. Because the carriers separate, they will locally screen the external electric field in the region where the photocarriers are generated by the laser pulse, as seen in Fig. 4.1(c). This in turn weakens the QCSE and decreases the absorption. After the excitation pulse has passed, the voltage recovers rapidly in time and the initial absorption level restores.

The voltage relaxation is governed by a diffusion process and can be described with an equation [111]

$$\frac{\partial V}{\partial t} = D\nabla_{xy}^2 V, \tag{4.1}$$

where

$$D = \frac{1}{R_{sq}C_A}, \tag{4.2}$$

with C_A being the capacitance per unit area of the device and R_{sq} being the sum of the square resistances of the n and p layers (i.e., the resistance between two opposite

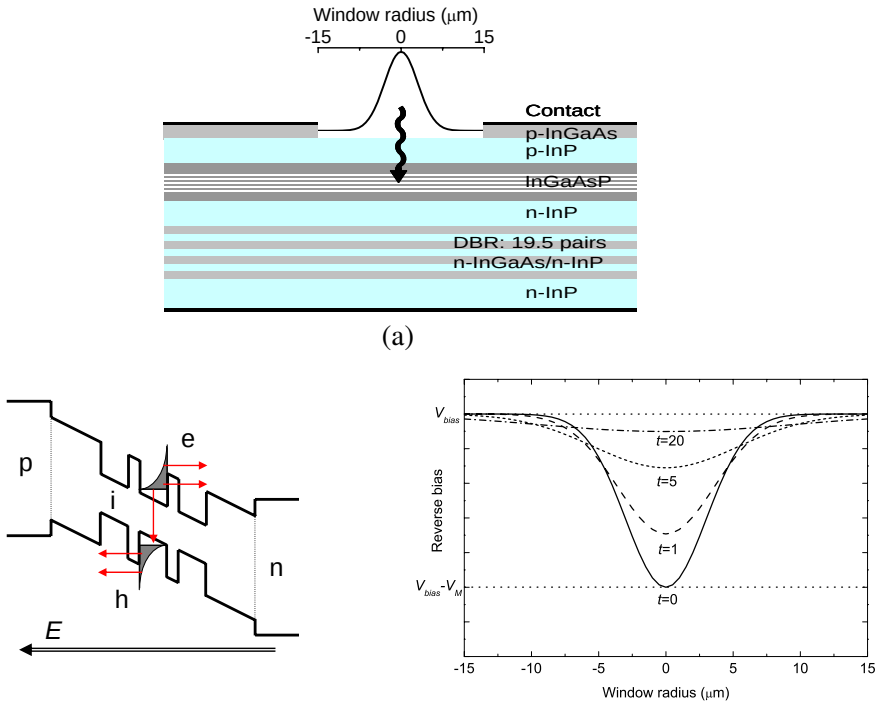

Fig. 4.1. *Structure and function of the reverse biased p-i-n absorber. (a) A Gaussian laser pulse hits the absorber, QW material absorbs the light and bound electron-hole pairs (excitons) are generated. (b) External electric field E separates the carriers and sweeps them out of the QWs via thermionic emission and tunneling through the QW barriers. (c) The separated carriers screen the external field leading to an approximately Gaussian voltage distribution across the device. The local reduction in reverse bias weakens the QCSE and, thus, decreases the absorption. After the pulse has passed, the voltage distribution relaxes and absorption returns to the initial level.*

sides of a square of the layer). For a laser pulse having a Gaussian cross section with $1/e^2$ intensity radius of w_0, we obtain an initial reverse voltage distribution in the form

$$V(r,t=0) = V_{bias} - V_M \exp\left(\frac{-r^2}{w_0^2/2}\right), \tag{4.3}$$

where the applied external reverse bias V_{bias} is assumed to be constant over the structure. V_M is the maximum voltage change due to the laser excitation and r is the radial distance from the center of the beam. The voltage distribution evolves as

$$V(r,t) = V_{bias} - V_M \left(\frac{\tau_{rel}}{t+\tau_{rel}}\right) \exp\left(\frac{-r^2}{4D(t+\tau_{rel})}\right), \tag{4.4}$$

with a characteristic time for the local voltage recovery

$$\tau_{rel} = \left(\frac{w_0}{\sqrt{2}}\right)^2 \frac{1}{4D}. \tag{4.5}$$

As can be seen, the voltage distribution relaxes faster for smaller laser spots and for smaller C_A and R_{sq}.

In conclusion, the saturation dynamics of a reverse-biased absorber depend on multiple physical mechanisms. The dominant effects are the emission and separation of charge carriers from the quantum wells followed by the diffusive relaxation of the screening voltage distribution. As discussed in [111], by engineering the structure appropriately, the overall absorption recovery time can be made to be picoseconds or even shorter, thus reaching the performance available with low-temperature grown or ion-implanted absorbers.

4.1.2 Device structure and characterization

The pin-SESAM structure is shown in Fig. 4.1(a). It was grown by solid-source molecular beam epitaxy on an n-InP substrate. The reflector consists of 19.5 pairs of Burstein-Moss shifted, λ/4 n^+-$Ga_{0.47}In_{0.53}As$ / n^+-InP layers, fabricated as described in [112]. The DBR reflectivity was measured to be ∼98 % in the spectral range from 1.525 to 1.580 μm. The absorber includes five 11.5-nm thick undoped InGaAsP QWs separated by 20-nm InGaAsP barriers lattice matched to InP, and a 220-nm separate confinement heterostructure with the same composition as the barriers. The quaternary QW structure facilitates sweep-out due to the low barriers to free carriers

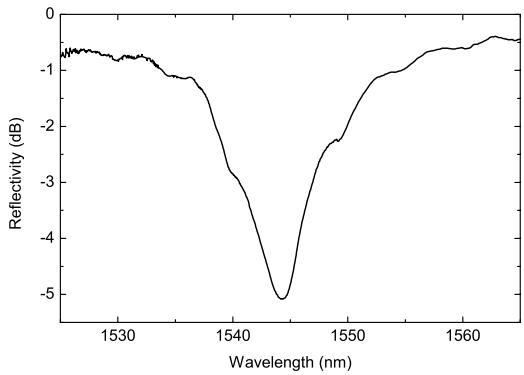

Fig. 4.2. *Low-intensity reflectivity of the pin-SESAM. In the experiments the fiber laser was operated at a near-resonant wavelength of 1548 nm.*

for both the conduction band and valence band wells. The active region is sandwiched between two InP cladding layers. The n-type cladding consists of 1.5 μm InP with n$\approx 10^{18}$ cm^{-3} and the p-type cladding is composed of 2 μm InP with p$\approx 10^{18}$ cm^{-3}. An $In_{0.53}Ga_{0.47}As$ cap layer with p$\approx 1.5 \cdot 10^{19}$ cm^{-3} was used for the p-contact. The structure was prepared in a single growth step. The mirror structure was completed using standard photolithography and wet chemical etching. The optical window on the top of the reflector has a diameter of 30 μm. The p$^+$-InGaAs contact layer was etched away in the window area in order to avoid signal absorption outside the MQW absorber region.

The reflection spectrum shown in Fig. 4.2 reveals the presence of a FP resonance at 1544 nm. At the resonant wavelength the low-intensity reflectivity was $\sim$32 % and the maximum modulation depth was measured to be $\sim$20 %. At a near-resonant wavelength of 1548 nm, where the fiber laser described in the following section was operated, the modulation depth was $\sim$8 %.

4.1.3 Mode-locked fiber laser using a pin-SESAM

The pin-SESAM was used as one of the mirrors in a linear cavity erbium-doped fiber laser shown schematically in Fig. 4.3. The aim was to examine the performance of the mirror in both starting the mode-locked operation and pulse shaping. This was achieved by minimizing the nonlinear effects and avoiding polarization-dependent components in the cavity to prevent pulse shaping through nonlinear polarization evolution. In order to fully avoid NPE, polarization maintaining (PM) components should have been used. Suitable PM fibers were, however, not available in the laboratory at the time of the experiment.

In the first cavity configuration the net dispersion had a normal value of +0.017 ps^2 at 1.55 μm, which prevented soliton shaping. The fiber cavity was comprised of 2.8 m of erbium-doped fiber with normal GVD of 0.0076 ps^2/m, 0.4 m of Corning Hi1060 WDM coupler fiber with dispersion of -0.0102 ps^2/m, and a loop mirror made of 0.5 m of dispersion shifted fiber with zero dispersion at 1.55 μm. In another cavity

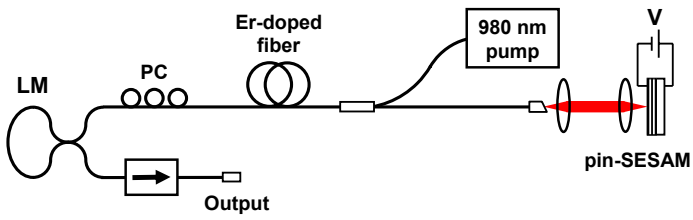

Fig. 4.3. *Laser setup with reverse biased saturable absorber mirror. PC: polarization controller, LM: loop mirror.*

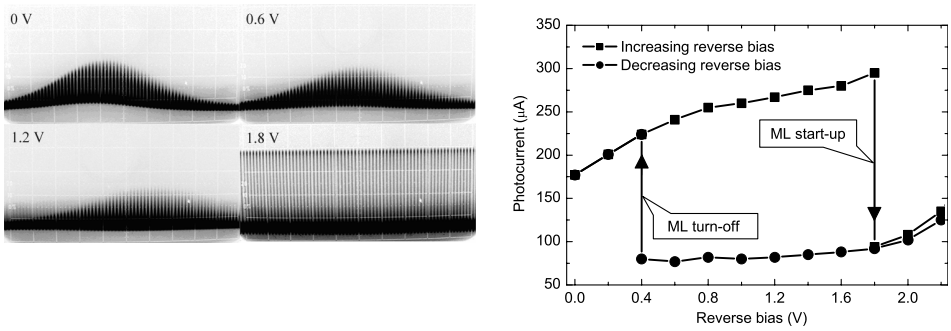

(a) (b)

Fig. 4.4. *(a) Oscilloscope traces of the laser output obtained with different reverse bias voltages (0.5 μs/div). With applied voltages above 1.8 V the cw mode-locked operation was achieved without low-frequency instability. (b) Photocurrent generated in the p-i-n structure as a function of reverse bias. The abrupt changes in photocurrent at 1.8 V and 0.4 V correspond to the start-up and turn-off of the cw mode-locked (ML) operation, respectively.*

configuration an additional 3.3 m long piece of SMF-28 fiber with GVD of -0.0217 ps^2/m was used to make the net dispersion anomalous (-0.054 ps^2), thus allowing soliton formation. The fiber ends were angle-polished to eliminate the influence of Fresnel reflections. AR-coated aspheric lenses were used to focus the beam to a 6.2-μm diameter spot on the pin-SESAM. The loop mirror served also as a 10 % output coupler. The laser was pumped with a single-mode grating-stabilized laser diode, which provided a power of 120 mW at 980 nm.

Figure 4.4(a) shows the operation regimes of the fiber laser for different values of the reverse bias. As expected, the reverse bias voltage applied to the pin-SESAM significantly influences the dynamic properties of the laser. At biases between 0 to 1.2 V, the laser output waveform shows mode-locked operation with distinct low-frequency instability. Self-starting cw mode-locking with a single pulse per round trip was observed for reverse biases above the value of V_0=1.2...1.8 V, depending on the absorber sample and alignment. The experimental observations made with a number of samples showed that passive mode-locked operation could be achieved with an appropriate optimization of the beam spot size at the p-i-n absorber.

The bias-dependent photocurrent generated in the p-i-n structure is shown in Fig. 4.4(b) for the pump power of 100 mW. With an increase in the reverse bias, the laser operates first in the Q-switched mode-locking until the bias reaches the value of V_0=1.8 V, corresponding to the electrical field of 32 kV/cm in the absorbing region. Above V_0 the recovery time of the absorber becomes fast enough to enable

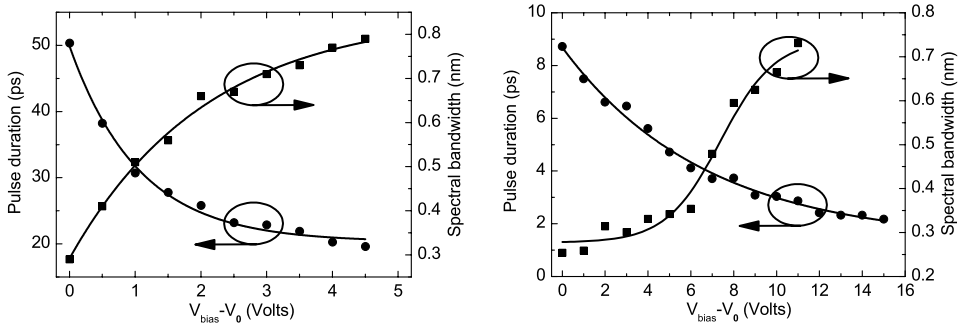

Fig. 4.5. *Measured mode-locked pulse duration and pulse bandwidth as a function of reverse bias applied to the pin-SESAM for (a) net normal and (b) net anomalous cavity dispersion. V_0 is the bias at cw mode-locking start-up.*

self-starting cw mode-locking. The onset of cw mode-locking is manifested as an abrupt decrease in the photocurrent indicating a reduction (bleaching) of the mirror absorption provided by the pulse train with a high repetition rate.

A hysteresis in the mode-locking start-up and turn-off is frequently observed versus pump power [69]. Similar behavior was found here by varying the reverse bias, as seen from Fig. 4.4(b). With a decrease in the reverse bias from a high value down to 0.4 V, the pin-SESAM sustains its highly saturated state corresponding to mode-locked operation. Below 0.4 V the absorber cannot support short pulse formation. Mode-locking turns off and the absorber jumps into the high absorption state distinguished as a regime with a high value of photocurrent.

Figures 4.5 (a) and (b) present the pulse characteristics for the bias above the mode-locking start-up voltage V_0 for the two different cavity configurations described above. A substantial decrease in pulse duration is observed both with net normal and anomalous dispersion regime. A corresponding spectral broadening by a factor of 2.5…3 was observed with an increase in the bias. Another interesting – but not desired – observation was made regarding the damage threshold of the absorbers. Namely, in case of net normal cavity dispersion, the pin-SESAMs could withstand only a few volts of reverse bias without breakdown in the p-i-n structure. Much higher bias values could be used with net anomalous dispersion. This behavior is attributed to arise from the higher pulse energies in the stretched-pulse regime compared to the soliton regime (see Fig. 3.1).

4.2 Semiconductor saturable absorber etalon

A semiconductor saturable absorber is typically fabricated on top of a high-reflective semiconductor, dielectric or metallic reflector forming a semiconductor saturable absorber mirror. As discussed in section 2.2.1, a high nonlinear modulation depth is often preferred for a SESAM used in mode-locked fiber lasers. The modulation depth can be enhanced by placing the absorber within a Fabry-Pérot cavity. However, the use of a resonant SESAM exhibiting higher loss near the resonant wavelength makes the mode-locking difficult to achieve at the desired wavelength. In order to operate the laser near the resonant wavelength, the cavity architectures should employ an additional wavelength selective element, e.g. an optical filter. The problem can be avoided by using the saturable absorber in the form of a FP etalon operating in transmission. With this geometry, the modulation depth enhanced near the FP resonance corresponds to the high transmission (low-loss) regime where the laser would tend to operate. An absorptive transmission etalon (ATE) can be naturally implemented in a ring cavity laser, as we have shown in [P3].

4.2.1 Device structure and characterization

The structure of the absorptive transmission etalon is shown in Fig. 4.6. It consists of an absorber region and spacer layers sandwiched between two distributed Bragg reflectors. The bottom DBR is made of 3.5 pairs of quarter-wave 89.3-nm AlAs/75.65-nm GaAs layers. The absorber region comprises six 6-nm InGaAs quantum wells with 15 nm GaAs barriers. The top DBR is comprised of 4.5 pairs of AlAs/GaAs. Two 126-nm GaAs buffer layers surrounding the absorber region set up the length of the ATE cavity and, therefore, define the resonant wavelength and the position of the absorber region in respect to the maxima of the standing-wave pattern of the optical

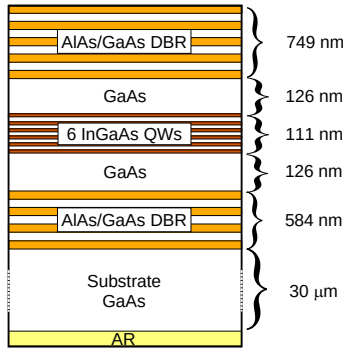

Fig. 4.6. *Structure of the absorptive transmission etalon.*

field within the cavity. The semiconductor substrate of the etalon was antireflection coated to avoid unwanted Fabry-Pérot effect between the absorber mirrors and the substrate/air interface. Before coating, the substrate was thinned down to 30 μm by wet etching. The saturation fluence of the ATE was measured to be $\sim$20 μJ/cm^2 and the modulation depth was $\sim$10%. Growth conditions ensured an absorption recovery time of about 40 ps.

4.2.2 Mode-locked fiber laser using an ATE

Figure 4.7 shows the setup of the mode-locked fiber laser employing the ATE as the mode-locking element. The gain medium was a 50-cm-long ytterbium-doped fiber with absorption of 414 dB/m at 976 nm. The ytterbium-doped fiber was pumped with a 980 nm laser diode delivering a power up to 130 mW. The ring laser cavity contained an optical isolator to ensure unidirectional propagation, a 980/1050-nm pumping fiber coupler, a 6% output coupler and a polarization controller. The cavity dispersion was adjusted by using a pair of 1250-lines/mm transmission gratings. The overall cavity length was about 6.5 m, which corresponds to a fundamental pulse repetition rate of 31.4 MHz. The laser delivered an average output power of $\sim$1 mW.

Stable mode-locked operation supported by the ATE could be initiated by adjusting the polarization inside the cavity. The pump power threshold for self-starting mode-locking was 100 mW. Once started, mode-locked operation was stable for hours. Polarization dependent loss of the grating pair suggests that nonlinear polarization evolution is a dominant pulse shaping mechanism, while the ATE plays mainly the role of a robust trigger for passive mode-locking. It should be mentioned that mode-locked operation was not observed without the ATE.

Figure 4.8(a) shows the output pulse spectra of the laser for different values of total cavity dispersion. As expected, the laser operates at the wavelength close to the

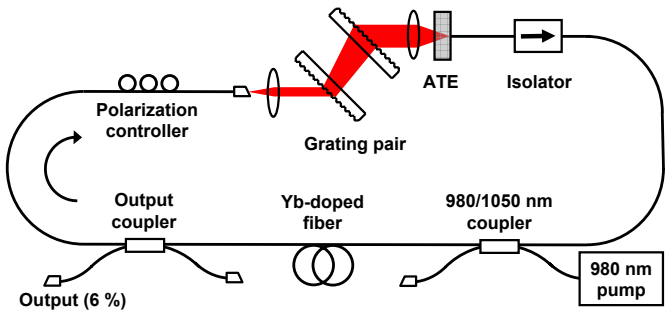

Fig. 4.7. *Configuration of the ring-cavity fiber laser using the ATE-mode-locker.*

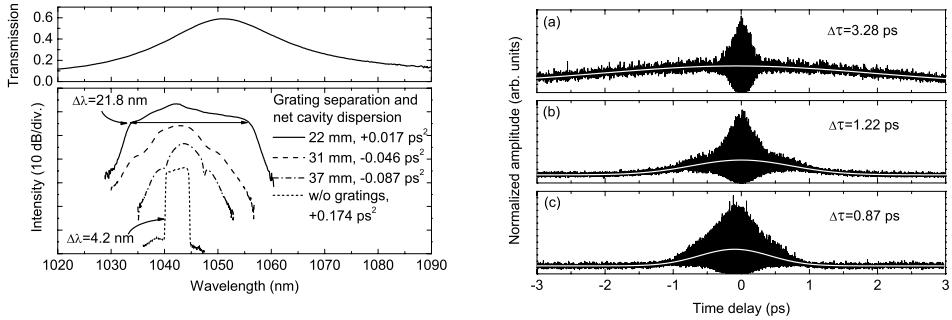

Fig. 4.8. *(a) Low intensity transmission spectrum of the ATE (top) and mode-locked spectra for different grating separations. The traces have been shifted for clarity. (b) Interferometric autocorrelation traces for the different grating separations: (from top) 22 mm, 31mm, and 37 mm. White curves show the Gaussian fit to the intensity autocorrelation.*

transmission maximum of the absorber. The slight shift from the resonance to the shorter wavelengths is most likely due to the non-uniformity of the gain spectrum. With a grating separation of 22 mm, the total cavity dispersion was normal with a value of +0.017 ps^2 and resulted in a very broad square-shaped spectrum with the bandwidth of 21.8 nm, indicating the stretched-pulse operation. With an increase in the grating separation the cavity dispersion becomes anomalous and, consequently, the laser switches to soliton pulse operation with the characteristic side-lobes in the spectrum. Without the grating compensator, the laser operates in the all-normal dispersion regime with a spectral width of 4.2 nm.

The autocorrelation traces corresponding to the three different grating separations are shown in Fig. 4.8(b). The traces, measured at the laser output shown in Fig. 4.7, correspond to strongly chirped pulses. As discussed in Section 3.3, the pulse duration and chirp vary along a stretched-pulse laser cavity. In order to reduce the pulse duration we placed the output after the grating compensator where the chirp is negative. The extracted pulses were then externally compressed from 1.6 ps down to 200 fs in a 4-m-long fiber delay line with normal GVD of 0.023 ps^2/m. The corresponding 6.6 nm wide spectrum indicated near transform-limited pulses with the time-bandwidth product of 0.36.

4.3 Discussion

The absorption recovery time and the nonlinear intensity response are the key parameters of a saturable absorber as discussed in Section 2.2 already. In this chapter I have

presented two unconventional approaches to affecting these parameters.

A p-i-n structure offers a way to control the SESAM parameters electrically. By varying the bias voltage it is possible to adjust both the amount of the absorption and the recovery time of the absorber mirror that allows to improve the pulse quality. Most importantly, the possibility to tune the absorber parameters on-the-fly allows for combining good mode-locking start-up capability with enhanced picosecond pulse shaping in the same device. Furthermore, the long-term stability of the pin-SESAM is expected to be better than in many defect-implanted structures, whose performance tend to degrade over time.

An absorptive transmission etalon was proposed for mode-locking fiber lasers. Contrary to the resonant absorbers operating in reflection mode, the low-loss state in the transmission etalon corresponds to the cavity resonance. Therefore, the operation wavelength sets spontaneously at the resonance of the etalon without using an intracavity filter. This ensures a high modulation depth and a reduced saturation fluence needed for reliable self-starting of mode-locking, in particular in lasers with high value of cavity dispersion.

An ATE is particularly attractive for ring cavity lasers. A unidirectional ring cavity is generally desired since it is less sensitive to the spurious intracavity reflections and, therefore, additionally improves the capability to self-starting mode-locking as compared to a standing-wave cavity. Another interesting cavity configuration would be a bi-directional ring cavity that enables pulse collision in the absorber. In such a configuration additional pulse shortening is expected due to the colliding-pulse mode-locking. An ATE placed in a linear cavity could initiate and support harmonic mode-locking. In this configuration, the pulse collision in the etalon that defines two subcavities with different lengths would enhance the operation with few pulses in the laser cavity.

5. INTRACAVITY DISPERSION MANAGEMENT IN FIBER LASERS

The lasers presented in the previous chapter were using dispersion shifted fiber and diffraction gratings for intracavity dispersion control at 1.5 μm and 1 μm spectral range, respectively. In addition to these conventional methods, several other schemes have been developed for dispersion management in different types of lasers. This chapter summarizes the results of the experiments I have carried out when searching for new techniques for dispersion control in fiber lasers. In Section 5.1, before going to my own results, I briefly introduce the basic concepts of the other compensation methods. In Section 5.2 I consider a semiconductor component based on a Gires-Tournois interferometer to produce tunable dispersion. In Section 5.3 I present the results demonstrating the potential of the novel photonic bandgap fiber technology for dispersion compensation at 1 μm. Finally, in Section 5.4 I compare the different methods in respect with their applicability to intracavity dispersion management in ultrashort-pulse fiber lasers.

5.1 Methods for dispersion compensation

Efficient dispersion management is important for modern fiber optical telecommunication systems operating at bit rates of 10 Gbit/s and beyond. A great deal of efforts has been put into the development of dispersion management techniques used in these systems. The dispersion control in mode-locked lasers has, however, many specific issues not applied for telecom. The various operation wavelengths, large spectral bandwidths and, in particular, the sign of cavity dispersion require individual methods for dispersion compensation, especially at wavelengths shorter than 1.3 μm, where the material dispersion of silica glass is normal. For example, in order to support pulse shortening by soliton formation in Yb-fiber lasers, one needs a compensator element with high enough anomalous dispersion. Both bulk optic and fiber optic methods have been proposed. They all have their pros and cons.

5.1.1 Bulk optic dispersion compensators

Prism pairs are the classical arrangement to provide an anomalous and controllable chromatic dispersion in a laser cavity [113, 114]. Prisms are generally used at minimum deviation (i.e., with incidence angle equal to the exiting angle) and cut at such an apex that rays enter and leave each prism at Brewster's angle. This approach keeps the Fresnel reflection losses low and provides coarsely tunable anomalous dispersion by changing the separation of the prisms. The amount of dispersion is, however, rather small. In addition to GDD compensation, prism pairs are used to compensate for the third order dispersion [115, 116].

Diffraction grating pairs are widely used for dispersion compensation both in solid state and fiber laser cavities [117]. The dispersion compensation effect arises from the fact that spectral components with shorter wavelengths travel a shorter distance than longer wavelengths. One can obtain large anomalous dispersion at any wavelength as long as gratings with a proper spatial frequency and separation are used. However, gratings introduce significant losses and increase the complexity of the system.

Chirped mirrors [118] are a special category of multilayer Bragg reflectors. They consist of a large number ($\sim$40) of alternating low- and high-refractive-index layers whose thickness progressively increases, in a suitable manner, when going towards the substrate. In this way, high-frequency components are reflected deeper in the multilayer structure. Hence the group delay of the reflected beam increases with decrease in ω, which results in anomalous dispersion ($\beta_2 < 0$). The dispersion can be designed to be approximately constant over the bandwidth of interest or to have linear dependence versus ω for compensating third order dispersion. In particular, *double-chirped mirrors* (DCMs) are used to precisely compensate GDD in mode-locked solid-state lasers to produce pulses with duration below 10 fs [119]. The amount of anomalous GDD obtainable with chirped mirrors is limited to about -100 fs^2.

A *Gires-Tournois interferometer* was proposed for pulse compression in the original paper of Gires and Tournois in 1964 [120]. It is based on an asymmetric Fabry-Pérot cavity composed of a partially reflective front mirror and a 100% reflective back mirror separated by a spacer layer as shown in Fig. 5.1. A GTI can be easily made to offer three orders of magnitude higher dispersion than a prism pair, although over a limited bandwidth. GTIs have been used for dispersion compensation in several studies [121, 122, 123, 124, 125, 126, 127, 128]. In particular, thin-film dielectric GTIs are used to compensate highly chirped ultrashort pulses [121, 129].

A special type of the Gires-Tournois dispersion compensator is a semiconductor GTI incorporating a saturable absorber. The device has the same basic structure as resonant SESAMs (or RSAMs), and thus it can be recognized as a *dispersive saturable absorber mirror* (D-SAM) [130]. In order to tell the different concepts apart, I am using the following definition: a D-SAM incorporates both a dispersion compensator

Fig. 5.1. *The basic structure of a Gires-Tournois interferometer. Back mirror reflectivity is 100 %.*

and a saturable absorber used for mode-locking whereas an absorbing GTI provides only the tunable dispersion compensation. The latter application is described in section 5.2.

5.1.2 Fiber optic dispersion compensators

Anomalous dispersion is readily available from conventional silica single-mode fiber (SMF) at wavelengths above 1.3 microns. By tailoring the waveguide contribution to the total dispersion one can fabricate different types of *dispersion modified fibers*. The wavelength-dependent effective refractive index depends on the core radius and the index difference between the core and the cladding. Designing techniques also use multiple cladding layers and tailored refractive index profiles.

A conventional *dispersion compensating fiber* (DCF) [131] has the normal dispersion of the order of -100 ps/(nm·km) at 1.5 microns. A shortcoming of the method is that relatively long lengths of DCF are required to compensate for the anomalous GVD of standard fiber. This increases the cost of telecom lines and may not be acceptable for laser intracavity compensation. Dispersion compensation schemes based on different types of DCF have been described for example in [132].

Zero dispersion wavelength can be tuned around 1550 nm. Such fibers are called *dispersion-shifted fibers* (DSF) [133]. They are best suited for applications involving single channel transmission at 1550 nm providing the benefits of zero dispersion as well as taking advantage of the low attenuation of silica-based fibers at that wavelength.

Other types of dispersion modified fibers have been made for high speed data transmission applications. In WDM applications the total chromatic dispersion should have an absolute value slightly above zero at all operation wavelengths to avoid four-wave mixing. *Non-zero dispersion-shifted fiber* (NZ-DSF) is designed to provide a small amount of dispersion in the 1550 nm region. Waveguide dispersion has also been used to produce *dispersion-flattened fibers* (DFF). They are designed so that the total dispersion is relatively small over a wide range extending from 1300 to 1600 nm.

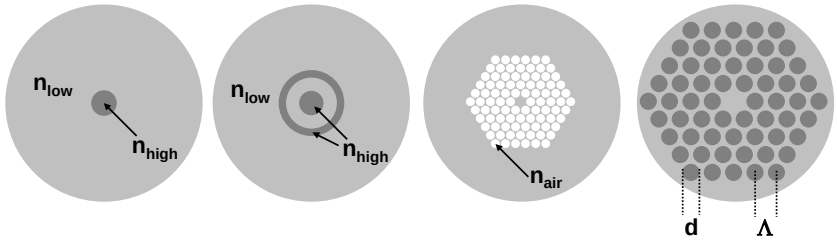

Fig. 5.2. *Cross-sectional profiles of selected fibers. From left: standard single-mode fiber; HOM fiber; index-guiding PCF; solid-core PBGF. Dark grey denotes higher refractive index, d=cladding rod diameter, Λ=pitch.*

In order to achieve the anomalous dispersion at wavelengths below 1.3 μm, special waveguide geometries of the fiber have to be considered. Some of them are depicted in Fig. 5.2. In *higher-order-mode (HOM) fibers* [134, 135] dispersion is modified since at a specified wavelength the guided mode of the fiber changes from being confined in the first core mode into the higher order mode(s). However, due to the multimode behavior, these fibers require some extra care when used in combination with standard single-mode fibers.

In *fiber tapers*, the light propagates through a thin waist that confines the optical field in an area much smaller than the original fiber core. The light is guided by the glass-air interface with an abrupt and large refractive index change that creates strong anomalous waveguide dispersion. By changing the diameter of the taper waist, one can control the amount of dispersion at the wavelength of interest. For example, with a waist diameter of the order of one micron, the zero-dispersion wavelength moves to the visible part of the optical spectrum. The reduced core size of the fiber enhances the nonlinear effects, which may or may not be desirable, depending on the application. Strong nonlinearity, particularly in combination with large anomalous GVD, will degrade the pulse quality and limit the maximum pulse energy. On the other hand, it can be used, for example, in supercontinuum generation. Being made of standard single-mode fiber, tapers can be easily fusion spliced in the laser cavity. Thus, neither back-reflections nor any significant insertion losses are induced.

Phototic crystal fibers can be designed to have dispersion properties very different from that of conventional fibers. In particular, anomalous waveguide dispersion can be achieved with a single-mode PCF at short wavelengths [136, 20], which is not possible with traditional index profiles.

Index-guiding photonic crystal fibers are based on a periodic arrangement of air holes in the cladding running parallel to the fused silica core. Although these solid core PCFs guide light similar to the standard step index fibers, the high effective index contrast and cladding micro-structures facilitate tailoring the fiber properties. The

dispersion profile of an index-guiding PCF strongly depends on the air-filling fraction and the core size. The amount of dispersion and the zero-dispersion wavelength are primarily determined by the core size of the fiber. Large dispersion values are typically achieved with small mode areas. The air-filling fraction of the fiber controls the higher-order dispersion [137]. Not surprisingly, a high air-filling fraction makes the PCF behave similar to a fiber taper with the same core diameter [138]. An advantage of PCF over the tapers is the more rugged mechanical structure. On the down side, splicing of a PCF with standard fibers may be somewhat cumbersome.

Photonic bandgap fibers are a class of photonic crystal fibers in which the light is not guided by total internal reflection [139]. Instead of index guiding mechanism, the light is confined in the core by a bandgap structure that prevents certain optical frequencies from penetrating into the cladding. Thus, light can be guided even in a hollow (air) core. PBGFs are also highly flexible in dispersion characteristics. The theory and experiments of dispersion compensation with PBGFs will be discussed in Section 5.3 in more detail.

Chirped fiber Bragg gratings (CFBGs) were first proposed for dispersion compensation in 1987 [140]. After that they have been used extensively in high bit rate (10–160 Gbit/s) telecommunication systems [141, 142, 143]. They provide an attractive scheme also for intracavity dispersion compensation in fiber lasers. CFBGs can be written in PM fibers and spliced with negligible loss. Moreover, they can be conveniently integrated as the cavity end mirrors. This possibility has been explored since the mid-nineties [144].

CFBG operation is based on the same principle as the dielectric chirped mirrors. A periodic set of perturbations of the effective refractive index in the core of an optical fiber acts as a mirror for wavelengths that satisfy the Bragg condition. A gradually varying perturbation period or effective index provides a spectrally dependent delay over a relatively wide bandwidth. The long wavelengths could, for example, reflect from the front of the grating, whereas the short wavelengths penetrate farther into the grating before being reflected. The sign of the dispersion can be changed simply by physically reversing the grating input and output. This makes it possible to achieve large amounts of both normal and anomalous dispersion at practically any wavelength in a short length of fiber. An ideal CFBG has a top-hat reflectivity profile and linear group delay. In practice, however, the spectral response of the actual gratings may have quite complicated and unregular shape. Some improvement in the performance has been gained using asymmetrically apodised CFBGs [145].

5.2 Dispersion tuning using an absorbing semiconductor Gires-Tournois interferometer

This section summarizes the results of the modeling and the experimental studies I have carried out in order to investigate the dispersion properties of nonlinear resonance structures such as an absorptive semiconductor Gires-Tournois interferometer. The main results have been published in [P1].

If a GTI cavity has no absorption and the back mirror is 100 % reflective, the total reflectivity of the device is unity at all wavelengths and no FP resonances appear. The interferometric resonant behaviour shows up in the phase delay, however. In the actual GTI devices, there is always some amount of loss that decreases the reflectivity, particularly at resonances. One can show that the resonant phase response depends strongly on the cavity loss. It is then obvious that by controlling the absorption, one could tune the group delay and, thus, dispersion of a GTI. It should be noted that the same basic principle applies to the structures with the gain used instead of absorption, and to other all-pass resonance structures as well. For example, the potential use of a GTI gain structure for fully integrated mode-locked semiconductor laser is discussed in [146]. In another recent study, active control of the group delay of a micro-ring resonator chain by changing the waveguide gain and loss has been demonstrated [147].

5.2.1 Theoretical considerations

The transfer function of a GTI describes the amplitude and phase variation of an optical field at frequency ω traversing the structure. It can be presented as

$$\Psi(\omega) = |\Psi| e^{i\Phi(\omega)}. \tag{5.1}$$

The field amplitude $|\Psi|$ (≤ 1) is shown to describe the spectrally dependent power reflectivity R_{GTI} by the relation (see appendix A)

$$|\Psi| \equiv R_{GTI}(\omega, A) = \frac{R + A + 2\sqrt{AR}\cos(\varphi - \omega t_0)}{1 + AR + 2\sqrt{AR}\cos(\varphi - \omega t_0)}. \tag{5.2}$$

Here R is the top mirror reflectivity, t_0 is the round-trip time of the cavity, and φ is the phase change on the high-reflective back mirror (usually assumed to be equal to π). The round-trip attenuation coefficient is given by $A = e^{-2\alpha d}$, where α is the linear absorption coefficient of the structure and d is the length of the GTI cavity. It should be noted that when $A = 1$, there is no loss in the structure. On the other hand, when $A = 0$, all power is absorbed. Different forms of Eq. 5.2 have been used widely to model the switching and modulation properties of GTI devices [148, 149, 150].

The phase change of the reflected light results from multiple reflections and from the accumulated loss inside the structure. The frequency dependent phase can be found from

$$\Phi(\omega,A) = \tan^{-1}\left(\frac{-\sqrt{A}(1-R)\sin(\varphi-\omega t_0)}{(A+1)\sqrt{R}+\sqrt{A}(1+R)\cos(\varphi-\omega t_0)}\right). \tag{5.3}$$

The group delay time τ is calculated by differentiating Eq. 5.3. If the material dispersion of the structure is neglected (i.e. refractive index is independent of ω), the group delay can be written as

$$\begin{aligned}\tau &= -\frac{\partial\Phi(\omega)}{\partial\omega} \\ &= \frac{-\left[\sqrt{A}(1+R)+(A+1)\sqrt{R}\cos(\varphi-\omega t_0)\right]\sqrt{A}(1-R)t_0}{\left[(A+1)\sqrt{R}+\sqrt{A}(1+R)\cos(\varphi-\omega t_0)\right]^2+\left[\sqrt{A}(1-R)\sin(\varphi-\omega t_0)\right]^2}\end{aligned} \tag{5.4}$$

In general, Eq. 5.4 cannot be written in a simplified form. However, at the cavity resonance frequency, i.e., at $\varphi-\omega t_0 = 2N\pi$ with $N\in\mathbb{N}$, we have $\sin(\varphi-\omega t_0)=0$ and $\cos(\varphi-\omega t_0)=-1$. In this case the group delay reduces to

$$\tau = \frac{(1-R)t_0}{(1+R)-(\sqrt{A}+1/\sqrt{A})\sqrt{R}}. \tag{5.5}$$

It can be easily seen that the group delay depends strongly on the level of absorption, moreover, it changes the sign from negative to positive when A passes the value R. When $A=R$, the numerator is equal to zero and this GTI configuration is referred to as an impedance matched design. It results in full extinction of the optical field, while the group delay $\tau\rightarrow\infty$, in other words, the incident light stays in the structure and gets fully absorbed. To generalize, operation close to impedance matching allows for very high group delay dispersion, but leads inevitably to high losses and narrow spectral bandwidth.

5.2.2 Device structure

The absorbing semiconductor GTIs I used in the dispersion tuning experiments were designed to operate at 1.55 μm wavelength range. The results are, however, applicable to other wavelengths as well. The samples were grown by the solid-source molecular beam epitaxy (SS-MBE) method. They consisted of a 0.1-μm InP buffer layer and a Burstein-Moss shifted distributed Bragg reflector made of 19.5 pairs of $\lambda/4$ n^+-$Ga_{0.47}In_{0.53}As$ / InP layers. The saturable absorber had 9-nm thick $Ga_{0.47}In_{0.53}As$ / 10-nm InP quantum wells, placed in an InP cavity. Different numbers of QWs were tested in order to investigate the device parameters, e.g. switching energy and the

amount of absorption. The whole structure was capped with 11-μm InP and 10-nm InGaAs layers.

A GTI structure with 28 (four groups of seven) 9-nm thick $Ga_{0.47}In_{0.53}As$ quantum wells with 10-nm thick intermediate InP barriers was examined in more detail. Different dielectric coatings were deposited on top of the basic structure to detune the top surface reflectivity from the initial value of $\sim$30 %. By using various high reflectivity coatings it is possible to meet the impedance matching condition at different absorption levels. In order to illustrate the consistency of the experimental results with the theory, I will describe the characteristics of a sample with 70 % top mirror reflectivity.

5.2.3 Device characterization

Dispersion tuning properties of the GTI sample were studied by bleaching the saturable absorption of the MQW structure using optical excitation. The structure was optically pumped with 980-nm pigtailed laser diode butt-coupled with the GTI-mirror, as shown in Fig. 5.3. The probe signal tunable near 1550 nm was combined with pump light by a selective coupler. The group delay was analyzed using phase-shift technique at the output of an optical circulator. All measured data were calibrated by replacing the GTI sample by a gold mirror used as a reference.

Figure 5.4(a) shows the measured group delay of the GTI sample as a function of wavelength near the cavity resonance for different pumping powers. To exclude the effect of a small pump-induced temperature shift from the consideration, the resonant wavelengths were normalized. The calculated dispersion with an absorption A within the GTI structure as a parameter is shown in Fig. 5.4(b). It can be seen, that the proper values of A-parameter leads to a good agreement between the theory and the experiment. Just as the theory suggests (see Eq. 5.5), the group delay changes its sign

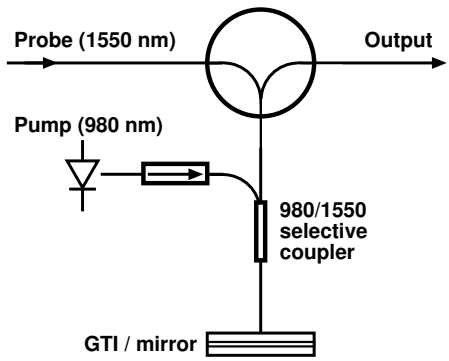

Fig. 5.3. *The setup used for testing the GTI group delay dependence on optical pumping.*

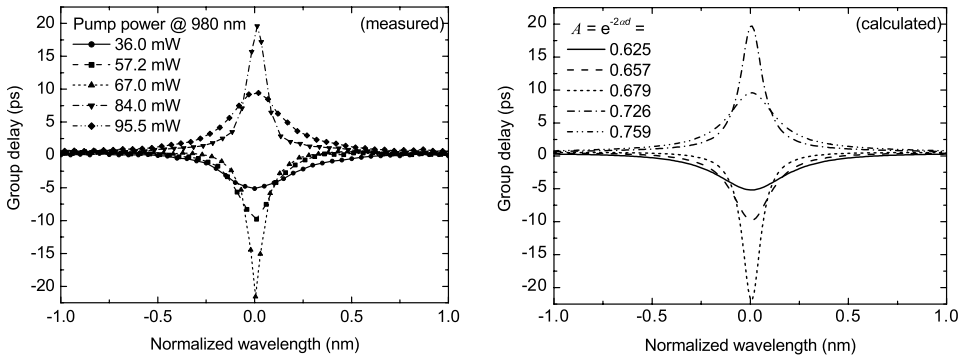

Fig. 5.4. *(a) Measured and (b) calculated group delays of the GTI sample as a function of wavelength around the cavity resonance. In calculation the attenuation A is used as an adjustable parameter. For the singular point, at which group delay shifts from negative to positive values, $P \approx 75.5$ mW and $A = 0.70$.*

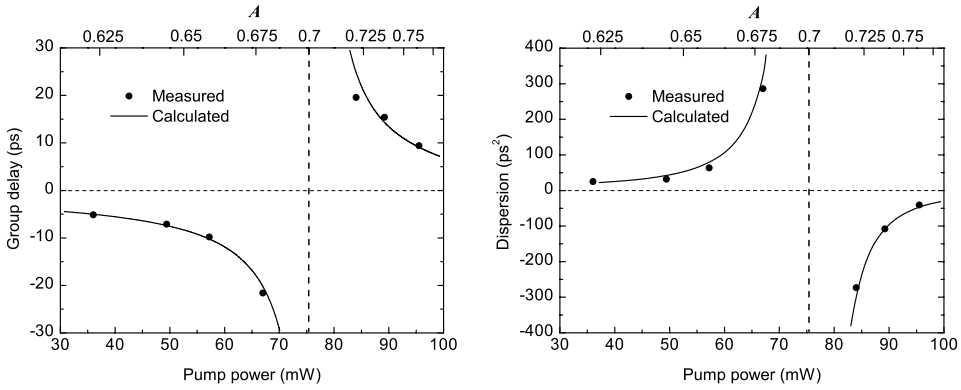

Fig. 5.5. *(a) Group delay dependence on pump power at resonant wavelength of the GTI. (b) Near resonant dispersion $\beta_2 = d\tau/d\omega$ as a function of pump power. The corresponding absorption scale is shown as the top horizontal axis.*

from negative to positive at the pump power level that corresponds to the impedance matched absorption condition.

Figure 5.5(a) shows the group delay versus pump power (or round-trip loss factor A) at the cavity resonance. The same dependence for dispersion β_2 is shown in Fig. 5.5(b). Singular point in $\tau(P)$ and $\beta_2(P)$ at pump power $P \approx 75.5$ mW corresponds to the condition $A = R = 0.70$, at which the group delay changes its sign.

5.3 Dispersion compensation using photonic bandgap fibers

Photonic bandgap fibers have more diverse and modifiable dispersion properties than standard index guiding fibers. In particular, the dispersion can be tailored to be anomalous at short wavelengths (<1.3 μm) where standard fibers have normal dispersion. Two mode-locked ytterbium fiber lasers using this scheme for intracavity dispersion control are presented here. In section 5.3.2 I introduce the use of a solid-core photonic bandgap fiber (SC-PBGF) in a typical linear cavity fiber laser setup. In the second experiment presented in section 5.3.3, both the laser gain and the dispersion compensation are provided by one ytterbium-doped PBG fiber (Yb-PBGF) segment. We have published the results of these studies in [P4], [P5], and [RP4].

5.3.1 Theoretical considerations

In order to accurately simulate the amplitude and phase response of photonic bandgap structures, the beam propagation model for the full structure should be used [151]. Due to the rather complicated geometries, this may not be particularly easy. The main spectral features of the fiber transmission and dispersion can be described analytically using simplified models such as Bragg reflection model, anti-resonant optical waveguiding (ARROW) [152, 153], and multipole simulations [154, 155]. These models give a good physical picture of the PBG fiber behavior.

The configuration known as Bragg fiber was proposed already in 1978 [156]. It gives perhaps the most intuitive explanation for light confinement in PBG fibers. The cladding is modeled as a 2-D cylindrical Bragg reflector formed of concentric low- and high-index layers whose indices may be higher than that of a core. The wavelengths meeting the Bragg condition are reflected back into the fiber core, whereas others are transmitted and lost. The appearing discrete bands of high and low transmission are a typical signature of photonic bandgap guidance.

It has been shown that light confinement in a solid-core PBG fiber does not actually require a periodic Bragg-type cladding structure. The ARROW model originally proposed for planar waveguides [157, 158] fundamentally differs from the Bragg model and the complete bandgap model in that the locations of the transmission bands depend only on the index and diameter of individual cladding inclusions, but not on their geometric arrangement [159]. This can be understood as follows: the light propagating in the core mode(s) couples to the cladding inclusions at wavelengths corresponding to the guided modes of these inclusions (i.e., when propagation constants $\beta = 2\pi n_{eff}/\lambda$ match each other). Thus, at these wavelengths light escapes from the core. More specifically, the transmission bands appear between the frequencies corresponding to the modal cut-offs of individual high-index rods. At cut-off

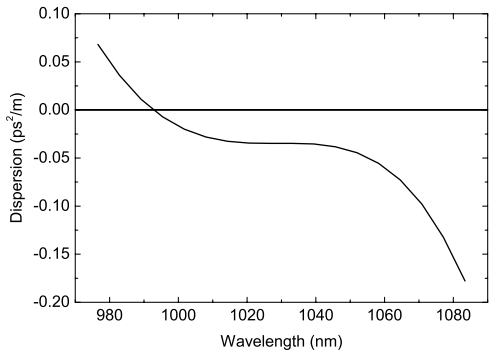

Fig. 5.6. *Typical dispersion characteristics within a transmission band of a PBG fiber.*

frequency, the effective refractive index of the particular rod mode equals the index of surrounding material, causing leakage of light from the core.

The complete bandgap model takes also the other contributing effects into account. Although the position and periodicity of the rods do not change the spectral location of the bandgaps, they do affect the bandgap shape and attenuation as a result of the changing coupling strength between the rods [160]. The periodic array of rods forms a set of supermodes which determines the actual bandgap shapes. The leakage rate depends on the number of cladding layers and decreases with an increasing number of layers. Moreover, any deviations in rod circularity decreases the degeneracy of supermodes and leads to narrowing and fragmenting of bandgaps [161]. In hollow-core photonic bandgap fibers (HC-PBGFs) the transmission bands are further reduced because of surface-confined modes guided in the small glass strands between the air holes [162]. These surface modes match the propagation constant of the hollow-core modes at certain wavelengths, causing increased coupling out of the fundamental core mode. This problem can be avoided in SC-PBG structures as long as the low-index regions between the cladding rods are significantly smaller than the core [160].

Figure 5.6 shows the typical dispersion characteristics in a PBG fiber within one of the transmission bands. The GVD is normal at the short-wavelength side of each transmission band, and anomalous at the long-wavelength side, approaching $\pm\infty$ at the edges of the band. Dispersion has a negative slope (i.e. positive β_3) across the whole band, and an inflection point near the zero dispersion wavelength.

Several methods have been proposed to give a theoretical reasoning for the observed dispersion behavior. The calculations reported in [163] predict the large anomalous dispersion at long wavelengths but not the change in sign of dispersion. In [164] the correct shape of the dispersion curve has been obtained using Bragg fiber model. The multipole simulations used in [165] give a good agreement between measured and calculated dispersion curves. Still again, a simple Bragg scattering model [166] gives

the most intuitive insight into the physical mechanisms that affect the phase response of light propagating in the PBG fibers.

The spectral position of the zero-GVD wavelength and the large amount of third-order dispersion are important characteristics of SC-PBG fibers. The anomalous waveguide dispersion due to the resonant-like PBG structure tends to shift the zero-GVD towards the short-wavelength edge of the transmission band [17]. On the other hand, in case of an all-solid PBG fiber, the strong silica material dispersion at short wavelengths moves the zero-GVD to the opposite direction [160]. In order to obtain the same amount of anomalous GVD in a SC-PBGF as with HC-PBGF at a certain wavelength λ_0, the long-wavelength edge of the transmission band has to be shifted closer to λ_0. This gives rise to an increase in waveguide dispersion and also shifts the zero-GVD towards the short-wavelength side of the transmission band [166]. As a consequence, however, the resulting TOD will be significantly higher as well. We have experimentally and numerically analyzed the influence of these dispersive effects on soliton pulse formation in fiber lasers as will be discussed later.

5.3.2 Solid-core photonic bandgap fiber laser

Figure 5.7(a) shows the microscope image of the SC-PBG fiber cross-section. The high-index Ge-doped rods around the undoped silica core are seen as light grey areas. The fiber diameter is 200 μm and the periodic structure has the spacing of 8.3 μm. The mode field diameter (MFD) in the SC-PBG fiber is $\sim$9 μm, i.e. slightly larger than the 6.4-μm MFD of the core in a standard fiber. Therefore, as the Eq. 3.2 suggests, the nonlinear parameter of the SC-PBG fiber is much smaller than that of the index-guiding PCFs used for dispersion compensation. Figure 5.7(b) shows a typical fusion splice between a standard single-mode fiber and the SC-PBG fiber. Thanks to the perfect matching between the fiber core indexes, the Fresnel reflection at the interface is avoided. Despite the clear difference in the outer diameters, the guided mode of the bandgap fiber has only a small mismatch with the mode of the normal fiber. The

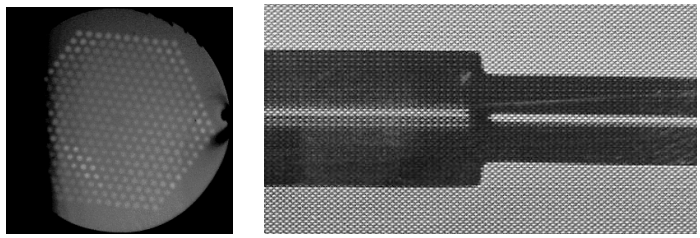

(a) (b)

Fig. 5.7. *(a) Cross-section of the SC-PBG fiber. (b) SC-PBG fiber (ϕ 200 μm) fusion spliced with a standard single-mode fiber (ϕ 125 μm).*

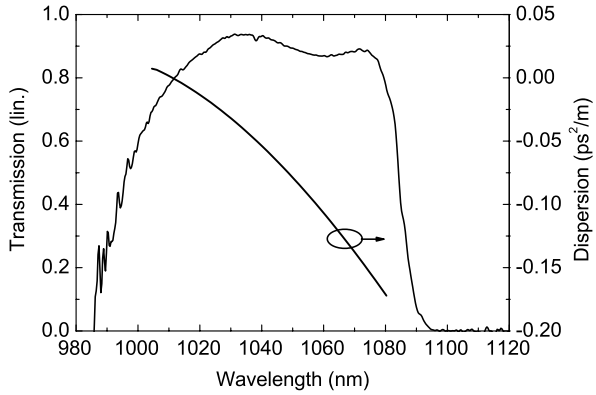

Fig. 5.8. *Transmission and dispersion of the SC-PBG fiber.*

measured double-pass splice loss was ∼1 dB, which corresponds very well to the MFD mismatch induced loss of 0.99 dB approximated by the equation

$$Loss[dB] = -10\log\frac{4}{\left(\frac{MFD_2}{MFD_1}+\frac{MFD_1}{MFD_2}\right)^2}, \tag{5.6}$$

where MFD_1 and MFD_2 are the mode field diameters of the two fibers. Note that the loss is independent of light propagation direction.

Figure 5.8 shows the measured transmission and dispersion spectra of the SC-PBG fiber. The short and long wavelength edges of the bandgap are seen at around 1000 nm and 1090 nm, respectively. The fiber exhibits anomalous GVD of -0.054 ps^2/m and the third order dispersion of $1.40\cdot10^{-3}$ ps^3/m at 1.04 μm.

The experimental setup of the mode-locked laser is illustrated in Fig. 5.9. The laser was pumped with a single-mode grating-stabilized laser diode, which provided a power of 120 mW at 980 nm. The free end of the SC-PBG fiber was butt-coupled to a high reflective (HR) mirror in order to avoid further splice loss and any unwanted

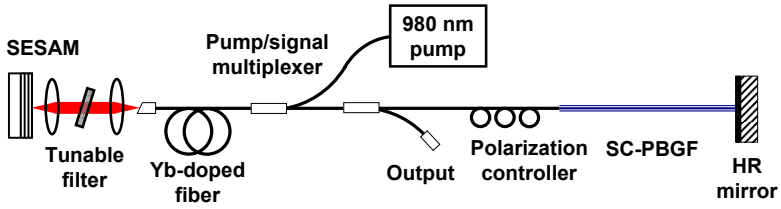

Fig. 5.9. *Mode-locked laser setup with a SC-PBG fiber for dispersion control.*

reflections from the fiber end. In the other end of the cavity an AR-coated aspheric lens with a focal length of 2.0 mm was used to focus the beam on the SESAM. The resonant-type SESAM was fabricated on an n-type GaAs substrate. The bottom mirror had 30 pairs of AlAs–GaAs quarter-wave layers forming a DBR. The DBR stop-

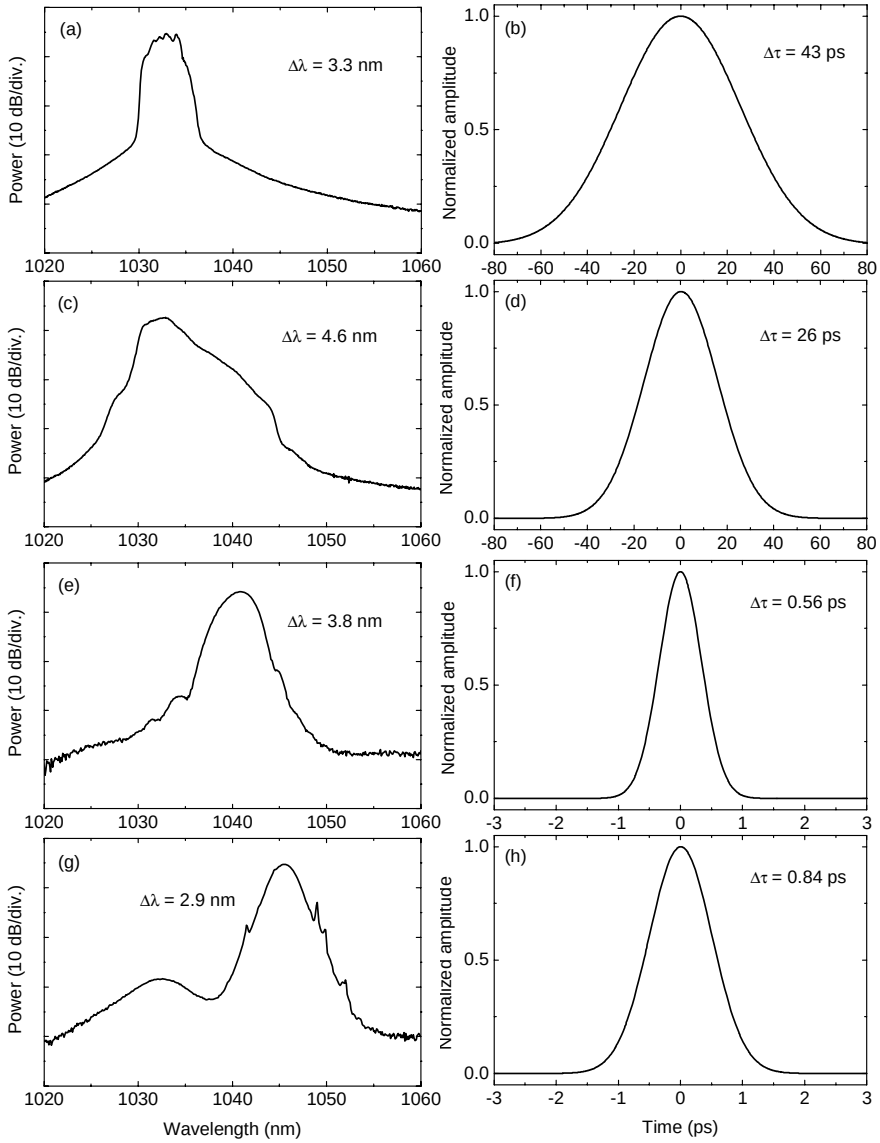

Fig. 5.10. *The intensity autocorrelation traces (right) and the corresponding spectra (left) obtained for tunable mode-locked operation. Plots (a)–(d) correspond to net normal cavity dispersion, (e)–(h) to net anomalous cavity dispersion.*

band was centered at 1050 nm and was ∼120 nm wide. The absorber comprised five InGaAs QWs with thickness of 6 nm and 16-nm GaAs barriers. The QW structure was sandwiched between 100-nm GaAs buffer and cap layers. Post-growth heavy-ion implantation was used for reducing the absorber recovery time to picosecond range.

The fiber segment of the cavity was comprised of 1.0 m of ytterbium-doped fiber, 2.7 m of standard single-mode fiber and a 2.8-m long SC-PBG fiber. The Yb-doped fiber had an unpumped loss of 414 dB/m at 976 nm and a normal GVD of +0.071 ps^2/m measured at 1.04 μm. The 10 % output coupler and the dichroic pump coupler were made of single-mode fiber with normal GVD of +0.023 ps^2/m. With this cavity configuration the round-trip dispersion equals to zero at around 1.04 μm. A birefringent filter at the Brewster angle was inserted into the air-segment of the cavity to tune the operation wavelength continuously around the zero-dispersion point. This allowed us to investigate mode-locked pulse operation both at normal and anomalous dispersion regimes and, in particular, to study the effects of the TOD.

Proper SESAM alignment has resulted in self-starting mode-locking with a fundamental repetition rate of ∼15 MHz. The laser delivers an average output power of ∼2 mW corresponding to the pulse peak power of 250 W. Without the filter, the laser operates at 1035 nm where the SC-PBG fiber has the transmission maximum, as seen in Fig. 5.8. Figure 5.10 shows the pulse spectra and intensity autocorrelations when the laser was tuned to different wavelengths. From Figs. 5.10(a)–(d), it is clear that owing to low value of anomalous dispersion generated by SC-PBG fiber at the short wavelengths (< 1035 nm), the laser operates with net normal cavity dispersion resulting in long pulses. This feature is expected from the dispersion curve shown in Fig. 5.8. In contrast, operation at longer wavelengths (Figs. 5.10(e)–(h)) shows substan-

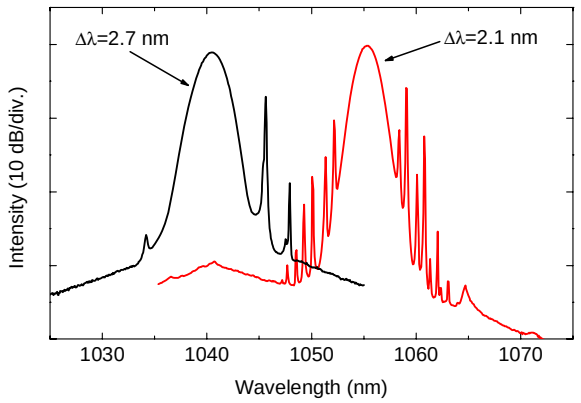

Fig. 5.11. *Mode-locked pulse spectra obtained with 0.55-m long ytterbium fiber. The total cavity dispersion calculated from the soliton sidebands equals -0.13 ps^2 at 1040 nm and -0.52 ps^2 at 1055 nm.*

tial soliton pulse compression indicating the total anomalous dispersion of the laser cavity.

To further illustrate the strong wavelength dependence of the SC-PBG fiber dispersion and, consequently, the high value of TOD, the length of an ytterbium fiber was decreased down to 0.55 m. This allowed us to operate with higher values of net anomalous dispersion. The spectral sidebands in the pulse spectra, shown in Fig. 5.11, give a clear signature of the soliton regime. The average cavity dispersion estimated from the soliton sidebands is -0.13 ps^2 at 1040 nm and -0.52 ps^2 at 1055 nm. The group-velocity dispersion derived from the spectral location of the sidebands agrees with total cavity GVD calculated from measured dispersion of the fibers comprised in the cavity.

5.3.3 Ytterbium-doped solid-core photonic bandgap fiber laser

An exciting and practically important option with a SC-PBG fiber is to use a rare-earth doped rod as the core element. A fiber with an ytterbium-doped core surrounded by the PBG structure can provide both the gain and the anomalous dispersion needed for a 1-μm soliton laser. Using such a fiber as the gain element and the dispersion compensator allows for a very simple and compact all-fiber cavity architecture with repetition rate above 100 MHz.

The experimental setup of the mode-locked laser is illustrated in Fig. 5.12. The Yb-PBG fiber used in the cavity had the same basic microstructure as the SC-PBG fiber described above. The Yb-doping is expected to have only a minor influence on the bandgap properties due to the small change in the refractive index of the core. The fiber cavity was comprised of 0.27 m of Yb-PBG fiber and 0.47 m of standard single-mode fiber. The free end of the PBG fiber was butt-coupled directly to a saturable absorber mirror. The laser output was taken from a variable coupler composed of a polarizing beam splitter and a half-wave plate placed in the free space section of the cavity. Rotating the half-wave plate was used to optimize the output coupling.

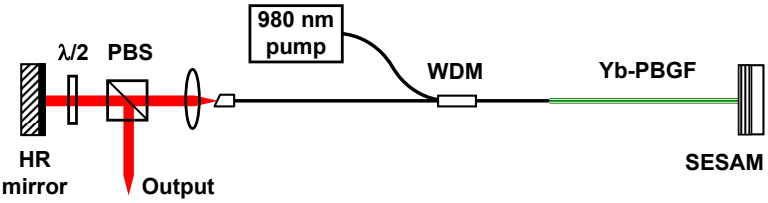

Fig. 5.12. *Laser setup with Yb-PBG fiber. PBS: polarizing beam splitter, λ/2: half-wave plate, WDM: pump/signal multiplexer, HR mirror: high reflectivity mirror. See Section 5.3.2 for details on the SESAM structure.*

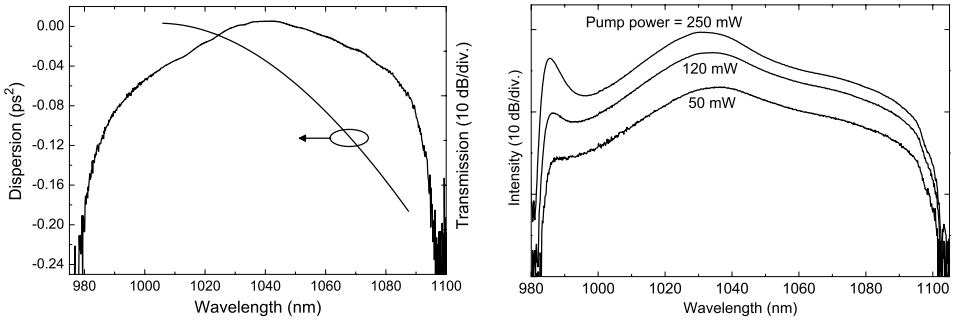

(a) (b)

Fig. 5.13. *(a) Dispersion of the whole fiber cavity and the transmission spectrum of the Yb-PBG fiber. (b) Amplified spontaneous emission from the Yb-PBG fiber.*

Depending on the other cavity parameters, the optimal value of the output coupling that allowed for stable mode-locked operation was ranged from 0.2 to 0.5. The laser was pumped with a single-mode grating-stabilized laser diode capable of delivering up to 300 mW of power at 980 nm.

Figure 5.13(a) shows the transmission band of the Yb-PBG fiber recorded using a white-light source. The bandgap ranges from 980 to 1100 nm covering both the pump wavelength and the laser transitions of the Yb-doped fiber. Although the transmission band shape of the PBG fiber is to certain extent affected by the high level of Yb doping, it is evident that the pump wavelength is located close to the short-wavelength edge of the band. The pump radiation is, therefore, weakly guided that in turn decreases the overall pump efficiency. With optimization of the band spectral position, an improvement in the output power would be expected.

The measured round-trip group-velocity dispersion of the laser cavity is seen in Fig. 5.13 as well. The dichroic pump coupler made of standard single-mode fiber has a normal GVD of +0.024 ps^2/m, while the PBG fiber exhibits anomalous GVD of -0.075 ps^2/m at 1035 nm. Thus, the total cavity has an anomalous round-trip dispersion of -0.017 ps^2 at 1035 nm corresponding to the operation wavelength of the laser.

Figure 5.13(b) shows the spectrum of amplified spontaneous emission (ASE) from Yb-doped bandgap fiber for different pump powers. The ASE spectrum matches closely the transmission band of the PBG fiber demonstrating an efficient filtering provided by the band spectral shape. This feature of the photonic bandgap structure was previously used to suppress undesired four-level transition in the Nd-doped fiber [167].

The laser exhibits self-starting mode-locked operation emitting the pulse train at the

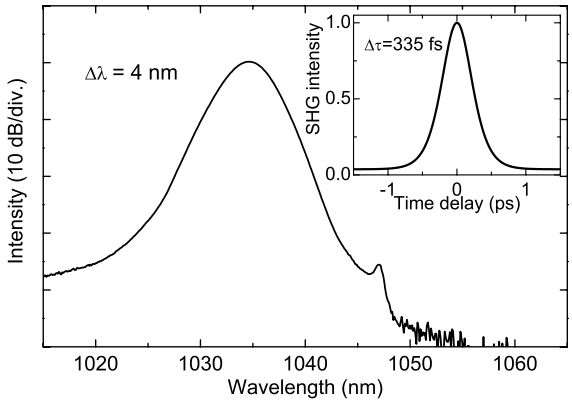

Fig. 5.14. *Mode-locked pulse spectrum. Inset: measured intensity autocorrelation.*

fundamental repetition rate of 117.5 MHz. An average power of 3 mW at the output corresponds to the pulse energy of 25.5 pJ. As it was mentioned above, this characteristic is expected to advance with improving the guiding of the pump radiation. Fig. 5.14 shows the optical spectrum of the pulse with a spectral width of 4.0 nm. The corresponding intensity autocorrelation is shown in the inset of Fig. 5.14. A sech^2-fit yields a pulse duration of 335 fs (FWHM), which corresponds to a time-bandwidth product of 0.37 indicating a nearly transform limited pulse operation.

The exceptionally large value of TOD was found to affect the shape of the soliton pulse spectrum. Namely, the spectral sidebands in the pulse spectrum show notable asymmetry. Typically, we observe 2–3 soliton sidebands in the long-wavelength tail of the spectrum which corresponds to a higher anomalous dispersion regime, while sidebands were never recorded at the short-wavelength wing of the spectrum. The same behavior was seen in numerical simulations [RP4]. For low values of higher-order dispersion, the pulse spectrum formation is governed by the second-order term resulting in a symmetric sideband distribution, as shown in Fig. 5.15 (trace a). With the round-trip TOD of 0.0014 ps^3, corresponding to a Yb-PBG fiber with a length of 30 cm, the sidebands become highly asymmetric and significant power is contained only in sidebands at the long wavelength tail of the pulse, as shown in Fig. 5.15 (trace b). The soliton character is maintained for the high TOD cavity, indicated by a transform limited time-bandwidth product of 0.32. Generally, these observations confirm a high immunity of the soliton pulses to higher-order dispersion.

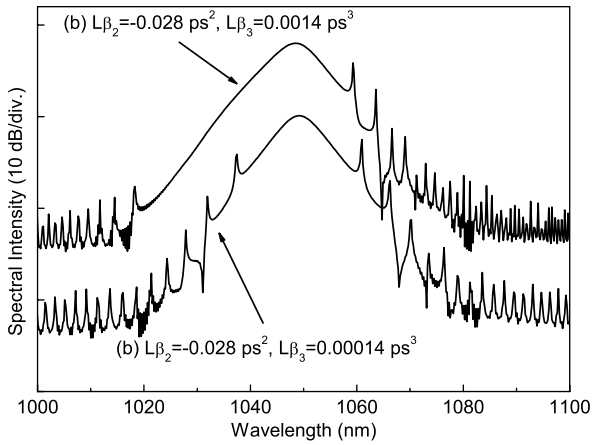

Fig. 5.15. *Simulated mode-locked spectra of a fiber laser for a low value of third-order dispersion (a) and with TOD corresponding to 30 cm of Yb-PBG fiber in the cavity(b).*

5.4 Discussion

The aim of my work presented in this chapter was to look for the best dispersion compensation method to be used in fiber lasers. The target was to find a solution that is easily applicable to mode-locked fiber lasers, minimizes the need for bulk optical components, provides a large and flat dispersion within a wide spectral bandwidth, and causes minimal insertion loss.

The requirements for dispersion compensation in fiber lasers and in bulk crystal solid-state (SS) lasers are different from each other. In comparison, a typical laser crystal is only a few millimeters or at most a centimeter long, whereas a fiber cavity is in lengths of several meters. The dispersive effects are very strong in fiber lasers due to such a long propagation length in the glass. Another difference is the fact that the conventional bulk optic dispersion compensators can rather easily be inserted in the free space cavity of a bulk crystal SS laser. In case of a fiber laser, some of the inherent advantages of the lasing medium are lost if bulk elements are used. In general, it is beneficial to maintain the all-fiber nature whenever possible.

Dispersion compensating fibers have been adopted as a basic solution for mode-locked erbium-doped fiber lasers operating at 1.5 μm wavelength range. Ultrashort pulse generation at the operation range of ytterbium- and neodymium-doped fibers is, however, problematic. As discussed earlier, the difficulty results from the high value of normal material dispersion of silica, which cannot be compensated by waveguide dispersion of standard DCFs. Table 5.1 summarizes the main characteristics of dispersion compensators available at 1.05$\pm$0.02 μm. Most of the parameter values shown in the table are taken from the configurations reported in the literature. In

Table 5.1. *Summary of the methods available for intracavity dispersion compensation at 1.05 μm range. The dispersion values for 5 mm of fused silica and for 1m of Hi1060 fiber are shown in order to illustrate the order of magnitude of dispersion compensation required in bulk crystal solid-state lasers and in fiber lasers, respectively. Insertion loss scale: Low — <0.5 dB, Moderate — 0.5–3 dB, High — >3 dB.*

	Cavity element	GDD [ps^2]	TOD [ps^3]	Insertion loss	Ref.
Bulk compensators	Prism pair, double pass, $l = 50$ cm	$-640{\cdot}10^{-6}$	$1.38{\cdot}10^{-6}$	Low	[113]
	Grating pair, double pass, 1200 lines/mm, $l = 1$ cm, $\beta = 55°$	-0.082	$0.23{\cdot}10^{-3}$	High	[117]
	Chirped mirror	$-45{\cdot}10^{-6}$	$56{\cdot}10^{-9}$	Low	[118]
	DCM	$-750{\cdot}10^{-6}$	Low, $\Delta\lambda \approx 40$ nm	Low	[168]
	Dielectric GTI	-0.050	Low, $\Delta\lambda \approx 2$ nm	Low	[129]
	D-SAM	$-400{\cdot}10^{-6}$	Low, $\Delta\lambda \approx 20$ nm	Low	[130]
	RSAM	-0.0030	$0.16{\cdot}10^{-3}$ *	Moderate	[146]
	Absorbing GTI	-0.55	High, $\Delta\lambda$<1 nm	High	[P1]
Fiber compensators	CFBG	-9.3	-1.43	-	[144]
		-0.25	-	High*	[169]
		-4.8	-	Low†	[170]
	Taper, $d_{waist} = 1.8$ μm, $l_{waist} = 20$ cm	-0.029	$0.03{\cdot}10^{-3}$ *	Low	[171]
	PCF, 1 m	-0.040	-	-	[20]
	Nd-PCF, 1 m	-0.015	$0.08{\cdot}10^{-3}$ *	-	[172]
	HC-PBGF, 1 m	-0.050	-	Moderate‡	[173]
		-0.072	$0.36{\cdot}10^{-3}$	Moderate‡	[174]
	SC-PBGF, 1 m	-0.085	$1.70{\cdot}10^{-3}$	Moderate‡	[175]
		-0.054	$1.40{\cdot}10^{-3}$	Moderate‡	[P4]
	Yb-PBGF, 1 m	-0.075	$2.30{\cdot}10^{-3}$	Moderate‡	[P5]
Fused silica, 5 mm		$85{\cdot}10^{-6}$	$0.21{\cdot}10^{-6}$		
Hi1060 fiber, 1 m		0.023	$0.04{\cdot}10^{-3}$		

* estimated from figure
* reflectivity 25 %, output-coupling 75 %
† reflectivity 97 %, output-coupling 3 %
‡ including splice losses

order to make it easier to assess the practicality of different techniques, the dispersion values for a 5-mm long bulk silica crystal and for a 1-m long piece of standard single-mode fiber are given at the bottom of the table.

The prism pair compensators have unpractically long separation (>1m) for a typical cavity of a fiber laser. Grating pairs offer higher dispersion resulted in a more realistic separation distance of about a centimeter. At the moment, they are most commonly used dispersion compensators in Yb-fiber laser. However, grating pairs are polarization dependent, lossy and difficult to align, which makes them less attractive for otherwise compact fiber lasers.

Although the dispersive dielectric (e.g. chirped) and semiconductor reflectors are discrete optical components, they can relatively easily be integrated in fiber lasers as cavity end mirrors. Still, they are mainly usable for dispersion compensation in solid-state lasers. Chirped mirrors and DCMs can provide anomalous dispersion over a large bandwidth ($\Delta\lambda$), however, they offer a compensation that is not sufficient for fiber cavities.

A dielectric GTI-based dispersion compensator has been successfully demonstrated also in a fiber laser [129]. An inherent problem, however, is the limited spectral bandwidth over which compensation is viable. The GDD introduced by GTI-mirrors is always accompanied by relatively high third and higher-order dispersion contributions, i.e. a constant GDD can be obtained only over a very limited wavelength range. Thus, GTI mirrors are useful for fiber cavities with length of a few tens of centimeters. This can be achieved using a gain fiber with a very high concentration of Yb-ions.

The GTI can be built either from dielectric or semiconductor material. Since the length of the semiconductor-based structure is limited to some micrometers, the semiconductor compensators such as the D-SAM (or RSAM) offer relatively low dispersion ($|\beta_2| \lesssim 0.01$ ps^2) [146]. The advantage of using a D-SAM structure is that it can provide both the high nonlinearity and dispersion needed for reliable generation of ultrashort optical pulses in mode-locked lasers.

Near-impedance matched absorbing semiconductor GTIs can have arbitrarily high dispersion values, but only at a price of very high losses and narrow bandwidths. In such a device, a small change in the level of absorption saturation can lead to a dramatic change of dispersion, even within the duration of an incident ultrashort pulse. Together with simultaneous collapse of resonance bandwidth, this may lead to interesting pulse shaping effects. Using a second pump pulse one could control the absorber characteristics to compensate dynamically for group-delay errors of ultrashort pulses. This could be used, for example, to accommodate environment-induced changes in the chromatic dispersion of the fiber.

Chirped fiber Bragg gratings commercially available generate the anomalous disper-

sion far above the value needed for a typical fiber laser. The amount of dispersion to be compensated in fiber lasers is approximately 100 times lower than that required for telecom applications. It is a very challenging task to fabricate highly reflective broadband gratings with such low dispersion. The small group-delay ripple and chirp linearity across the reflection band of the CFBG necessitates very fine control of the writing conditions. Nevertheless, compact all-fiber systems for a variety of operation regimes have been demonstrated recently [169, 170, 176, 177]. The problems with narrow bandwidth and too large values of anomalous dispersion still hinder CFBGs' applicability to sub-picosecond soliton fiber lasers. With advances in fabrication, they may still become a serious candidate for these systems as well.

Fiber tapers can offer high enough dispersion to compensate for about 1m of standard single-mode fiber at 1 μm. The low insertion loss and the small value of TOD are clear benefits of the technique. The increased nonlinearity due to the small core sizes may, however, limit their use in high power applications. With improvements in reliability and packaging, tapers have a clear potential for all-fiber dispersion compensation in short-cavity fiber lasers.

The amount of dispersion generated by the properly designed index-guiding PCFs is well suited for fiber lasers. The increased nonlinearity due to the small core sizes still limits their applicability. Photonic bandgap structures enable even greater freedom in tailoring the fiber parameters. For instance, in hollow-core PBG fibers the nonlinearities are practically avoided. Unfortunately, they suffer from poor matching with the standard fibers and, consequently, may generate high intracavity loss. Particularly in a mode-locked laser cavity, a hollow-core PBG fiber spliced with standard fiber could provide Fresnel back-reflection which affects badly the mode-lock starting capability and quality of the pulse operation. Thus, they are better suited for extracavity pulse stretching and compression. Good matching with the standard fiber can be achieved by using solid-core PBG fibers. Furthermore, SC-PBG fibers are all-solid structures that exhibit no surface modes and allow for high anomalous dispersion with reduced non-linear effects as compared with index-guiding PCFs. One major limitation to the pulse width and quality may still arise from the very high third-order dispersion generated in the SC-PBG fibers.

To date, SC-PBG fibers offer one of the most promising "all-fiber" alternatives to the bulk gratings used for intracavity dispersion compensation in short-wavelength fiber lasers. The possibility of using the ytterbium-doped PBG fiber simultaneously as the gain medium and the dispersion compensator gives additional value to the technique. It is clear that very compact femtosecond lasers can be realized using this approach. In general, PBG fiber systems have a great potential, but the technology is not fully matured yet and further improvements are still needed.

6. CONCLUSIONS

This dissertation presents results on ultrashort pulse generation in fiber lasers using semiconductor saturable absorbers and novel techniques for dispersion compensation. The main achievements of the work include:

Two promising approaches for semiconductor saturable absorbers were described. First, the reverse-biased saturable absorber mirror allows to adjust both the level of absorption saturation and the recovery time. The possibility to tune the absorber parameters electrically offers good mode-locking start-up capability together with enhanced picosecond pulse shaping in the same device.

In the second approach, a transmission-type saturable absorber was implemented in a ring cavity ytterbium fiber laser. With this geometry, the resonantly enhanced modulation depth of the absorber matches the high transmission low-loss regime. This allowed for reliable start-up of mode-locking without any additional wavelength-selective elements in the fiber cavity.

An absorptive semiconductor Gires-Tournois interferometer can also be used as an optically tunable delay line. The device can provide very high amounts of dispersion, but only at a cost of high loss and narrow spectral bandwidth. Due to these limitations, it was concluded that absorptive GTIs or other D-SAM-type devices are not particularly well suited for dispersion compensation in mode-locked fiber lasers. However, this type of component may find other applications as adaptive group-delay error compensators in high-speed all-optical signal regeneration or as optical delay lines in slow light experiments.

Two mode-locked soliton lasers utilizing novel solid-core photonic bandgap fiber were demonstrated. The first system confirms the capability of a photonic bandgap fiber to compensate for intracavity dispersion in fiber lasers. This kind of an all-fiber approach is advantageous due to its simplicity and robustness compared with the techniques that use free space optics such as grating pairs. In the second laser system, a solid-core ytterbium-doped photonic bandgap fiber is used as both the gain medium and the dispersion compensator, simultaneously. The integration of two functions in one cavity element allows

for compact, high repetition rate soliton fiber lasers operating at 1 μm. This approach represents a significant step towards a practical laser design.

I expect these results to be useful in realizing new reliable fiber sources for various applications where ultrashort laser pulses are needed.

BIBLIOGRAPHY

[1] I. Morita, K. Tanaka, N. Edagawa, and M. Suzuki, "40 Gb/s Single-Channel Soliton Transmission Over Transoceanic Distances by Reducing Gordon-Haus Timing Jitter and Soliton-Soliton Interaction," *IEEE J. Light. Tech.*, vol. 17, no. 12, p. 2506, Dec. 1999.

[2] W. Denk, J. Strickler, and W. Webb, "Two-photon laser scanning fluorescence microscopy," *Science*, vol. 248, no. 4951, pp. 73–76, 1990.

[3] H. Kano and H. Hamaguchi, "Characterization of a supercontinuum generated from a photonic crystal fiber and its application to coherent Raman spectroscopy," *Opt. Lett.*, vol. 28, no. 23, pp. 2360–2362, 2003.

[4] J. M. Schmitt, "Optical coherence tomography (OCT): a review," *IEEE Sel. Topics Quantum Electron.*, vol. 5, no. 4, pp. 1205–1215, 1999.

[5] N. Katzenellenbogen and D. Grischkowsky, "Efficient generation of 380 fs pulses of thz radiation by ultrafast laser pulse excitation of a biased metal-semiconductor interface," *Appl. Phys. Lett.*, vol. 58, no. 3, pp. 222–224, 1991.

[6] S. A. Diddams, D. J. Jones, J. Ye, S. T. Cundiff, J. L. Hall, J. K. Ranka, R. S. Windeler, R. Holzwarth, T. Udem, and T. W. Hänsch, "Direct link between microwave and optical frequencies with a 300 THz femtosecond laser comb," *Phys. Rev. Lett.*, vol. 84, no. 22, pp. 5102–5105, 2000.

[7] T. Udem, R. Holzwarth, and T. W. Hänsch, "Optical frequency metrology," *Nature*, vol. 416, pp. 233–237, Mar. 2002.

[8] X. Liu, D. Du, and G. Mourou, "Laser ablation and micromachining with ultrashort laser pulses," *IEEE J. Quantum Electron.*, vol. 33, no. 10, pp. 1706–1716, 1997.

[9] T. Juhasz, F. Loesel, R. Kurtz, J. Horvath, C. Bille, and G. Mourou, "Corneal refractive surgery with femtosecond lasers," *IEEE Sel. Topics Quantum Electron.*, vol. 5, no. 4, pp. 902–910, 1999.

[10] S. O. Konorov, V. P. Mitrokhin, A. B. Fedotov, D. A. Sidorov-Biryukov, V. I. Beloglazov, N. B. Skibina, A. V. Shcherbakov, E. Wintner, M. Scalora, and A. M. Zheltikov, "Laser ablation of dental tissues with picosecond pulses of 1.06-μm radiation transmitted through a hollow-core photonic-crystal fiber," *Appl. Opt.*, vol. 43, no. 11, pp. 2251–2256, 2004.

[11] K. Kim, Z. Guo, J. Li, and S. Kumar, "Radiation heat transfer in tissue welding and soldering with ultrafast lasers," in *Proc. 29th Annual IEEE Bioengineering Conf.*, Mar. 2003, pp. 185–186.

[12] W. Watanabe, N. Arakawa, S. Matsunaga, T. Higashi, K. Fukui, K. Isobe, and K. Itoh, "Femtosecond laser disruption of subcellular organelles in a living cell," *Opt. Express*, vol. 12, no. 18, pp. 4203–4213, 2004.

[13] G. Cheng, F. Shan, A. Freyer, and T. Guo, "Compact 50-Hz Terawatt Ti:Sapphire Laser for X-ray and Nonlinear Optical Spectroscopy," *Appl. Opt.*, vol. 41, no. 24, pp. 5148–5154, 2002.

[14] P. Russell, "Photonic crystal fibers," *Science*, vol. 299, no. 5605, pp. 358–362, 2003.

[15] T. A. Birks, J. C. Knight, and P. S. Russell, "Endlessly single-mode photonic crystal fiber," *Opt. Lett.*, vol. 22, no. 13, pp. 961–963, 1997.

[16] N. G. R. Broderick, T. M. Monro, P. J. Bennett, and D. J. Richardson, "Nonlinearity in holey optical fibers: measurement and future opportunities," *Opt. Lett.*, vol. 24, no. 20, pp. 1395–1397, 1999.

[17] D. G. Ouzounov, F. R. Ahmad, D. Müller, N. Venkataraman, M. T. Gallagher, M. G. Thomas, J. Silcox, K. W. Koch, and A. L. Gaeta, "Generation of megawatt optical solitons in hollow-core photonic band-gap fibers," *Science*, vol. 301, no. 5640, pp. 1702–1704, 2003.

[18] J. C. Knight, J. Arriaga, T. A. Birks, A. Ortigosa-Blanch, W. J. Wadsworth, and P. S. Russell, "Anomalous dispersion in photonic crystal fiber," *IEEE Photon. Technol. Lett.*, vol. 12, no. 7, pp. 807–809, 2000.

[19] J. K. Ranka, R. S. Windeler, and A. J. Stentz, "Visible continuum generation in air silica microstructure optical fibers with anomalous dispersion at 800nm," *Opt. Lett.*, vol. 25, no. 1, pp. 25–27, 2000.

[20] H. Lim, F. Ö. Ilday, and F. W. Wise, "Femtosecond ytterbium fiber laser with photonic crystal fiber for dispersion control," *Opt. Express*, vol. 10, no. 25, pp. 1497–1502, 2002.

[21] G. P. Agrawal, *Nonlinear fiber optics*, 3rd ed. San Diego, USA: Academic Press, 2001.

[22] M. Rusu, "Frequency conversion using ultrafast fiber lasers," Ph.D. dissertation, Tampere University of Technology, Tampere, Finland, 2006.

[23] U. Keller, "Recent developments in compact ultrafast lasers," *Nature*, vol. 424, pp. 831–838, Aug. 2003.

[24] O. Svelto, *Principles of Lasers*, 4th ed. New York, NY: Plenum Press, 1998.

[25] T. F. Carruthers and I. N. Duling III, "10-GHz, 1.3-ps erbium fiber laser employing soliton pulse shortening," *Opt. Lett.*, vol. 21, no. 23, pp. 1927–1929, 1996.

[26] M. Nakazawa and E. Yoshida, "A 40-GHz 850-fs regenaratively fm mode-locked polarization-maintaining erbium fiber ring laser," *IEEE Photon. Technol. Lett.*, vol. 12, no. 12, pp. 1613–1615, Dec. 2000.

[27] U. Keller, K. J. Weingarten, F. X. Kärtner, D. Kopf, B. Braun, I. D. Jung, R. Fluck, C. Honninger, N. Matuschek, and J. Aus der Au, "Semiconductor saturable absorber mirrors (SESAMs) for femtosecond to nanosecond pulse generation in solid-state lasers," *IEEE Sel. Topics Quantum Electron.*, vol. 2, no. 3, pp. 435–453, 1996.

[28] R. Herda, O. G. Okhotnikov, E. U. Rafailov, W. Sibbett, P. Crittenden, and A. Starodumov, "Semiconductor quantum-dot saturable absorber mode-locked fiber laser," *IEEE Photon. Technol. Lett.*, vol. 18, no. 1, pp. 157–159, Jan. 2006.

[29] S. Y. Set, H. Yaguchi, Y. Tanaka, and M. Jablonski, "Laser mode locking using a saturable absorber incorporating carbon nanotubes," *IEEE J. Light. Tech.*, vol. 22, no. 1, pp. 51–56, 2004.

[30] C. S. Goh, K. Kikuchi, S. Y. Set, D. Tanaka, T. Kotake, M. Jablonski, S. Yamashita, and T. Kobayashi, "Femtosecond mode-locking of a ytterbium-doped fiber laser using a carbon-nanotube-based mode-locker with ultra-wide absorption band," in *Proc. Conf. on Lasers and Electro-Optics (CLEO)*, Baltimore, USA, May 2005, p. CThG2.

[31] M. E. Fermann, L.-M. Yang, M. L. Stock, and M. J. Andrejco, "Environmentally stable kerr-type mode-locked erbium fiber laser producing 360-fs pulses," *Opt. Lett.*, vol. 19, no. 1, pp. 43–45, 1994.

[32] D. H. Sutter, G. Steinmeyer, L. Gallmann, N. Matuschek, F. Morier-Genoud, U. Keller, V. Scheuer, G. Angelow, and T. Tschudi, "Semiconductor saturable-absorber mirror-assisted kerr-lensmode-locked ti:sapphire laser producing pulses in the two-cycle regime," *Opt. Lett.*, vol. 24, no. 9, pp. 631–633, May 1999.

[33] L. F. Mollenauer and R. H. Stolen, "Soliton laser," *Opt. Lett.*, vol. 9, no. 1, pp. 13–15, 1984.

[34] M. Hofer, M. E. Fermann, F. Haberl, M. H. Ober, and A. J. Schmidt, "Mode locking with cross-phase and self-phase modulation," *Opt. Lett.*, vol. 16, no. 7, pp. 502–504, 1991.

[35] A. G. Bulushev, E. M. Dianov, and O. G. Okhotnikov, "Passive mode locking of a laser with a nonlinear fiber reflector," *Opt. Lett.*, vol. 15, no. 17, pp. 968–970, 1990.

[36] S. Tsuda, W. H. Knox, S. T. Cundiff, W. Y. Jan, and J. E. Cunningman, "Mode-locking ultrafast solid-state lasers with saturable bragg reflectors," *IEEE Sel. Topics Quantum Electron.*, vol. 2, no. 3, pp. 454–464, 1996.

[37] D. S. Chemla and D. A. B. Miller, "Room-temperature excitonic nonlinear-optical effects in semiconductor quantum-well structures," *J. Opt. Soc. Am. B*, vol. 2, no. 7, pp. 1155–1173, 1985.

[38] M. Guina, "Absorptive semiconductor reflectors for controlling dynamic properties of fiber lasers," Ph.D. dissertation, Tampere University of Technology, Tampere, Finland, 2002.

[39] R. Paschotta and U. Keller, "Passive mode locking with slow saturable absorbers," *Appl. Phys. B*, vol. 73, no. 7, pp. 653–662, 2001.

[40] R. Herda and O. Okhotnikov, "Dispersion compensation-free fiber laser mode-locked and stabilized by high-contrast saturable absorber mirror," *IEEE J. Quantum Electron.*, vol. 40, no. 7, pp. 893–899, July 2004.

[41] ——, "Semiconductor all-optical modulator for synchronization of independent fiber laser oscillators and active mode-locking," *IEEE J. Quantum Electron.*, vol. 41, no. 6, pp. 774–778, June 2005.

[42] C. Porzi, L. Poti, A. Bogoni, M. Guina, and O. Okhotnikov, "All-optical wavelength conversion in a vertical cavity semiconductor switch," in *Proc. SPIE, Optical Components and Materials III*, ser. Presented at the Society of Photo-Optical Instrumentation Engineers (SPIE) Conference, M. J. Digonnet and S. Jiang, Eds., vol. 6116, Mar. 2006, pp. 136–144.

[43] F. Koyama, "Recent advances of VCSEL photonics," *IEEE J. Light. Tech.*, vol. 24, no. 12, pp. 4502–4513, Dec. 2006.

[44] F. X. Kärtner, J. Aus der Au, and U. Keller, "Mode-locking with slow and fast saturable absorbers - what's the difference?" *IEEE Sel. Topics Quantum Electron.*, vol. 4, no. 2, pp. 159–168, Mar. 1998.

[45] N. Xiang, "Monolithic semiconductor saturable absorber mirrors for ultrashort optical pulse generation," Ph.D. dissertation, Tampere University of Technology, Tampere, Finland, 2003.

[46] R. Herda and O. G. Okhotnikov, "Effect of amplified spontaneous emission and absorber mirror recovery time on the dynamics of mode-locked fiber lasers," *Appl. Phys. Lett.*, vol. 86, no. 1, p. 011113, 2005.

[47] S. Schmitt-Rink, D. S. Chemla, and D. A. B. Miller, "Theory of transient excitonic optical nonlinearities in semiconductor quantum-well structures," *Phys. Rev. B*, vol. 32, no. 10, pp. 6601–6609, Nov 1985.

[48] Y.-C. Chen, P. Wang, J. J. Coleman, D. P. Bour, K. K. Lee, and R. G. Waters, "Carrier recombination rates in strained-layer InGaAs-GaAs quantumwells," *IEEE J. Quantum Electron.*, vol. 27, no. 6, pp. 1451–1455, June 1991.

[49] S. Marcinkevi$\hat{c}$ius, U. Olin, and G. Treideris, "Room temperature carrier recombination in InGaAs/GaAs quantum wells," *J. Appl. Phys.*, vol. 74, no. 5, pp. 3587–3589, Sept. 1993.

[50] S. Gupta, J. F. Whitaker, and G. A. Mourou, "Ultrafast carrier dynamics in III-V semiconductors grown by molecular-beam epitaxy at very low substrate temperatures," *IEEE J. Quantum Electron.*, vol. 28, no. 10, pp. 2464–2472, Oct. 1992.

[51] M. Haiml, U. Siegner, F. Morier-Genoud, U. Keller, M. Luysberg, P. Specht, and E. R. Weber, "Femtosecond response times and high optical nonlinearity in beryllium-doped low-temperature grown GaAs," *Appl. Phys. Lett.*, vol. 74, no. 9, pp. 1269–1271, 1999.

[52] S. Suomalainen, A. Vainionpää, O. Tengvall, T. Hakulinen, S. Karirinne, M. Guina, O. G. Okhotnikov, T. G. Euser, and W. L. Vos, "Long-wavelength fast semiconductor saturable absorber mirrors using metamorphic growth on GaAs substrates," *Appl. Phys. Lett.*, vol. 87, no. 12, p. 121106, 2005.

[53] J. T. Gopinath, E. R. Thoen, E. M. Koontz, M. E. Grein, L. A. Kolodziejski, E. P. Ippen, and J. P. Donnelly, "Recovery dynamics in proton-bombarded semiconductor saturable absorber mirrors," *Appl. Phys. Lett.*, vol. 78, no. 22, pp. 3409–3411, 2001.

[54] E. Lugagne Delpon, J. L. Oudar, N. Bouche, R. Raj, A. Shen, N. Stelmakh, and J. M. Lourtioz, "Ultrafast excitonic saturable absorption in ion-implanted InGaAs/InAlAs multiple quantum wells," *Appl. Phys. Lett.*, vol. 72, no. 7, pp. 759–761, 1998.

[55] V. D. S. Dhaka, N. V. Tkachenko, E.-M. Pavelescu, H. Lemmetyinen, T. Hakkarainen, M. Guina, J. Konttinen, O. Okhotnikov, M. Pessa, K. Arstila, and J. Keinonen, "Ni^{+}-irradiated InGaAs/GaAs quantum wells: picosecond carrier dynamics," *New J. Phys.*, vol. 7, p. 131, 2005.

[56] S. Suomalainen, M. Guina, T. Hakulinen, O. G. Okhotnikov, T. G. Euser, and S. Marcinkevicius, "1 μm saturable absorber with recovery time reduced by lattice mismatch," *Appl. Phys. Lett.*, vol. 89, no. 7, p. 071112, 2006.

[57] L. Joulaud, J. Mangeney, J.-M. Lourtioz, P. Crozat, and G. Patriarche, "Thermal stability of ion-irradiated InGaAs with (sub-) picosecond carrier lifetime," *Appl. Phys. Lett.*, vol. 82, no. 6, pp. 856–858, 2003.

[58] V. D. S. Dhaka, N. V. Tkachenko, H. Lemmetyinen, E.-M. Pavelescu, J. Konttinen, M. Pessa, K. Arstila, and J. Keinonen, "Room-temperature self-annealing of heavy-ion-irradiated InGaAs/GaAs quantum wells," *Electron. Lett.*, vol. 41, no. 23, pp. 1304–1305, Nov. 2005.

[59] H. Haus, "Theory of mode locking with a fast saturable absorber," *J. Appl. Phys.*, vol. 46, pp. 3049–3058, 1975.

[60] J. N. Kutz, B. C. Collings, K. Bergman, S. Tsuda, S. T. Cundiff, W. H. Knox, P. Holmes, and M. Weinstein, "Mode-locking pulse dynamics in a fiber laser with a saturable bragg reflector," *J. Opt. Soc. Am. B*, vol. 14, no. 10, pp. 2681–2690, Oct. 1997.

[61] B. E. A. Saleh and M. C. Teich, *Fundamentals of photonics*. USA: John Wiley & Sons, Inc., 1991.

[62] I. N. Duling III, "Subpicosecond all-fiber erbium laser," *Electron. Lett.*, vol. 27, pp. 544–545, 1991.

[63] F. X. Kärtner, D. Kopf, and U. Keller, "Solitary-pulse stabilization and shortening in actively mode-locked lasers," *J. Opt. Soc. Am. B*, vol. 12, pp. 486–496, 1995.

[64] L. E. Nelson, D. J. Jones, K. Tamura, H. A. Haus, and E. P. Ippen, "Ultrashort-pulse fiber ring lasers," *Applied Physics B: Lasers and Optics*, vol. 65, no. 2, pp. 277–294, Aug. 1997.

[65] S. M. J. Kelly, "Characteristic sideband instability of periodically amplified average soliton," *Electron. Lett.*, vol. 28, no. 8, pp. 806–808, Apr. 1992.

[66] M. L. Dennis and I. N. Duling III, "Experimental study of sideband generation in femtosecond fiber lasers," *IEEE J. Quantum Electron.*, vol. 30, no. 6, pp. 1459–1477, 1994.

[67] K. Tamura, L. E. Nelson, H. A. Haus, and E. P. Ippen, "Soliton versus non-soliton operation of fiber ring lasers," *Appl. Phys. Lett.*, vol. 64, pp. 149–151, 1994.

[68] D. Anderson, M. Desaix, M. Lisak, and M. L. Quiroga-Teixeiro, "Wave breaking in nonlinear-optical fibers," *J. Opt. Soc. Am. B*, vol. 9, pp. 1358–, 1992.

[69] K. Tamura, E. P. Ippen, H. A. Haus, and L. E. Nelson, "77-fs pulse generation from a stretched-pulse mode-locked all-fiber ring laser," *Opt. Lett.*, vol. 18, pp. 1080–1082, 1993.

[70] K. Tamura, E. P. Ippen, H. S. Haus, L. E. Nelson, and C. R. Doerr, "Stretched-pulse fiber laser," U.S. Patent 5 513 194, April, 1996. [Online]. Available: http://www.freepatentsonline.com/5513194.html

[71] N. J. Smith, N. J. Doran, W. Forysiak, and F. M. Knox, "Soliton transmission using periodic dispersion compensation," *IEEE J. Light. Tech.*, vol. 15, no. 10, pp. 1808–1822, 1997.

[72] L. F. Mollenauer and P. V. Mamyshev, "Massive wavelength-division multiplexing with solitons," *IEEE J. Quantum Electron.*, vol. 34, no. 11, pp. 2089–2102, 1998.

[73] P.-A. Bélanger, "On the profile of pulses generated by fiber lasers," *Opt. Express*, vol. 13, no. 20, pp. 8089–8096, 2005.

[74] F. Ö. Ilday, J. R. Buckley, H. Lim, F. W. Wise, and W. G. Clark, "Generation of 50-fs, 5-nj pulses at 1.03 μm from a wave-breaking-free fiber laser," *Opt. lett.*, vol. 28, no. 15, pp. 1365–1367, Aug. 2003.

[75] F. O. Ilday, J. R. Buckley, F. W. Wise, and W. G. Clark, "Self-similar evolution of parabolic pulses in a laser," *Phys. Rev. Lett.*, vol. 92, no. 21, p. 213902, May 2004.

[76] L. E. Nelson, S. B. Fleischer, G. Lenz, and E. P. Ippen, "Efficient frequency doubling of a femtosecond fiber laser," *Opt. Lett.*, vol. 21, no. 21, pp. 1759–1761, 1996.

[77] L. Lefort, J. H. V. Price, D. J. Richardson, G. J. Spüler, R. Paschotta, U. Keller, A. R. Fry, and J. Weston, "Practical low-noise stretched-pulse Yb^{3+}-doped fiber laser," *Opt. Lett.*, vol. 27, no. 5, pp. 291–293, 2002.

[78] H. Lim, F. Ö. Ilday, and F. W. Wise, "Generation of 2 nJ pulses from a femtosecond ytterbium fiber laser," *Opt. Lett.*, vol. 28, no. 8, pp. 660–662, 2003.

[79] M. Guina, N. Xiang, A. Vainionpää, and O. G. Okhotnikov, "Self-starting stretched-pulse fiber laser mode-locked and stabilized with slow and fast semiconductor saturable absorbers," *Opt. Lett.*, vol. 26, no. 22, pp. 1809–1811, Nov. 2001.

[80] B. Resan, L. Archundia, and P. Delfyett, "Experimental characterization and numerical simulations of dispersion-managed breathing-mode semiconductor mode-locked ring laser," in *Proc. Lasers and Electro-Optics Society, 2003. LEOS 2003. The 16th Annual Meeting of the IEEE*, vol. 2, Oct. 2003, pp. 559–560.

[81] P. Maine, D. Strickland, P. Bado, M. Pessot, and G. Mourou, "Generation of ultrahigh peak power pulses by chirped pulse amplification," *IEEE J. Quantum Electron.*, vol. QE-24, pp. 398–403, Feb. 1988.

[82] P. A. Bélanger, L. Gagnon, and C. Paré, "Solitary pulses in an amplified nonlinear dispersive medium," *Opt. Lett.*, vol. 14, no. 17, pp. 943–945, 1989.

[83] D. Anderson, M. Desaix, M. Karlsson, M. Lisak, and M. L. Quiroga-Teixeiro, "Wave-breaking-free pulses in nonlinear-optical fibers," *J. Opt. Soc. Am. B*, vol. 10, no. 7, pp. 1185–1190, July 1993.

[84] M. E. Fermann, V. I. Kruglov, B. C. Thomsen, J. M. Dudley, and J. D. Harvey, "Self-similar propagation and amplification of parabolic pulses in optical fibers," *Phys. Rev. Lett.*, vol. 84, no. 26, pp. 6010–6013, June 2000.

[85] J. Limpert, T. Schreiber, T. Clausnitzer, K. Zöllner, H. Fuchs, E. Kley, H. Zellmer, and A. Tünnermann, "High-power femtosecond Yb-doped fiber amplifier," *Opt. Express*, vol. 10, no. 14, pp. 628–638, 2002.

[86] C. Nielsen, B. Ortaç, T. Schreiber, J. Limpert, R. Hohmuth, W. Richter, and A. Tünnermann, "Self-starting self-similar all-polarization maintaining Yb-doped fiber laser," *Opt. Express*, vol. 13, no. 23, pp. 9346–9351, 2005.

[87] L. M. Zhao, D. Y. Tang, and J. Wu, "Gain-guided solitons in a positive group-dispersion fiber laser," *Opt. Lett.*, vol. 31, no. 12, pp. 1788–1790, 2006.

[88] C. Finot, F. Parmigiani, P. Petropoulos, and D. Richardson, "Parabolic pulse evolution in normally dispersive fiber amplifiers preceding the similariton formation regime," *Opt. Express*, vol. 17, no. 8, pp. 3161–3170, 2006.

[89] T. Schreiber, B. Ortaç, J. Limpert, and A. Tünnermann, "On the study of pulse evolution in ultra-short pulse mode-locked fiber lasersby numerical simulations," *Opt. Express*, vol. 15, no. 13, pp. 8252–8262, 2007.

[90] B. Ortaç, A. Hideur, M. Brunel, C. Chédot, J. Limpert, A. Tünnermann, and F. Ö. Ilday, "Generation of parabolic bound pulses from a Yb-fiber laser," *Opt. Express*, vol. 14, no. 13, pp. 6075–6083, 2006.

[91] J. R. Buckley, F. W. Wise, F. Ö. Ilday, and T. Sosnowski, "Femtosecond fiber lasers with pulse energies above 10 nJ," *Opt. Lett.*, vol. 30, no. 14, pp. 1888–1890, 2005.

[92] V. L. Kalashnikov, E. Podivilov, A. Chernykh, S. Naumov, A. Fernandez, R. Graf, and A. Apolonski, "Approaching the microjoule frontier with femtosecond laser oscillators: theory and comparison with experiment," *New J. Phys.*, vol. 7, p. 217, 2005. [Online]. Available: http://stacks.iop.org/1367-2630/7/217

[93] L. M. Zhao, D. Y. Tang, T. H. Cheng, and C. Lu, "Gain-guided solitons in dispersion-managed fiber lasers with large net cavity dispersion," *Opt. Lett.*, vol. 31, no. 20, pp. 2957–2959, 2006.

[94] S. Naumov, A. Fernandez, R. Graf, P. Dombi, F. Krausz, and A. Apolonski, "Approaching the microjoule frontier with femtosecond laser oscillators," *New J. Phys.*, vol. 7, p. 216, 2005. [Online]. Available: http://stacks.iop.org/1367-2630/7/216

[95] A. Chong, J. Buckley, W. Renninger, and F. Wise, "All-normal-dispersion femtosecond fiber laser," *Opt. Express*, vol. 14, no. 21, pp. 10 095–10 100, 2006.

[96] J. W. Lou, M. Currie, and F. K. Fatemi, "Experimental measurements of solitary pulse characteristics from an all-normal-dispersion yb-doped fiber laser," *Opt. Express*, vol. 15, no. 8, pp. 4960–4965, 2007.

[97] B. Ortaç, O. Schmidt, T. Schreiber, J. Limpert, A. Tünnermann, and A. Hideur, "High-energy femtosecond yb-doped dispersion compensation free fiber laser," *Opt. Express*, vol. 15, no. 17, pp. 10 725–10 732, 2007.

[98] A. M. Fox, M. D. A. B., G. Livescu, J. E. Cunningham, and W. Y. Jan, "Quantum well carrier sweep out: relation to electroabsorption and exciton saturation," *IEEE J. Quantum Electron.*, vol. 27, no. 10, pp. 2281–2295, 1991.

[99] J. R. Karin, R. J. Helkey, D. J. Derickson, R. Nagarajan, D. S. Allin, J. E. Bowers, and R. L. Thornton, "Ultrafast dynamics in field-enhanced saturable absorbers," *Appl. Phys. Lett.*, vol. 64, no. 6, pp. 676–678, 1994.

[100] E. P. Burr, J. Song, A. J. Seeds, and C. C. Button, "60 ps recovery time in an InGaAsP quaternary multiple quantum well saturable absorber employing carrier sweep-out," in *Proc. Conf. on Lasers and Electro-Optics Europe (CLEO Europe)*, Nice, France, Sept. 2000, p. CTuD2.

[101] Y.-K. Chen and M. C. Wu, "Monolithic colliding-pulse mode-locked quantum-well lasers," *IEEE J. Quantum Electron.*, vol. 28, no. 10, pp. 2176–2185, 1992.

[102] D. J. Derickson, R. J. Helkey, A. Mar, J. R. Karin, J. G. Wasserbauer, and J. E. Bowers, "Short pulse generation using multisegment mode-locked semiconductor lasers," *IEEE J. Quantum Electron.*, vol. 28, no. 10, pp. 2186–2202, 1992.

[103] J. F. Martins-Filho, E. A. Avrutin, C. N. Ironside, and J. S. Roberts, "Monolithic multiple colliding pulse mode-locked quantum-well lasers: experiment and theory," *IEEE Sel. Topics Quantum Electron.*, vol. 1, no. 2, pp. 539–551, 1995.

[104] I. Ogura, Y. Hashimoto, H. Kurita, T. Shimizu, and H. Yokoyama, "Picosecond all-optical gate using a saturable absorber in mode-locked laser diodes," *IEEE Photon. Technol. Lett.*, vol. 10, no. 4, pp. 603–605, 1998.

[105] S. Hojfeldt, F. Romstad, and J. Mork, "Absorption recovery in strongly saturated quantum-well electroabsorption modulators," *IEEE Photon. Technol. Lett.*, vol. 15, no. 5, pp. 676–678, 2003.

[106] K. Jasim, Q. Zhang, A. V. Nurmikko, E. Ippen, A. Mooradian, G. Carey, and W. Ha, "Picosecond pulse generation from passively modelocked vertical cavity diode laser at up to 15 GHz pulse repetition rate," *Electron. Lett.*, vol. 40, no. 1, pp. 34–36, 2004.

[107] Q. Zhang, K. Jasim, A. V. Nurmikko, E. Ippen, A. Mooradian, G. Carey, and W. Ha, "Characteristics of a high-speed passively mode-locked surface-emitting semiconductor InGaAs laser diode," *IEEE Photon. Technol. Lett.*, vol. 17, no. 3, pp. 525–527, 2005.

[108] B. Stormont, E. U. Rafailov, I. G. Cormack, A. Mooradian, and W. Sibbett, "Extended-cavity surface-emitting diode laser as active mirror controlling modelocked Ti:sapphire laser," *Electron. Lett.*, vol. 40, no. 12, pp. 732–734, 2004.

[109] A. A. Lagatsky, E. U. Rafailov, W. Sibbett, D. A. Livshits, A. E. Zhukov, and V. M. Ustinov, "Quantum-dot-based saturable absorber with p-n junction for mode-locking of solid-state lasers," *IEEE Photon. Technol. Lett.*, vol. 17, no. 2, pp. 294–296, 2005.

[110] D. A. B. Miller, D. S. Chemla, T. C. Damen, A. C. Gossard, W. Wiegmann, T. H. Wood, and C. A. Burrus, "Band-edge electroabsorption in quantum well structures: The quantum-confined stark effect," *Phys. Rev. Lett.*, vol. 53, no. 22, pp. 2173–2176, Nov 1984.

[111] A. Miller, D. T. Reid, and D. M. Finlayson (ed.), *Ultrafast photonics*. Bristol, UK: SUSSP Publications & Institute of Physics, 2004.

[112] N. Xiang, O. G. Okhotnikov, A. Vainionpää, M. Guina, and M. Pessa, "Broadband semiconductor saturable absorber mirror at 1.55 μm using Burstein-Moss shifted $Ga_{0.47}In_{0.53}As$/ InP distributed Bragg reflector," *Electron. Lett.*, vol. 37, no. 6, pp. 374–375, 2001.

[113] R. L. Fork, O. E. Martinez, and J. P. Gordon, "Negative dispersion using pairs of prisms," *Opt. Lett.*, vol. 9, no. 5, pp. 150–152, 1984.

[114] J. D. Kafka and T. Baer, "Prism-pair dispersive delay lines in optical pulse compression," *Opt. Lett.*, vol. 12, no. 6, pp. 401–403, 1987.

[115] R. L. Fork, C. H. B. Cruz, P. C. Becker, and C. V. Shank, "Compression of optical pulses to six femtoseconds by using cubic phase compensation," *Opt. Lett.*, vol. 12, no. 7, pp. 483–485, 1987.

[116] J. R. Buckley, S. W. Clark, and F. W. Wise, "Generation of ten-cycle pulses from an ytterbium fiber laser with cubic phase compensation," *Opt. Lett.*, vol. 31, no. 9, pp. 1340–1342, 2006.

[117] E. B. Treacy, "Optical pulse compression with diffraction gratings," *IEEE J. Quantum Electron.*, vol. QE-5, pp. 454–458, 1969.

[118] R. Szipöcs, K. Ferencz, C. Spielmann, and F. Krausz, "Chirped multilayer coatings for broadband dispersion control in femtosecond lasers," *Opt. Lett.*, vol. 19, no. 8, pp. 201–203, 1994.

[119] A. Stingl, M. Lenzner, C. Spielmann, F. Krausz, and R. Szipöcs, "Sub-10-fs mirror-dispersion-controlled Ti:sapphire laser," *Opt. Lett.*, vol. 20, pp. 602–604, 1995.

[120] F. Gires and P. Tournois, "Interféromètre utilisable pour la compression d'impulsions lumineuses modulées en fréquence," *C. R. Acad. Sci.*, vol. 258, pp. 6112–6115, 1964.

[121] J. Kuhl and J. Heppner, "Compression of femtosecond optical pulses with dielectric multilayer interferometers," *IEEE J. Quantum Electron.*, vol. QE-22, no. 1, pp. 182–185, 1986.

[122] K. D. Li, W. H. Knox, and N. M. Pearson, "Broadband cubic-phase compensation with resonant Gires-Tournois interferometers," *Opt. Lett.*, vol. 14, no. 9, pp. 450–452, 1989.

[123] L. J. Cimini, Jr., L. J. Greenstein, and A. A. M. Saleh, "Optical equalization to combat the effects of laser chirp and fiber dispersion," *IEEE J. Light. Tech.*, vol. 8, no. 5, pp. 649–659, 1990.

[124] M. Beck, I. A. Walmsley, and J. D. Kafka, "Group delay measurements of optical components near 800 nm," *IEEE J. Quantum Electron.*, vol. 27, no. 8, pp. 2074–2081, 1991.

[125] A. H. Gnauck, C. R. Giles, L. J. Cimini, Jr., J. Stokes, L. W. Stulz, S. K. Korotky, and J. J. Veselka, "8-Gb/s–130 km Transmission Experiment Using Er-doped Fiber Preamplifier and Optical Dispersion Equalization," *IEEE Photon. Technol. Lett.*, vol. 3, no. 12, pp. 1147–1149, 1991.

[126] N. U. Wetter, E. P. Maldonado, and N. D. V. Jr., "Calculations for Broadband Intracavity Chirp Compensation with Thin-Film Gires-Tournois Interferometers," *Revista de Física Aplicada e Instrumentação*, vol. 13, no. 2, pp. 31–33, 1998.

[127] M. Jablonski, Y. Tanaka, H. Yaguchi, K. Furuki, K. Sato, N. Higashi, and K. Kikuchi, "Entirely thin-film allpass coupled-cavity filters in a parallel configuration for adjustable dispersion-slope compensation," *IEEE Photon. Technol. Lett.*, vol. 13, no. 11, pp. 1188–1190, 2001.

[128] M. Hacker, G. Stobrawa, and R. Sauerbrey, "Femtosecond-pulse sequence compression by Gires-Tournois interferometers," *Opt. Lett.*, vol. 28, no. 3, pp. 209–211, 2003.

[129] L. Orsila, L. A. Gomes, N. Xiang, T. Jouhti, and O. G. Okhotnikov, "Modelocked ytterbium fiber lasers," *Appl. Opt.*, vol. 43, no. 9, pp. 1902–1906, Mar. 2004.

[130] D. Kopf, G. Zhang, R. Fluck, M. Moser, and U. Keller, "All-in-one dispersion-compensating saturable absorber mirror for compact femtosecond laser sources," *Opt. Lett.*, vol. 21, no. 7, pp. 486–488, 1996.

[131] C. Lin, H. Kogelnik, and L. G. Cohen, "Optical-pulse equalization of low-dispersion transmission in single-mode fibers in the 1.3–1.7-μm spectral region," *Opt. Lett.*, vol. 5, no. 11, pp. 476–478, 1980.

[132] A. Pizzinat, A. Schiffini, F. Alberti, A. Paoletti, D. Caccioli, P. Griggio, P. Minzioni, and F. Matera, "Numerical and Experimental Comparison of Dis-

persion Compensation Techniques on Different Fibers," *IEEE Photon. Technol. Lett.*, vol. 14, no. 10, pp. 1415–1417, 2002.

[133] L. G. Cohen, C. Lin, and W. G. French, "Tailoring zero chromatic dispersion into the 1.5–1.6 μ-m low-loss spectral region of single mode fibers," *Electron. Lett.*, vol. 15, no. 12, pp. 334–335, 1979.

[134] A. H. Gnauck, L. D. Garrett, Y. Danziger, U. Levy, and M. Tur, "Dispersion and dispersion-slope compensation of NZDSF over the entire C band using higher-order-mode fibre," *Opt. Lett.*, vol. 36, no. 23, pp. 1946–1947, 2000.

[135] S. Ramachandran, S. Ghalmi, J. W. Nicholson, M. F. Yan, P. Wisk, E. Monberg, and F. V. Dimarcello, "Demonstration of anomalous dispersion in a solid, silica-based fiber at λ<1300 nm," in *Proc. Optical Fiber Communication Conf. (OFC)*, Anaheim, USA, Mar. 2006, p. PDP3.

[136] D. Mogilevtsev, T. A. Birks, and P. S. J. Russell, "Group-velocity dispersion in photonic crystal fibers," *Opt. Lett.*, vol. 23, no. 21, pp. 1662–1664, 1998.

[137] A. Ferrando, E. Silvestre, J. J. Miret, J. A. Monsoriu, M. V. Andres, and P. S. Russell, "Designing a photonic crystal fibre with flattened chromatic dispersion," *Electron. Lett.*, vol. 35, no. 4, pp. 325–327, 1999.

[138] T. A. Birks, D. Mogilevtsev, J. C. Knight, and P. S. Russell, "Dispersion compensation using single material fibers," *IEEE Photon. Technol. Lett.*, vol. 11, no. 6, pp. 674–676, 1999.

[139] J. C. Knight, "Photonic crystal fibres," *Nature*, vol. 424, pp. 847–851, 2003.

[140] F. Ouellette, "Dispersion cancellation using linearly chirped Bragg grating filters in optical waveguides," *Opt. Lett.*, vol. 12, no. 10, pp. 847–849, 1987.

[141] L. Dong, M. Cole, A. Ellis, R. Laming, and T. Widdowson, "40 Gbit/s 1.55 μm RZ transmission over 109 km of non-dispersion shifted fibre with long continuously chirped fibre gratings," *Electron. Lett.*, vol. 33, no. 18, pp. 1563–1565, 1997.

[142] A. Gnauck, L. Garrett, F. Forghieri, V. Gusmeroli, and D. Scarano, "8$\times$20 Gb/s 315-km, 8$\times$10 Gb/s 480-km WDM transmission over conventional fiber using multiple broad-band fiber gratings," *IEEE Photon. Technol. Lett.*, vol. 10, no. 10, pp. 1495–1497, 1998.

[143] B. Eggleton, B. Mikkelsen, G. Raybon, A. Ahuja, J. A. Rogers, P. S. Westbrook, T. N. Nielsen, S. Stulz, and K. Dreyer, "Tunable dispersion compensation in a 160-Gb/s TDM system by a voltage controlled chirped fiber Bragg grating," *IEEE Photon. Technol. Lett.*, vol. 12, no. 8, pp. 1022–1024, 2000.

[144] M. Hofer, M. H. Ober, R. Hofer, M. E. Fermann, G. Sucha, D. Harter, K. Sugden, I. Bennion, C. A. C. Mendonca, and T. H. Chiu, "High-power neodymium soliton fiber laser that uses a chirped fiber grating," *Opt. Lett.*, vol. 20, no. 16, pp. 1701–1703, Aug. 1995.

[145] M. N. Zervas and D. Taverner, "Asymmetrically apodised linearly-chirped fibre Bragg gratings with improved dispersion characteristics," in *Proc. ECOC'98*, Madrid, Spain, Sept. 1998, pp. 417–418.

[146] M. Moenster, U. Griebner, W. Richter, and G. Steinmeyer, "Resonant saturable absorber mirrors for dispersion control in ultrafast lasers," *IEEE J. Quantum Electron.*, vol. 43, no. 2, pp. 174–181, 2007.

[147] F. J. Fraile-Peláez and P. Chamorro-Posada, "Active control and stability in microring resonator chains," *Opt. Express*, vol. 15, no. 6, pp. 3177–3189, 2007.

[148] E. Garmire, "Criteria for Optical Bistability in a Lossy Saturating Fabry-Perot," *IEEE J. Quantum Electron.*, vol. 25, no. 3, pp. 289–295, 1989.

[149] J. F. Heffernan, M. H. Moloney, J. Hegarty, J. S. Roberts, and M. Whitehead, "All optical, high contrast absorptive modulation in an asymmetric Fabry-Perot étalon," *Appl. Phys. Lett.*, vol. 58, no. 25, pp. 2877–2879, 1991.

[150] H. S. Loka and P. W. E. Smith, "Ultrafast All-Optical Switching with an Asymmetric Fabry-Pérot Device Using Low-Temperature-Grown GaAS: Material and Device Issues," *IEEE J. Quantum Electron.*, vol. 36, no. 1, pp. 100–111, 2000.

[151] R. Scarmozzino, A. Gopinath, R. Pregla, and S. Helfert, "Numerical techniques for modeling guided-wave photonic devices," *IEEE Sel. Topics Quantum Electron.*, vol. 6, no. 1, pp. 150–162, 2000.

[152] N. M. Litchinitser, A. K. Abeeluck, C. Headley, and B. J. Eggleton, "Antiresonant reflecting photonic crystal optical waveguides," *Opt. Lett.*, vol. 27, no. 18, pp. 1592–1594, 2002.

[153] P. Steinvurzel, B. Kuhlmey, T. White, M. Steel, C. de Sterke, and B. Eggleton, "Long wavelength anti-resonant guidance in high index inclusion microstructured fibers," *Opt. Express*, vol. 12, no. 22, pp. 5424–5433, 2004.

[154] T. P. White, B. T. Kuhlmey, R. C. McPhedran, D. Maystre, G. Renversez, C. M. de Sterke, and L. C. Botten, "Multipole method for microstructured optical fibers. I. Formulation," *J. Opt. Soc. Am. B*, vol. 19, no. 10, pp. 2322–2330, 2002.

[155] B. T. Kuhlmey, T. P. White, G. Renversez, D. Maystre, L. C. Botten, C. M. de Sterke, and R. C. McPhedran, "Multipole method for microstructured optical fibers. II. Implementation and results," *J. Opt. Soc. Am. B*, vol. 19, no. 10, pp. 2331–2340, 2002.

[156] P. Yeh, A. Yariv, and E. Marom, "Theory of Bragg fiber," *J. Opt. Soc. Am. B*, vol. 68, no. 9, pp. 1196–1201, 1978.

[157] M. A. Duguay, Y. Kokubun, T. L. Koch, and L. Pfeiffer, "Antiresonant reflecting optical waveguides in SiO_2-Si multilayer structures," *Appl. Phys. Lett.*, vol. 49, no. 1, pp. 13–15, 1986.

[158] T. Baba and Y. Kokubun, "Dispersion and radiation loss characteristics of antiresonant reflecting optical waveguides - Numerical results and analytical expressions," *IEEE J. Quantum Electron.*, vol. 28, no. 7, pp. 1689–1700, 1992.

[159] N. M. Litchinitser, A. K. Abeeluck, C. Headley, and B. J. Eggleton, "Antiresonant reflecting photonic crystal optical waveguides," *Opt. Lett.*, vol. 27, no. 18, pp. 1977–1979, 2002.

[160] F. Luan, A. K. George, T. D. Hedley, G. J. Pearce, D. M. Bird, J. C. Knight, and P. S. J. Russell, "All-solid photonic bandgap fiber," *Opt. Lett.*, vol. 29, no. 20, pp. 2369–2371, 2004.

[161] A. Argyros, T. A. Birks, S. G. Leon-Saval, C. M. B. Cordeiro, and P. S. J. Russell, "Guidance properties of low-contrast photonic bandgap fibres," *Opt. Express*, vol. 13, no. 7, pp. 2503–2511, 2005.

[162] J. West, C. Smith, N. Borrelli, D. Allan, and K. Koch, "Surface modes in air-core photonic band-gap fibers," *Opt. Express*, vol. 12, no. 8, pp. 1485–1496, 2004.

[163] J. Broeng, T. Søndergaard, S. E. Barkou, P. M. Barbeito, and A. Bjarklev, "Waveguidance by the photonic bandgap effect in optical fibres," *J. Opt. A: Pure Appl. Opt.*, vol. 1, no. 4, pp. 477–482, 1999.

[164] S. Johnson, M. Ibanescu, M. Skorobogatiy, O. Weisberg, T. Engeness, M. Soljacic, S. Jacobs, J. Joannopoulos, and Y. Fink, "Low-loss asymptotically single-mode propagation in large-core OmniGuide fibers," *Opt. Express*, vol. 9, no. 13, pp. 748–779, 2001.

[165] A. Fuerbach, P. Steinvurzel, J. Bolger, and B. Eggleton, "Nonlinear pulse propagation at zero dispersion wavelength in anti-resonant photonic crystal fibers," *Opt. Express*, vol. 13, no. 8, pp. 2977–2987, 2005.

[166] J. Jasapara, T. H. Her, R. Bise, R. Windeler, and D. J. DiGiovanni, "Group-velocity dispersion measurements in a photonic bandgap fiber," *J. Opt. Soc. Am. B*, vol. 20, no. 8, pp. 1611–1615, 2003.

[167] A. Wang, A. K. George, and J. C. Knight, "Three-level neodymium fiber laser incorporating photonic bandgap fiber," *Opt. Lett.*, vol. 31, no. 10, pp. 1388–1390, 2006.

[168] R. Paschotta, G. J. Spühler, D. H. Sutter, N. Matuschek, U. Keller, M. Moser, R. Hövel, V. Scheuer, G. Angelow, and T. Tschudi, "Double-chirped semiconductor mirror for dispersion compensation in femtosecond lasers," *Appl. Phys. Lett.*, vol. 75, no. 15, pp. 2166–2168, Oct. 1999.

[169] I. Hartl, G. Imeshev, L. Dong, G. C. Cho, and M. E. Fermann, "Ultra-compact dispersion compensated femtosecond fiber oscillators and amplifiers," in *Proc. Conf. on Lasers and Electro-Optics (CLEO)*, Baltimore, USA, May 2005, p. CThG1.

[170] O. Katz, Y. Sintov, Y. Nafcha, and Y. Glick, "Passively mode-locked ytterbium fiber laser utilizing chirped-fiber-bragg-gratings for dispersion control," *Opt. Communications*, vol. 269, no. 1, pp. 156–165, 2007.

[171] M. Rusu, R. Herda, S. Kivistö, and O. G. Okhotnikov, "Fiber taper for dispersion management in a mode-locked ytterbium fiber laser," *Opt. Lett.*, vol. 31, no. 15, pp. 2257–2259, Aug. 2006.

[172] M. Moenster, P. Glas, R. Iliew, R. Wedell, and G. Steinmeyer, "Microstructure fiber soliton laser," *IEEE Photon. Technol. Lett.*, vol. 18, no. 23, pp. 2502–2504, 2006.

[173] H. Lim and F. W. Wise, "Control of dispersion in a femtosecond ytterbium laser by use of hollow-core photonic bandgap fiber," *Opt. Express*, vol. 12, no. 10, pp. 2231–2235, 2004.

[174] Crystal Fibre A/S, [Online; accessed 14-April-2007]. [Online]. Available: http://www.crystal-fibre.com/datasheets/HC-1060-02.pdf

[175] C. K. Nielsen, K. G. Jespersen, and S. R. Keiding, "A 158 fs 5.3 nJ fiber-laser system at 1 μm using photonic bandgap fibers for dispersion control and pulse compression," *Opt. Express*, vol. 14, no. 13, pp. 6063–6068, 2006.

[176] M. Plötner, B. Ortaç, R. Kinney, T. Schreiber, J. Limpert, and A. Tünnermann, "Self-starting wave-breaking-free environmentally stable Yb-doped all-fiber laser," in *Proc. Conf. on Lasers and Electro-Optics Europe (CLEO Europe)*, Münich, Germany, June 2007, pp. CJ–1872.

[177] O. Katz and Y. Sintov, "Strictly all-fiber picosecond ytterbium fiber laser utilizing chirped-fiber-bragg-gratings for dispersion control," *Opt. Communications*, 2007, to be published.

[178] E. Hecht, *Optics*, 3rd ed. Massachusetts: Addison-Wesley, 1998.

APPENDIX A: REFLECTIVITY AND GROUP DELAY OF AN ABSORBING GTI

The derivation of amplitude (Eq. 5.2) and phase (Eq. 5.3) response of an absorbing GTI is presented in this appendix. The procedure follows the Stokes notation used for example in [178].

The incoming field is denoted as $E_0 e^{i\omega t}$, where E_0 is the amplitude of the field and ω is the optical frequency. The top mirror amplitude-transmission coefficients are represented by t for the amplitude of a wave transmitted into the GTI and t' for the amplitude leaving the structure. The external and internal amplitude-reflectivity coefficients are r and r', respectively. They are related as $r = -r'$, where the minus sign indicates a phase change by π. In addition we can write $tt' = 1 - r^2$. The round-trip amplitude-attenuation in the resonator is represented by a.

Following the illustration in Fig. A.1 the components of the reflected field can be

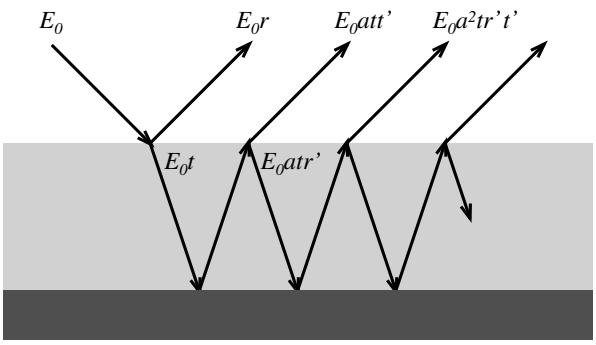

Fig. A.1. *Origin of the reflected field components in an absorbing GTI.*

written as

$$\begin{aligned}
\tilde{E}_{1r} &= E_0 r e^{i\omega t} \\
\tilde{E}_{2r} &= E_0 a t t' e^{i(\omega t - \delta)} \\
\tilde{E}_{3r} &= E_0 a^2 t r' t' e^{i(\omega t - 2\delta)} \\
\tilde{E}_{4r} &= E_0 a^3 t r'^2 t' e^{i(\omega t - 3\delta)} \\
&\vdots \\
\tilde{E}_{Nr} &= E_0 a^{N-1} t r'^{N-2} t' e^{i(\omega t - (N-1)\delta)}.
\end{aligned}$$

The phase change between adjacent field components $\delta = \varphi - \omega t_0$, where t_0 is the round-trip time of the cavity. The phase change φ on the back mirror is let be a free variable. Typically it is also set equal to π.

The total reflected field is

$$\begin{aligned}
\tilde{E}_r &= \tilde{E}_{1r} + \tilde{E}_{2r} + \tilde{E}_{3r} + \cdots + \tilde{E}_{Nr} + \ldots \\
&= E_0 e^{i\omega t} \left[r + a t t' e^{-i\delta} + a^2 t r' t' e^{-i2\delta} + \ldots \right] \\
&= E_0 e^{i\omega t} \left[r + a t t' e^{-i\delta} (1 + a r' e^{-i\delta} + a^2 r'^2 e^{-i2\delta} + \ldots) \right].
\end{aligned}$$

The geometric series in parentheses converges to the finite sum $1/(1 - a r' e^{-i\delta})$. Thus, $\tilde{E}_r$ reduces to form

$$\begin{aligned}
\tilde{E}_r &= E_0 e^{i\omega t} \left[r + \frac{a t t' e^{-i\delta}}{1 - a r' e^{-i\delta}} \right] \\
&= E_0 e^{i\omega t} \left[r + \frac{a(1 - r^2) e^{-i\delta}}{1 + a r e^{-i\delta}} \right] \\
&= E_0 e^{i\omega t} \left[\frac{r + a e^{-i\delta}}{1 + a r e^{-i\delta}} \right],
\end{aligned}$$

where also the relations $r' = -r$ and $t t' = 1 - r^2$ are used. The term in square brackets is the transfer function Ψ of an absorbing GTI.

The amplitude and phase variations of the transfer function can be separated as fol-

lows:

$$\begin{aligned}\Psi(\delta) &= \frac{r+ae^{-i\delta}}{1+are^{-i\delta}} \\ &= \frac{r+a(\cos\delta - i\sin\delta)}{1+ar(\cos\delta - i\sin\delta)} \\ &= \frac{[1+ar(\cos\delta + i\sin\delta)][r+a(\cos\delta - i\sin\delta)]}{(1+ar\cos\delta)^2+(ar\sin\delta)^2} \\ &= \frac{(a^2+1)r+a(1+r^2)\cos\delta - i\,a(1-r^2)\sin\delta}{1+(ar)^2+2ar\cos\delta} \\ &= |\Psi|e^{i\Phi(\delta)}.\end{aligned}$$

The power reflectivity of the GTI structure is given by

$$\begin{aligned}R_{GTI}(\omega) = |\Psi|^2 &= \Psi\Psi^* \\ &= \frac{(r+ae^{-i\delta})(r+ae^{i\delta})}{(1+are^{-i\delta})(1+are^{i\delta})} \\ &= \frac{r^2+a^2+ar(e^{-i\delta}+e^{i\delta})}{1+(ar)^2+ar(e^{-i\delta}+e^{i\delta})} \\ &= \frac{r^2+a^2+2ar\cos\delta}{1+(ar)^2+2ar\cos\delta} \\ &= \frac{R+A+2\sqrt{AR}\cos(\varphi-\omega t_0)}{1+AR+2\sqrt{AR}\cos(\varphi-\omega t_0)}.\end{aligned}$$

On the last row the amplitude quantities r and a have been replaced with their intensity counterparts $A = a^2$ and $R = r^2$. Also the round-trip phase term δ is changed to $\varphi - \omega t_0$. This is the final form used in Eq. 5.2. The same formula has been presented in several different ways in literature [148, 149, 150].

For the total phase $\Phi(\delta)$ we have

$$\tan\Phi(\delta) = \frac{\Im(\Phi)}{\Re(\Phi)} = \frac{-a(1-r^2)\sin\delta}{(a^2+1)r+a(1+r^2)\cos\delta}.$$

Now Eq. 5.3 follows immediately after substitution of the intensity and phase quantities:

$$\Phi(\omega) = \tan^{-1}\left(\frac{-\sqrt{A}(1-R)\sin(\varphi-\omega t_0)}{(A+1)\sqrt{R}+\sqrt{A}(1+R)\cos(\varphi-\omega t_0)}\right).$$

The effect of absorption on the total phase is best understood by drawing a phasor diagram. For a nonabsorbing GTI, the amplitude E_{r1} and phase Φ_1 of the total reflected field result from the components in the way illustrated in Fig. A.2 (a). When the ef-

fect of absorption is included, the total reflected amplitude is changed to E_{r2} and the total phase to Φ_2 as shown in Fig. A.2 (b). Despite the fact that the phase difference δ between the components remains unchanged, the resultant phases Φ_1 and Φ_2 are, indeed, not equal.

Finally, the group delay time τ is derived by taking the derivative $-d\Phi/d\omega$.

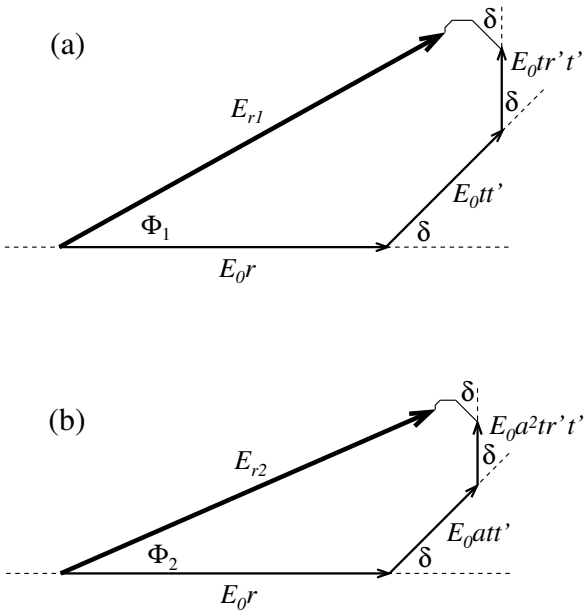

Fig. A.2. *Phasor diagram of (a) a nonabsorbing GTI and (b) an absorbing GTI. The angle* δ *depends on wavelength.*

APPENDIX B: PUBLICATIONS

PUBLICATION 1

A. Isomäki, A. Vainionpää, J. Lyytikäinen, and O. G. Okhotnikov, "Semiconductor mirror for dynamic dispersion compensation", *Appl. Phys. Lett.*, Vol. 82, No. 17, pp. 2773–2774 (2003)

Semiconductor mirror for dynamic dispersion compensation

A. Isomäki,[a] A. Vainionpää, J. Lyytikäinen, and O. G. Okhotnikov
Optoelectronics Research Centre, Tampere University of Technology, P.O. Box 692, FIN-33101 Tampere, Finland

(Received 27 December 2002; accepted 1 March 2003)

We report on a monolithic Gires–Tournois semiconductor interferometer used to generate a tunable delay. Controllable saturable absorption in optically pumped multiple-quantum-well semiconductor reflector was shown to provide promising means for rapid changing the group delay of the reflector, and represents an attractive form of dynamic dispersion compensation. © *2003 American Institute of Physics.* [DOI: 10.1063/1.1569990]

Dynamically tunable dispersion is an important issue for ultrafast technologies including optical communication systems operating at channel transmission rates above 40 Gbit/s. Thin-film dielectric Gires–Tournois interferometers (GTIs) are widely used to compensate highly chirped ultrashort pulses. Large amounts of negative group delay dispersion provided by the GTI are essential in mode-locked lasers in order to compensate for normal dispersion. The GTI can be easily made to offer 3 orders of magnitude higher dispersion than a prism pair, although over a limited bandwidth. It should be noted that GTI dispersion depends on the cavity loss. By placing intensity-dependent or saturable absorption into the GTI cavity, one can achieve a mechanism for tunable dispersion. In this letter, we explore an approach combining microcavity with epitaxially grown semiconductor multiple quantum wells (MQWs) to generate tunable delay. To achieve large optical nonlinearity in the surface-reflection device, a GTI representing a low-finesse Fabry–Pérot geometry composed of a pair of asymmetric mirrors separated by MQW saturable absorber section was explored.[1] Dispersion compensators based on surface-normal MQW structures have a great potential because they allow for realizing compact polarization-independent devices capable of high-speed tuning and low insertion loss. We studied a monolithic vertical-cavity GTI structure operated in reflection as a tunable dispersion compensator in the 1.55 μm spectral range. Since the group delay of the GTI depends on the cavity loss, the intensity-dependent absorption in MQW material was employed to control by the optical pumping, the GTI reflectivity, and consequently, the device dispersion.

Our devices were grown by the solid-source molecular beam epitaxy method. They consisted of a 0.1 μm InP buffer layer and a Burstein–Moss shifted distributed Bragg reflector[2] made of 19.5 pairs of $\lambda/4$ n^+-$Ga_{0.47}In_{0.53}As$/InP layers. The saturable absorber structure with 28 (four groups of seven) 9 nm thick $Ga_{0.47}In_{0.53}As$/10 nm InP quantum wells was placed into the impedance-matched cavity to achieve high pump-induced reflectivity. The reflectivity for the top dielectric mirror provided impedance-matched cavity was found from absorption measurements to be of ~60%.[1] The whole structure was capped with 11 μm InP and 10 nm InGaAs

It is usually assumed that there is no loss in a Gires–Tournois interferometer used for pulse compression and dispersion compensation.[3,4] However, one can show that GTI group delay and, therefore, its dispersion depend strongly on the cavity loss. It is then obvious that saturable absorption provides an attractive mechanism for tunable dispersion. The transfer function of a GTI can be presented as $H(\omega)=e^{i\Phi(\omega)}$ with

$$\tan(\Phi)=\frac{\sqrt{a}(1-R)\sin(\varphi-\omega t_0)}{(a+1)\sqrt{R}-\sqrt{a}(1+R)\cos(\varphi-\omega t_0)},$$

where R is the reflectivity of the front mirror, φ is the phase change on reflection from the high reflectivity back mirror, and t_0 is the round-trip time of the interferometer. The loss term is given by $a=e^{-2\alpha d}$, where α is the linear absorption coefficient and d the distance between GTI mirrors. The group delay time of the GTI is calculated by differentiating $\Phi(\omega)$. At the cavity resonance wavelength group delay reduces to form

$$\tau=\frac{(1-R)t_0}{1+R-(\sqrt{a}+1/\sqrt{a})\sqrt{R}}.$$

It can be easily seen that group delay depends on the GTI absorption, moreover, it changes the sign from negative to positive when a passes the value R.

In the experiment a GTI was used for dynamic dispersion tuning by bleaching the saturable absorption of the MQW structure using optical excitation. The structure was optically pumped with 980 nm pigtailed laser diode butt coupled with the GTI mirror. The tunable probe signal near 1550 nm wavelength was combined with pump light by a selective coupler and the group delay was analyzed through optical circulator using a conventional phase-shift technique.[5] Figures 1(a) and 1(b) show measured and computed group delays of the GTI mirror as a function of wavelength around the cavity resonance, respectively. To compare the group delays at different pump powers, the actual spectra were shifted to have the cavity resonances at the same value. This was done to compensate for the temperature-induced shift in the position of the cavity resonance with increased pump power. The thermal (positive) nonlinearity is dominant

[a]Author to whom correspondence should be addressed; electronic mail: antti.isomaki@orc.tut.fi

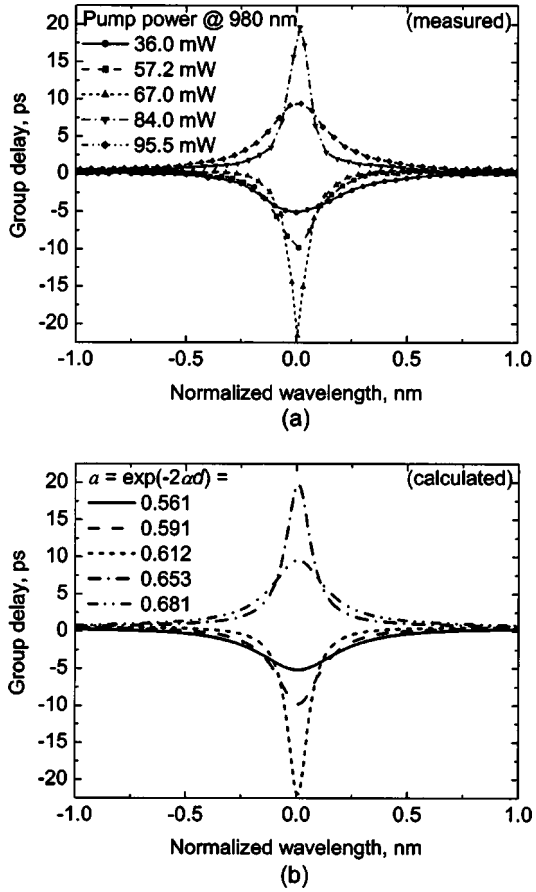

FIG. 1. (a) Measured and (b) computed group delays of GTI as a function of wavelength around the GTI cavity resonance.

over the carrier-induced refractive index changes with the continuous-wave laser used for pumping.[6] The net wavelength shift of $+0.75$ nm in the position of the GTI resonance was observed for pump powers between 36 and 95.5 mW. It should be noted that the thermal shift of the resonance can also be used for changing the dispersion on particular wavelength at low speeds, however.

It can be seen that there is a good agreement between theory and experiment. At the cavity resonance, the optical field is trapped in a spacer layer containing a MQW saturable absorber resulting in the highest group delay. In addition, close to cavity resonant wavelength due to the strong interaction of the optical field with the absorber, the semiconductor Gires–Tournois interferometer provides for a large change of group delay (± 20 ps) with the change in the pump power from $P=36$ to 95.5 mW. Figure 2 shows dispersion versus pump power near the cavity resonance. The slope of the group delay/pump dependence corresponds to $dD/dP \approx 45$ ps/nm/mW at a pump power of ~ 67 mW. A singular point in the $D(P)$ dependence at pump power $P \approx 76$ mW corresponds to the condition $a=R$, at which the group delay changes its sign.

GTI exploiting saturable absorption for dispersion tuning provides a certain amount of losses because the very operation principle of the compensator requires the presence of nonlinear absorption in the cavity. If we limit the value of device losses to 3 dB, the achievable variation in dispersion

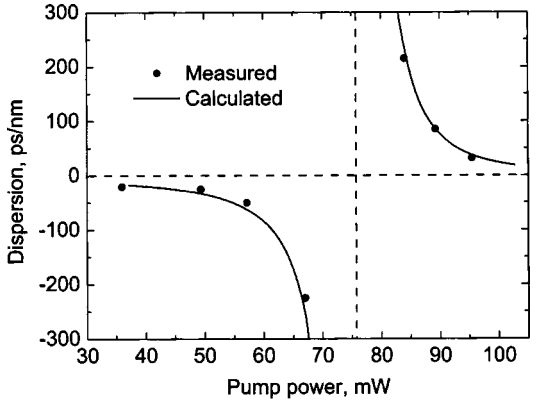

FIG. 2. Calculated and measured dispersion against pump power near cavity resonance.

due to absorption bleaching is $\Delta D = 0.43$ ps/nm for a GTI with $d=15$ μm and $R=0.7$. If the top mirror reflectivity was changed to $R=0.9$, the maximum variation in dispersion could be further increased to $\Delta D = 5.6$ ps/nm. However, at the same time the optical bandwidth decreases from ~ 1 to ~ 0.5 nm. Therefore, the magnitude of dispersion variation should be optimized depending on required bandwidth and available loss budget. It should also be mentioned that near impedance-matched GTI, the pump-induced dispersion can change its sign, i.e., the dispersion can be switched from normal dispersion to anomalous and vice versa. The new form of dynamic dispersion compensation based on controllable saturable absorption in optically pumped multiple quantum well semiconductor reflector provides a promising means for rapidly changing the group delay and can be useful for ultrafast technologies including optical communication systems operating at channel transmission rates above 40 Gbit/s.

In conclusion, a nonlinear semiconductor mirror was demonstrated for dynamic dispersion compensation. The compensator is an optical device based on the intrinsically fast nonlinear optical processes, which would perform operations at very high speeds. The microcavity effect in the form of a Gires–Tournois interferometer allows for the enhancement and manipulation of dispersion. The use of GTI provides a very simple scheme for large and rapid dispersion tuning since the MQW saturable absorber allows for recovery time of ~ 1 ps. By choosing semiconductor absorber material and its thickness, it is possible to make resonant Gires–Tournois interferometers to compensate dynamically for quadratic group-delay errors of ultrashort pulses. Optimized GTI-based dispersion compensators can also be used in high-speed data transmission to accommodate environment-induced changes in the chromatic dispersion of the fiber link.

[1] J. F. Heffernan, M. H. Moloney, J. Hegarty, J. S. Roberts, and M. Whitehead, Appl. Phys. Lett. **58**, 2877 (1991).
[2] N. Xiang, O. G. Okhotnikov, A. Vainionpää, M. Guina, and M. Pessa, Electron. Lett. **37**, 374 (2001).
[3] F. Gires and P. Tournois, C. R. Acad. Sci., Ser. III **258**, 6112 (1964).
[4] J. Kuhl and J. Heppner, IEEE J. Quantum Electron. **22**, 182 (1986).
[5] *Fiber Optic Test and Measurement*, edited by D. Dericson (Prentice-Hall, Englewood Cliffs, NJ, 1998).
[6] M. H. Moloney, J. F. Heffernan, J. Hegarty, R. Grey, and M. Whitehead, Appl. Phys. Lett. **63**, 435 (1993).

PUBLICATION 2

A. Isomäki, A. Vainionpää, S. Suomalainen, and O. G. Okhotnikov, "Self-starting mode-locked fiber laser using biased semiconductor absorber mirror", in *Congress on Optics and Optoelectronics*, Warsaw, Poland, 28 August - 2 September (2005) Lasers and Applications, edited by Krzysztof M. Abramski, Antonio Lapucci, Edward F. Plinski, Proc. SPIE Vol. 5958, 59580R (2005)

Self-starting mode-locked fiber laser using biased semiconductor absorber mirror

A. Isomäki*, A. Vainionpää, S. Suomalainen, O.G. Okhotnikov
Optoelectronics Research Centre, Tampere University of Technology,
P.O. Box 692, FIN-33101, Tampere, Finland

ABSTRACT

We present an erbium-doped fiber laser mode-locked using a reverse-biased InGaAsP multiple quantum-well saturable absorber. We have examined the performance of a p-type–intrinsic–n-type (PIN) structured semiconductor absorber mirror both in starting the pulse operation and in pulse shaping. We have also found that applying a reverse bias is a useful means to suppress the Q-switching instability. By varying the reverse bias voltage applied to the absorber mirror, we could change the recovery time of the device owing to the electric-field-induced carrier sweep-out. Through the sweep-out process we were able to control the mode-locking start-up capability and the pulse duration of the fiber laser. In the experiment the mode-locked pulse duration could be reduced from 50 to 20 ps by application of an 80 kV/cm sweep-out field in the intrinsic region of the PIN absorber. The equivalent spectral broadening by a factor of 2.5 was observed as well.

Keywords: Fiber laser, mode-locked laser, reverse bias, carrier sweep-out, quantum-well devices

1. INTRODUCTION

Semiconductor saturable absorbers mirrors (SESAMs) have been used successfully to initiate and to sustain mode-locking in a wide range of fiber lasers[1-4]. The main advantage of the SESAM is the possibility to control important parameters such as absorption recovery time, saturation fluence and insertion loss through the device design, growth conditions and heavy ion implantation. Exploiting the SESAM as a cavity mirror in the fiber laser results in compact size, environmentally stable and simple ultrashort pulse sources that can cover wide wavelength range and generate optical pulses with durations from picoseconds to femtoseconds.

The study of the semiconductor reflectors has revealed that mode-locking of the laser can be initiated and stabilized by the saturation dynamics of a slow absorber. However, the pulses develop a trailing wing due to the slowly recovering absorber; therefore, an absorber with a fast response is still desirable. The response speed of the semiconductor absorbers can be increased by introducing capture and recombination centers during or after epitaxial crystal growth[5, 6]. Low-temperature growth or post-growth heavy-ion irradiation are most popular methods of reducing the recovery time of the saturable absorption.

Another approach for controlling the recovery time of the semiconductor absorber has been demonstrated by placing it into a p-i-n structure that allows exploiting the sweep-out process for reducing the recovery time[7]. In p-i-n absorbers, the sweep-out of carriers from the active region is the main process that determines the device speed. P-i-n structures provide an attractive flexibility in controlling both the amount of absorption and its response time[8-10]. Reverse biased absorbers are broadly used in monolithic edge-emitting mode-locked semiconductor lasers[11]. In this Letter, we demonstrate that absorbers based on the p-i-n structure can efficiently mode-lock a fiber laser. The pulse width can be conveniently adjusted by changing the reverse bias applied to the p-i-n absorber mirror.

2. DEVICE GEOMETRY

The device structure was grown by solid-source molecular beam epitaxy on an n-InP substrate. The reflector consists of 19.5 Burstein-Moss shifted, $\lambda/4$ n^+-$Ga_{0.47}In_{0.53}As$ / n^+-InP layers, fabricated as described in [1]. The DBR reflectivity was

*antti.isomaki@orc.tut.fi; phone +358 3 3115 3432; fax +358 3 3115 3400; http://www.orc.tut.fi/

measured to be ≈98 % in the spectral range from 1.525 to 1.580 μm. The absorber includes five 0.85 % compressively strained 11.5-nm thick undoped InGaAsP quantum-wells separated by 20-nm InGaAsP barriers lattice matched to InP, and a 220-nm separate confinement heterostructure with the same composition as the barriers. The photo-luminescence peak wavelength of the quantum wells was positioned close to the long-wavelength edge of the DBR stopband at λ≈1600 nm. The active region is sandwiched between two InP cladding layers. The n-type cladding consists of 1.5 μm InP with $n \approx 1 \times 10^{18}$ cm^{-3} and the p-type cladding is composed of 2 μm InP with $p \approx 1 \times 10^{18}$ cm^{-3}. An $In_{0.53}Ga_{0.47}As$ cap layer with $p \approx 1.5 \times 10^{19}$ cm^{-3} was used for the p-contact. The structure was prepared in a single growth step. The mirror structure was completed using standard photolithography and wet chemical etching with SiO_2 used for electrical insulation. The optical window on the top of the reflector has a diameter of 30 μm. The p^+-InGaAs contact layer was etched away in the optical area defined by the window in order to avoid signal absorption outside the MQW absorber region. The absorber structure was used as one of the mirrors in a linear cavity erbium-doped fiber laser.

3. EXPERIMENT

The SESAM was studied in a fiber laser test bed that was constructed to examine the performance of the mirror in both starting the pulse operation and pulse shaping. This was achieved by minimizing the nonlinear effects and avoiding polarization-dependent components in the cavity to prevent pulse shaping through nonlinear polarization rotation. The soliton shaping could be prevented by using the erbium-doped fiber with normal dispersion and purposely made components fabricated of dispersion-shifted fiber. The fiber Fabry-Perot cavity is comprised of 2.8 m of erbium-doped fiber having dispersion of -6 ps/nm/km, 0.5 m of dispersion shifted fiber, 0.4 m of Corning Hi1060 WDM coupler fiber with dispersion of 8 ps/nm/km. Additional 3.3-m long segment of SMF-28 fiber with dispersion of 17 ps/nm/km was used optionally when the cavity with overall anomalous dispersion was needed. The fiber ends were angle-polished to eliminate the influence of the Fresnel reflection. AR-coated aspheric lenses with focal lengths of 2.0 mm were used to focus the beam on the p-i-n absorber served as a cavity mirror. A 90%-reflectivity mirror was used as another cavity end reflector and output coupler. The laser was pumped with a single-mode grating-stabilized laser diode, which provided a power of 120 mW at 980 nm. The laser cavity has the fundamental repetition rate of ~13.5 MHz.

Summarizing the experimental observations made with a number of p-i-n mirror structures studied, we deduce that passive mode-locked operation can be achieved with an appropriate optimization of the beam spot size at the p-i-n absorber. By varying the bias voltage it is possible to adjust both the amount of the absorption and the recovery time of the absorber mirror and increase the pulse quality. The current through the p-i-n structure was negligible (<1 mA); therefore, thermal effects are expected to be insignificant for the mirror performance.

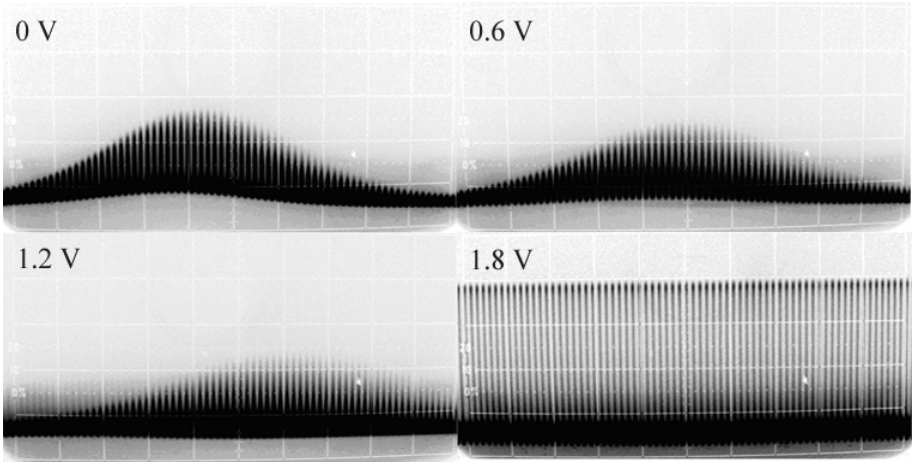

Fig. 1. Oscilloscope traces of the laser output obtained with different reverse bias voltages (0.5 μs/div). With applied voltages above 1.8 V the cw mode-locked operation was achieved without Q-switching instability.

Fig. 1 shows the measured reverse bias dependent operation regimes of the fiber laser. As expected, the reverse bias voltage applied to the p-i-n absorber significantly influences the dynamic properties of the laser. At 0 to 1.2 V biases, the laser output shows the waveform corresponding to Q-switched mode-locked operation. For reverse biases higher than 1.2 to 1.8 V, depending on the absorber sample and alignment, the laser starts cw mode-locked operation. Self-starting mode-locking to a single pulse per round trip was observed at a launched pump power up to 120 mW for reverse biases above the start-up value V_0.

The p-i-n mirror characterization was carried out by measuring the device photocurrent as a function of the reverse bias. The bias and, therefore, operating regime dependent photocurrent is shown in Fig. 2 for the pump power of 100 mW. With an increase in the reverse bias, the laser operates first in the Q-switched mode-locking until the bias reaches the value of V_0=1.8 V, as was shown in Fig. 1. Above V_0 the recovery time of the absorber becomes fast enough to enable self-starting cw mode-locking. The onset of cw mode-locking is manifested as an abrupt decrease in the photocurrent indicating a reduction (bleaching) of the mirror absorption provided by the pulse train with high repetition rate.

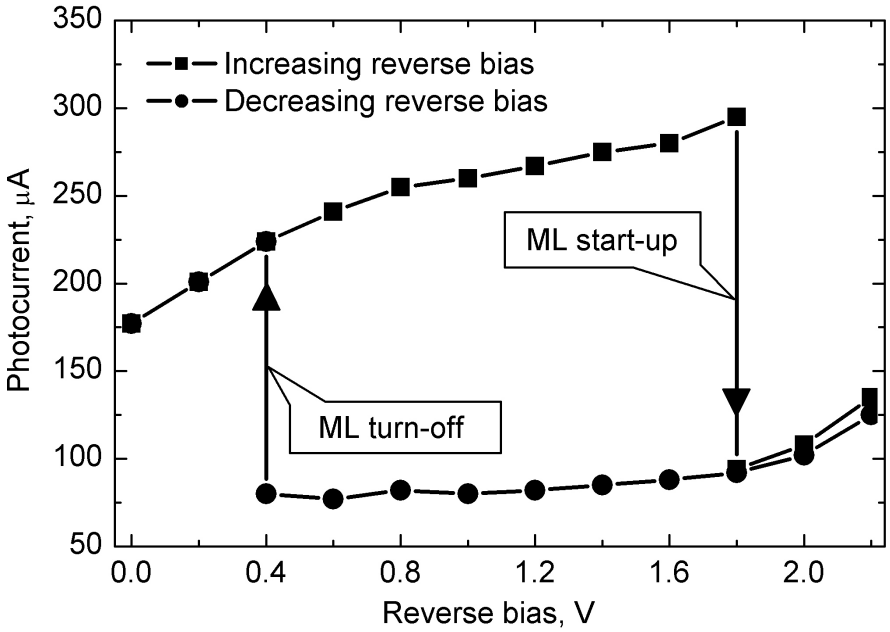

Fig. 2. Photocurrent generated in the p-i-n structure as a function of reverse bias. The abrupt changes in photocurrent at 1.8 V and 0.4 V correspond to the start-up and turn-off of the cw mode-locked (ML) operation, respectively.

A mode-locking hysteresis is usually observed versus pump power[12]. Similar behavior was found here by varying the reverse bias, as seen from Fig. 2. With a decrease in the reverse bias from a high value down to 0.4 V, the p-i-n absorber mirror sustains its highly saturated state corresponding to mode-locked operation. Below 0.4 V the recovery time of the absorber becomes too long to support short pulse formation. Mode-locking turns off and the absorber jumps into the high absorption state distinguished as a regime with a high value of photocurrent.

Fig. 3 presents the pulse characteristics for the bias above the mode-locking start-up voltage V_0. A decrease in pulse duration and equivalent spectral broadening up to the factor of 2.5 were observed with an increase in the bias. The pulse durations were derived from the autocorrelation traces assuming a double exponential pulse shape, which provided the best fit to the experimental data. Fig. 4 points out how the pulses evolve at various bias values. The inset shows the optical spectrum of the pulses obtained at $V-V_0$=4.5 V, corresponding to the electrical field of 80×10^3 V·cm^{-1} in the

absorbing region. The corresponding change in the absorption with the reverse bias was too small to be measured directly, especially in situ condition, and, therefore, did not play essential role in the pulse width reduction. Thus, tuning the reverse bias voltage provides a convenient method for adjusting the recovery time of the absorber mirror.

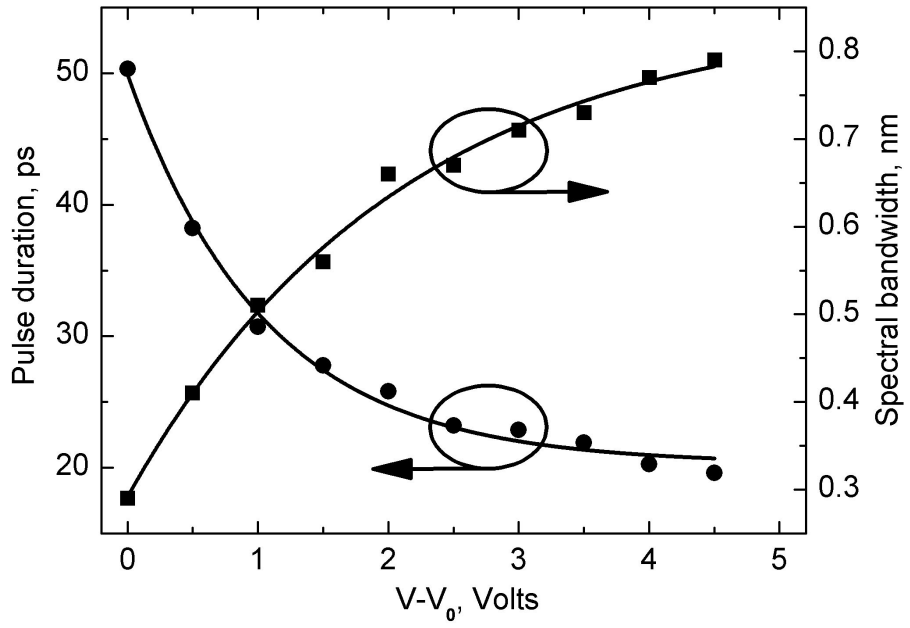

Fig. 3. Measured mode-locked pulse duration and pulse bandwidth as a function of reverse bias applied to the p-i-n absorber mirror. V_0 is a voltage of cw mode-locking start-up.

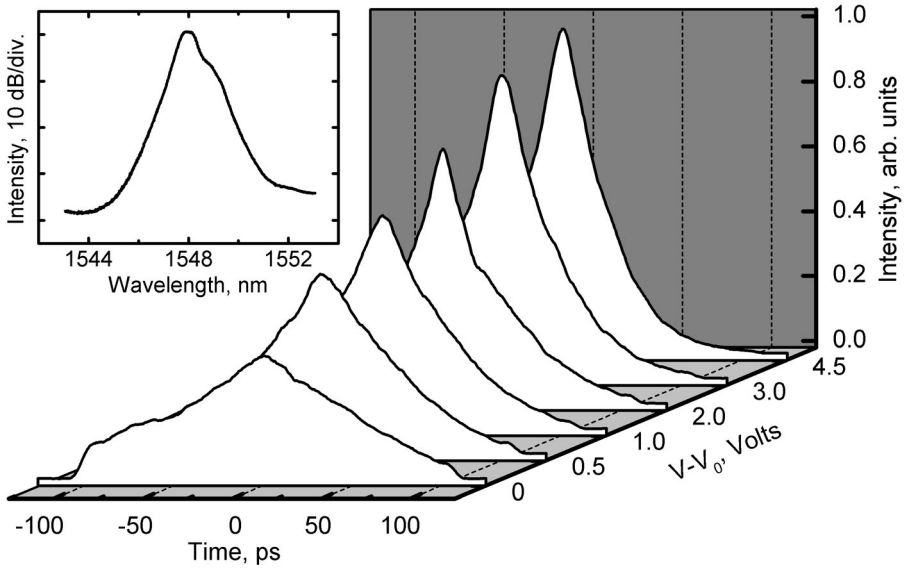

Fig. 4. The evolution of the pulses at different reverse biases. The inset shows the optical spectrum corresponding to the bias $V-V_0=4.5$ V.

4. CONCLUSIONS

In conclusion, we have used a reverse-biased InGaAsP multiple quantum-well reflector to mode-lock an erbium-doped fiber laser. By varying a bias applied to a p-i-n absorber structure, we could change the recovery time of the device owing to the sweep-out process and, consequently, control the mode-locking start-up capability and pulse duration. We were able to adjust the mode-locked pulse duration from 50 to 20 ps by increasing the reverse bias. We have also found that applying a reverse bias is a useful means in suppression the Q-switching instability.

REFERENCES

1. N. Xiang, O.G. Okhotnikov, A. Vainionpää, M. Guina and M. Pessa, "Broadband semiconductor saturable absorber mirror at 1.55 μm using Burstein-Moss shifted $Ga_{0.47}In_{0.53}As$ / InP distributed Bragg reflector", Electron. Lett., **37**, 374-375, 2001.
2. O.G. Okhotnikov, L. Gomes, N. Xiang, T. Jouhti, and A. B. Grudinin, "Mode-locked ytterbium fiber laser tunable in the 980 – 1070 nm spectral range", Opt. Lett., **28**:17, 1522-1524, 2003.
3. O.G. Okhotnikov, L. Gomes, N. Xiang, T. Jouhti, A. K. Chin, R. Singh and A.B. Grudinin, "980 nm picosecond fiber laser", IEEE Photon. Technol. Lett., **15**, 1519-1521, 2003.
4. M. Rusu, S. Karirinne, M. Guina, A.B. Grudinin and O.G. Okhotnikov, "Femtosecond neodymium-doped fiber laser operating in the 894-909 nm spectral range", IEEE Photon. Technol. Lett., **16**, 1029-1031, 2004.
5. H. S. Loka, and P. W. E. Smith, "Ultrafast all-optical switching in an asymmetric Fabry-Pérot device using low-temperature-grown GaAs", IEEE Photon. Technol. Lett., **10**, 1733-1735, 1998.
6. M. J. Lederer, B. Luther-Davis, H. H. Tan, and C. Jagadish, "An antiresonant Fabry-Perot saturable absorber for passive mode-locking fabricated by metal-organic vapor phase epitaxy and ion implantation design, characterization, and mode-locking," IEEE J. Quantum Electron., **34**, 2150-2161, 1998.
7. I. Ogura, Y. Hashimoto, H. Kurita, T. Shimizu, and H. Yokoyama, "Picosecond all-optical gate using a saturable absorber in mode-locked laser diodes", IEEE Photon. Technol. Lett., **4**, 603-605, 1998.
8. E. P. Burr, J. Song, A. J. Seeds, and C. C. Button, "60 ps recovery time in an InGaAsP quaternary multiple quantum well saturable absorber employing carrier sweep-out", *Conference on Lasers and Electro-Optics Europe, 2000, Conference Digest*, paper CTuD2, 10-15 September 2000.
9. A. V. Uskov, J. R. Karin, J. E. Bowers, J. G. McInerney, J. L. Bihan, and R. Nagarajan, "Effects of carrier cooling and carrier heating in saturation dynamics and pulse propagation through bulk semiconductor absorbers," IEEE J. Quantum Electron., **34**, 2162–2171, 1998.
10. S. Hojfeldt, F. Romstad, and J. Mork, "Absorption recovery in strongly saturated quantum-well electroabsorption modulators", IEEE Photon. Technol. Lett., **15**, 676-678, 2003.
11. J. F. Martins-Filho, E. A. Avrutin, C. N. Ironside, and J. S. Roberts, "Monolithic multiple colliding pulse mode-locked quantum-well lasers: experiment and theory," IEEE J. Select. Topics Quantum Electron., **1**, 539-551, 1995.
12. K. Tamura, E. P. Ippen, H. A. Haus, and L. E. Nelson, "77-fs pulse generation from a stretched-pulse mode-locked all-fiber ring laser", Opt. Lett., **18**:13, 1080-1082, 1993.

PUBLICATION 3

A. Isomäki, M. D. Guina, P. Tuomisto, and O. G. Okhotnikov, "Fiber laser mode-locked with a semiconductor saturable absorber etalon operating in transmission", *IEEE Photon. Tech. Lett.*, Vol. 18, No. 20, pp. 2150–2152 (2006)

Fiber Laser Mode-Locked With a Semiconductor Saturable Absorber Etalon Operating in Transmission

Antti Isomäki, Mircea D. Guina, Pietari Tuomisto, and Oleg G. Okhotnikov

***Abstract*—We demonstrate a ring cavity ytterbium fiber laser mode-locked with a semiconductor saturable absorber used in transmission. The resonant cavity-enhanced nonlinear response corresponding to the low-loss transmission state enables a robust self-starting mode-locking. Such a transfer function is opposite to that of the resonant absorber operating in the reflection mode, where the highest modulation depth matches the high-loss state. The device ensures ultrashort pulse operation with the wavelength self-adjusted to the optimal value corresponding to the low-loss state of the laser cavity. When using a saturable absorber etalon in transmission mode, the mode-locking mechanism is also highly tolerant to the total cavity dispersion.**

***Index Terms*—Mode-locked lasers, optical fiber lasers, quantum-well devices, ultrafast optics.**

I. Introduction

SATURABLE absorbers are nonlinear optical elements that impose an intensity-dependent attenuation on a light beam incident upon them; an incident radiation of low intensity is absorbed, while a high intensity radiation passes the saturable absorber with much less attenuation. These devices have found applications in a large variety of fields. In particular, passive mode-locking based on semiconductor saturable absorber is a powerful technique to produce short optical pulses with a rather simple architecture of the laser cavity [1]–[3].

Typically, a semiconductor saturable absorber is fabricated on top of a high-reflective semiconductor, dielectric or metallic reflector forming a semiconductor saturable absorber mirror (SESAM) [4]. The nonlinear properties of an absorber used in mode-locked lasers can be enhanced by placing it within a Fabry–Pérot cavity. The parameters of such an absorption etalon are largely determined by the cavity length and the position of the active material within the cavity. If the operation wavelength is substantially detuned from the cavity resonance, the device has an antiresonant behavior. Thus, it provides a high reflectivity over a broad spectral range [5], but the nonlinear reflectivity modulation depth is relatively small. Advanced SESAM devices having lower saturation fluence and more control over dispersion and the modulation depth than classical SESAMs have been proposed recently [6]. These devices are particularly suited for passively mode-locked solid-state lasers. However, for fiber lasers a higher modulation depth is usually required for reliable start-up of mode-locking, in particular with high values of total cavity dispersion [7]. By changing the cavity length, the resonant wavelength of the etalon can be matched to the laser operation wavelength. This kind of design has a twofold function. First, the resonant operation gives a substantial increase in the modulation depth [8]. Second, a large value of dispersion can be produced near the resonant wavelength. It has been recently shown that the amount of dispersion induced by a resonant absorber could be sufficient to balance the dispersion of a fiber laser cavity [9], [10]. However, the use of a resonant SESAM exhibiting higher loss near the resonant wavelength makes the mode-locking difficult to achieve and forces the laser to operate away from the spectral range with anomalous dispersion [11]. In order to operate the laser near the resonant wavelength, the cavity architectures should employ additional wavelength selective elements, e.g., optical filters. These problems can be avoided by using the saturable absorber in a form of a Fabry–Pérot etalon operating in transmission. With this geometry, the cavity-enhanced modulation depth and the high dispersion values correspond simultaneously to the high-transmission regime where the laser would preferably operate.

The semiconductor saturable absorbers operating in transmission demonstrated so far did not exploit the cavity effect [12], [13]. In this letter, we demonstrate the attractive potential of such an absorptive transmission etalon (ATE) for mode-locking fiber lasers. The transmission mode ensures a high modulation depth needed for mode-locked fiber lasers and can be naturally implemented in a ring cavity. Particularly, we show that an ATE is able to initiate passive mode-locking in a laser with an arbitrary amount of cavity dispersion.

II. ATE Design and Characterization

The ATE consists of an absorber region and spacer layers sandwiched between two distributed Bragg reflectors (DBRs). The bottom DBR is made of 3.5 pairs of quarter-wave 89.3-nm AlAs/75.65-nm GaAs layers. The absorber region comprises six 6-nm InGaAs quantum wells with 15-nm GaAs barriers. The top DBR is comprised of 4.5 pairs of AlAs–GaAs. Two 126-nm GaAs buffer layers surrounding the absorber region set up the length of the ATE cavity and, therefore, define the resonant wavelength and the position of the absorber region in respect to the maxima of the standing-wave pattern of the optical field within the cavity. The semiconductor substrate of the etalon was antireflection-coated to avoid unwanted Fabry–Pérot effects between the absorber mirrors and the substrate–air interface. Before coating, the substrate was thinned down to 30 μm by wet

Manuscript received April 19, 2006; revised August 7, 2006. This work was supported by the Finnish Academy of Sciences, by the EU FP6 Uranus Project, and by the Graduate School in Electronics, Telecommunications and Automation (GETA).

A. Isomäki, P. Tuomisto, and O. G. Okhotnikov are with the Optoelectronics Research Centre, Tampere University of Technology, FIN-33101 Tampere, Finland (e-mail: antti.isomaki@tut.fi; pietari.tuomisto@tut.fi; oleg.okhotnikov@tut.fi).

M. D. Guina is with the Optoelectronics Research Centre, Tampere University of Technology, FIN-33101 Tampere, Finland, and also with RefleKron Ltd., FIN-33720 Tampere, Finland (e-mail: mircea.guina@tut.fi).

Digital Object Identifier 10.1109/LPT.2006.883894

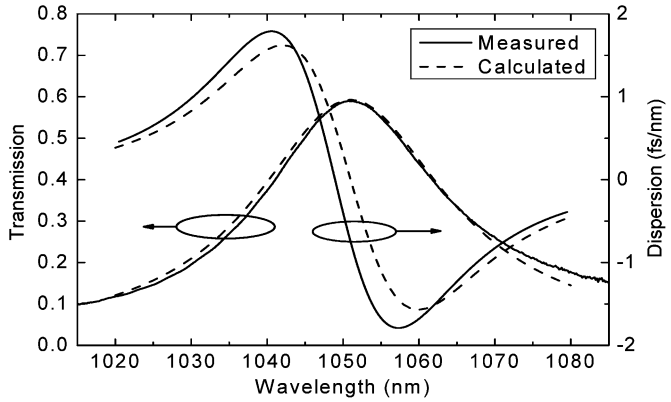

Fig. 1. Calculated and measured transmission spectrum and group-velocity dispersion of the ATE with resonance at 1050 nm.

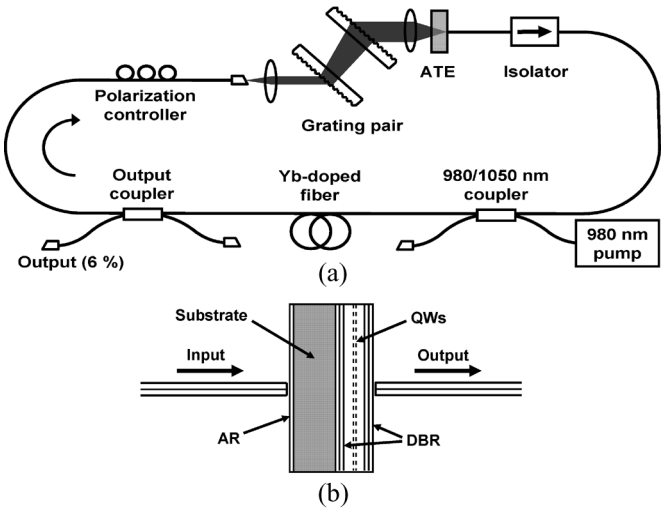

Fig. 2. Schematics of (a) the ring-cavity fiber laser setup and (b) all-fiber coupling geometry of an ATE.

etching. The saturation fluence of the ATE was measured to be $\sim$20 μJ/cm^2 and the modulation depth was $\sim$10%. Growth conditions ensured an absorption recovery time of about 40 ps.

Fig. 1 shows the transmission spectrum and group-velocity dispersion of the etalon. The dispersion was measured using a phase-locked interferometer similar to that described in [14]. Both the measurement and the numerical modeling indicate a transmission increase at the resonant wavelength of 1050 nm. Due to the short cavity length of the etalon, the induced dispersion of $<$2 fs/nm is low and it cannot affect the total cavity dispersion significantly. The modeling agrees well with the measured data.

III. Laser Performance

Fig. 2(a) shows the setup of the mode-locked fiber laser employing the ATE as the mode-locking element. The gain medium was a 50-cm-long ytterbium-doped fiber with absorption of 414 dB/m at 976 nm. The ytterbium-doped fiber was pumped with a 980-nm laser diode delivering a power up to 130 mW. The ring laser cavity contained an optical isolator to ensure unidirectional propagation, a 980/1050-nm pumping fiber coupler, a 6% output coupler and a polarization controller. The cavity dispersion was adjusted by using a pair

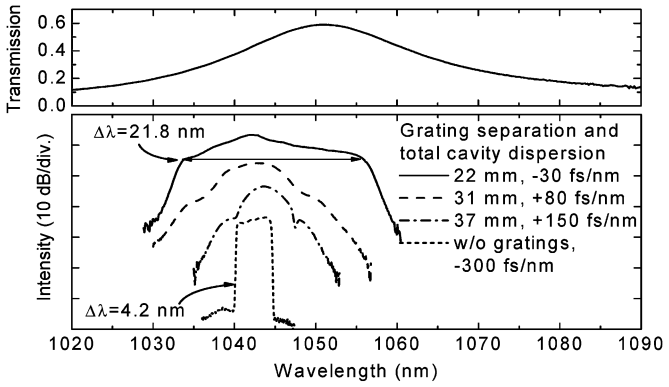

Fig. 3. Low intensity transmission spectrum of the ATE (top) and mode-locked pulse spectra for different grating separations. The traces have been shifted for clarity.

of 1250-lines/mm transmission gratings that inflicted the loss of $\sim$1 dB. In a mode-locked state when the absorption is being completely saturated, the ATE had a Q-factor of 40 with an insertion loss of $\sim$1.5 dB for the lens coupling geometry shown in Fig. 2(a). Fig. 2(b) shows the all-fiber butt-coupling geometry of the etalon that we used in a compact laser without the grating pair compensator. The estimated insertion loss in this coupling scheme was found to be close to that measured for the setup presented above in Fig. 2(a). Stable mode-locked operation supported by the ATE could be initiated by adjusting the polarization inside the cavity. Once started, mode-locked operation was stable for hours. Polarization-dependent loss of the grating pair suggests that nonlinear polarization evolution is a dominant pulse shaping mechanism, while the ATE plays mainly the role of robust trigger of passive mode-locking. The pump power threshold for self-starting mode-locking was 100 mW. The overall cavity length was about 6.5 m which corresponds to a fundamental pulse repetition rate of 31.4 MHz. The laser delivered an average output power of $\sim$1 mW.

Fig. 3 shows the output pulse spectra of the laser for different values of total cavity dispersion. As expected, the laser operates in the wavelength region close to the transmission maximum of the absorber. The slight shift from the resonance to the shorter wavelengths is most likely due to the nonuniformity of the gain spectrum. With a grating separation of 22 mm, the total cavity dispersion was normal with a value of $-$30 fs/nm and resulted in a very broad square-shaped spectrum with the bandwidth of 21.8 nm, indicating a stretched pulse operation. With an increase in the grating separation, the cavity dispersion becomes anomalous and, consequently, the laser switches to soliton pulse operation with the characteristic sidelobes in the spectrum. Without dispersion compensation, the laser operates in stretched pulse regime with a 3-dB spectral width of 4.2 nm. The corresponding autocorrelation traces for three grating separations are shown in Fig. 4. These traces, taken from the output coupler shown in Fig. 2, correspond to strongly chirped pulses.

Since the pulse duration and chirp vary along the fiber cavity, we measured the pulses also at the output of the grating compensator. In this experiment the gratings with 29-mm separation set the operation wavelength to 1050 nm. The external pulse compression in a fiber pigtail with dispersion of $-$40 fs/nm/m proves that the chirp is linear. At the output of a 4-m-long fiber the pulse

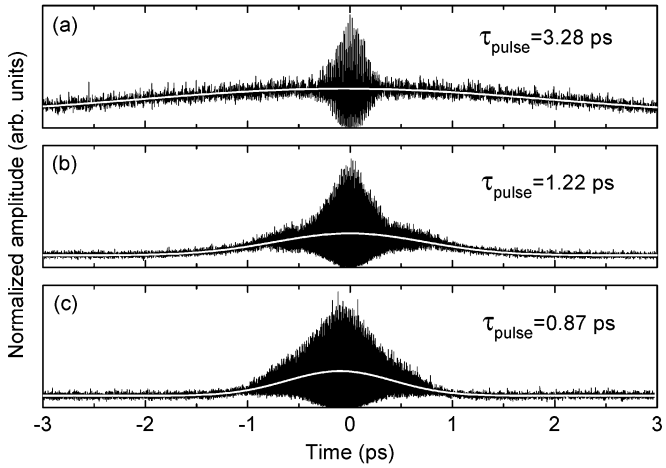

Fig. 4. Interferometric autocorrelation traces for three different grating separations: (a) 22, (b) 31, and (c) 37 mm. White curves show the Gaussian fit to the intensity autocorrelation.

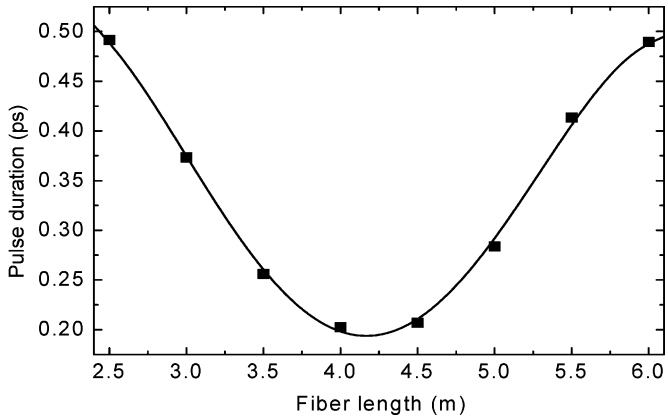

Fig. 5. Pulse duration measured at the output of the grating compensator as a function of the length of the external fiber delay line.

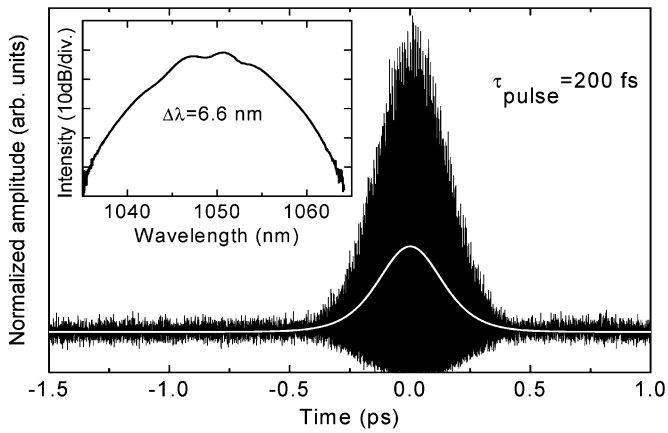

Fig. 6. Autocorrelation of the shortest pulse obtained using a 4-m-long fiber delay line. The inset shows the corresponding spectrum.

was compressed from 1.6 ps down to 200 fs, as shown in Fig. 5, while the pulse spectra remained essentially unchanged. The autocorrelation of the shortest pulse obtained at the output of the fiber delay line is shown in Fig. 6. The corresponding spectrum, shown in the inset of Fig. 6, indicates near-transform-limited pulses with the time-bandwidth product of 0.36.

IV. Conclusion

An ATE has been proposed for mode-locking fiber lasers. Contrary to the etalons operating in reflection mode, the low-loss state in the transmission etalon corresponds to the cavity resonance. Therefore, the operation wavelength sets spontaneously at the resonance of the etalon without using an intracavity filter and thus ensures a high modulation depth needed for reliable self-starting of mode-locking. An ATE could also be designed to compensate for the fiber dispersion. This option supplies, however, a limited amount of anomalous dispersion and can only be applied for short cavity lasers $(L < 1\ \mathrm{m})$.

An ATE is particularly attractive for ring cavity lasers. A unidirectional ring cavity is desirable since it is less sensitive to the spurious intracavity reflections and, therefore, additionally improves the capability to self-starting mode-locking as compared to a standing-wave laser cavity.

References

[1] E. A. De Souza, C. E. Soccolich, W. Pleibel, R. H. Stolen, J. R. Simpson, and D. J. DiGiovanni, "Saturable absorber modelocked polarisation maintaining Erbium-doped fibre laser," *Electron. Lett.*, vol. 29, pp. 447–449, 1993.

[2] F. X. Kärtner, I. D. Jung, and U. Keller, "Soliton mode-locking with saturable absorbers," *IEEE J. Sel. Topics Quantum Electron.*, vol. 2, no. 3, pp. 540–556, Sep. 1996.

[3] B. C. Collings, K. Bergman, S. T. Cundiff, S. Tsuda, J. N. Kutz, J. E. Cunningham, W. Y. Jan, M. Koch, and W. H. Knox, "Short cavity Erbium/Ytterbium fiber laser mode-locked with a saturable Bragg reflector," *IEEE J. Sel. Topics Quantum Electron.*, vol. 3, no. 8, pp. 1065–1075, Aug. 1997.

[4] U. Keller, K. J. Weingarten, F. X. Kärtner, D. Kopf, B. Braun, I. D. Jung, R. Fluck, C. Hönninger, N. Matuschek, and J. Aus der Au, "Semiconductor saturable absorber mirrors (SESAMs) for femtosecond to nanosecond pulse generation in solid-state lasers," *IEEE J. Sel. Topics Quantum Electron.*, vol. 2, no. 3, pp. 435–452, Sep. 1996.

[5] L. R. Brovelli, U. Keller, and T. H. Chiu, "Design and operation of antiresonant Fabry–Perot saturable semiconductor absorbers for mode-locked solid-state lasers," *J. Opt. Soc. Amer. B*, vol. 12, pp. 311–322, 1995.

[6] G. J. Spühler, K. J. Weingarten, R. Grange, L. Krainer, M. Haiml, V. Liverini, M. Golling, S. Schön, and U. Keller, "Semiconductor saturable absorber mirror structures with low saturation fluence," *Appl. Phys. B*, vol. 81, pp. 27–32, 2005.

[7] R. Herda and O. G. Okhotnikov, "Dispersion compensation-free fiber laser mode-locked and stabilized by high-contrast saturable absorber mirror," *IEEE J. Quantum Electron.*, vol. 40, no. 7, pp. 893–899, Jul. 2004.

[8] J. Heffernan, M. Moloney, J. Hegarty, J. Roberts, and M. Whitehead, "All optical, high contrast absorptive modulation in an asymmetric Fabry–Perot etalon," *Appl. Phys. Lett.*, vol. 58, pp. 2877–2879, 1991.

[9] M. Guina, N. Xiang, and O. G. Okhotnikov, "Stretched-pulse fiber lasers based on semiconductor saturable absorbers," *Appl. Phys. B*, vol. 74, pp. S193–S200, 2002.

[10] L. Orsila, L. A. Gomes, N. Xiang, T. Jouhti, and O. G. Okhotnikov, "Mode-locked Ytterbium fiber lasers," *Appl. Opt.*, vol. 43, pp. 1902–1906, 2004.

[11] D. Kopf, G. Zhang, R. Fluck, M. Moser, and U. Keller, "All-in-one dispersion-compensating saturable absorber mirror for compact femtosecond laser sources," *Opt. Lett.*, vol. 21, pp. 486–488, 1996.

[12] M. Zirngbil, L. W. Stulz, J. Stone, J. Hugi, D. DiGiovanni, and P. B. Hansen, "1.2 ps pulses from passively mode-locked laser diode pumped Er-doped fibre ring laser," *Electron. Lett.*, vol. 27, pp. 1734–1735, 1991.

[13] Y. Deng, M. W. Koch, F. Lu, G. W. Wicks, and W. H. Knox, "Colliding-pulse passive harmonic mode-locking in a femtosecond Yb-doped fiber laser with a semiconductor saturable absorber," *Opt. Express*, vol. 12, pp. 3872–3877, 2004.

[14] M. Beck and I. A. Walmsley, "Measurements of group delay with high temporal and spectral resolution," *Opt. Lett.*, vol. 15, pp. 492–494, 1990.

PUBLICATION 4

A. Isomäki and O. G. Okhotnikov, "All-fiber ytterbium soliton mode-locked laser with dispersion control by solid-core photonic bandgap fiber", *Opt. Express*, Vol. 14, No. 10, pp. 4368–4372 (2006)

All-fiber ytterbium soliton mode-locked laser with dispersion control by solid-core photonic bandgap fiber

A. Isomäki and O. G. Okhotnikov

Optoelectronics Research Centre, Tampere University of Technology,
P.O. Box 692, FIN-33101, Tampere, Finland
antti.isomaki@tut.fi

Abstract: We exploit an anomalous dispersion generated by a solid-core photonic bandgap fiber for dispersion compensation in an ytterbium fiber laser passively mode-locked with a semiconductor saturable absorber. The bandgap-guiding fiber, adequately compatible with standard fiber based on guiding via total internal reflection, allows for an environmentally robust all-fiber subpicosecond soliton oscillator at 1 μm.

OCIS codes: (060.2340) Fiber optics components; (140.3510) Lasers, fiber; (260.2030) Dispersion; (320.7090) Ultrafast lasers

References and links

1. B. C. Collings, K. Bergman, S. T. Cundiff, S. Tsuda, J. N. Kutz, J. E. Cunningham, W. Y. Jan, M. Koch, and W. H. Knox, "Short cavity erbium/ytterbium fiber lasers mode-locked with a saturable Bragg reflector," IEEE J. Sel. Top. Quantum Electron. **3**, 1065-1075 (1997).
2. F. Ö. Ilday, J. R. Buckley, H. Lim, F. W. Wise, and W. G. Clark, "Generation of 50-fs, 5-nJ pulses at 1.03 μm from a wave-breaking-free fiber laser," Opt. Lett. **28**, 1365-1367 (2003).
3. L. A. Gomes, L. Orsila, T. Jouhti, and O. G. Okhotnikov, "Picosecond SESAM based ytterbium mode-locked fiber lasers," IEEE J. Sel. Top. Quantum Electron. **10**, 129-136 (2004).
4. O. G. Okhotnikov, L. A. Gomes, N. Xiang, T. Jouhti, and A. B. Grudinin, "Mode-locked ytterbium fiber laser tunable in the 980-1070 -nm spectral range," Opt. Lett. **28**, 1522-1524 (2003).
5. B. Barnett, L. Rahman, M. Islam, Y. Chen, P. Bhattacharya, W. Riha, K. Reddy, A. Howe, K. Stair, H. Iwamura, S. Friberg, and T. Mukai, "High-power erbium-doped fiber laser mode locked by a semiconductor saturable absorber," Opt. Lett. **20**, 471-473 (1995).
6. R. Herda and O. G. Okhotnikov, "Dispersion compensation-free fiber laser mode-locked and stabilized by high-contrast saturable absorber mirror," IEEE J. Quantum Electron. **40**, 893-899 (2004).
7. R. L. Fork, O. E. Martinez, and J. P. Gordon, "Negative dispersion using pairs of prisms," Opt. Lett. **9**, 150-152 (1984).
8. E. B. Treacy, "Optical pulse compression with diffraction gratings," IEEE J. Quantum Electron. **QE-5**, 454-458 (1969).
9. H. Lim, F. Ö. Ilday, and F. W. Wise, "Femtosecond ytterbium fiber laser with photonic crystal fiber for dispersion control," Opt. Express **10**, 1497-1502 (2002).
10. J. C. Knight, "Photonic crystal fibres," Nature **424**, 847-851 (2003).
11. D. G. Ouzounov, F. R. Ahmad, D. Muller, N. Venkataraman, M. T. Gallagher, M. G. Thomas, J. Silcox, K. W. Koch, and A. L. Gaeta, "Generation of megawatt optical solitons in hollow-core photonic band-gap fibers," Science **301**, 1702-1704 (2003).
12. F. Luan, A. K. George, T. D. Hedley, G. J. Pearce, D. M. Bird, J. C. Knight and P. S. J. Russell, "All-solid photonic bandgap fiber," Opt. Lett. **29**, 2369-2371 (2004).

1. Introduction

Recently, mode-locked fiber lasers have gained an enormous interest owing to their excellent beam and pulse quality, small footprint and user-friendly operation [1, 2]. The semiconductor saturable absorber mirror (SESAM) technology has dramatically improved the performance of mode-locked fiber lasers by providing both robust self-starting and strong pulse shaping

#69016 - $15.00 USD Received 16 March 2006; revised 24 April 2006; accepted 26 April 2006

mechanisms [3-5]. Despite excellent performance reported to date, Yb-doped fiber laser development remains hindered by the issue of chromatic dispersion compensation. Owing to both doped and standard single mode fibers exhibiting normal chromatic dispersion around 1 μm, fiber lasers without proper dispersion management tend to operate at these wavelengths in a stretched pulse regime associated with long pulse width and problematic start-up of mode-locked operation [6]. To overcome these problems, normal dispersion of the laser cavity should be compensated by an appropriate cavity element with anomalous dispersion. Regularly, dispersion compensation is achieved with bulk optical components such as prisms [7] and diffraction gratings [8]. These solutions, however, suffer from disadvantages that limit their applicability to fiber lasers: prisms exhibit too low dispersion and require impractically large separation, while diffraction gratings are strongly polarization dependent and lossy. Furthermore, the use of intracavity bulk optical elements violates the "all-fiber" nature of the laser. Recently, the photonic crystal technology has been used to build dispersion compensators which allow for robust and all-fiber compact systems [9]. Unlike conventional optical fibers, photonic bandgap (PBG) fibers do not guide light by total internal reflection but rely on a photonic bandgap in the fiber's cladding [10]. A hollow-core PBG fiber consists of a hollow core surrounded by a cladding whose periodicity creates a bandgap for the photons guided in the fiber's core. Using hollow-core fibers should be useful for high peak power ultrashort pulse applications [11].

Whereas hollow-core PBG fibers are attractive alternative to bulk elements, they suffer from poor matching with the standard fibers and, consequently, may generate high intracavity loss. Particularly in a mode-locked laser cavity, a hollow-core PBG fiber spliced with standard fiber could provide Fresnel back-reflection which affects badly the starting capability and quality of the pulse operation. Better matching with the standard fiber could be achieved by using solid-core photonic crystal fibers. These fibers with light guided by total internal reflection typically have a solid silica-based core surrounded by a silica-air photonic crystal cladding [10]. Anomalous dispersion in this type of crystal fiber could be generated with rather small core diameters. Because of high nonlinearity, these fibers are widely used in supercontinuum generation, but poor matching with standard fibers prevents using them inside the laser cavity. An alternative solution is based on a solid-core photonic bandgap fiber (SC-PBG) made of a pure silica core and an array of higher index (e.g. Ge-doped) strands in the cladding. Such an all-solid approach has the advantage of easy splicing to a standard fiber. Furthermore, the structure exhibits no surface modes [12] and allows for high anomalous dispersion with less critical non-linear thresholds than index guiding photonic crystal fibers.

In this Letter, we report on the use of a solid-core photonic bandgap fiber to compensate the dispersion of an ytterbium mode-locked laser. We demonstrate that using semiconductor saturable absorber mirror together with photonic bandgap fiber allows for self-starting all-fiber mode-locked laser around 1-μm wavelength range.

2. Experimental

The experimental setup of the mode-locked laser is illustrated in Fig. 1. The fiber cavity is comprised of 1.0 m of ytterbium-doped fiber, 2.7 m of standard single mode fiber and a 2.8-m long segment of SC-PBG fiber. The Yb-doped fiber has an unpumped loss of 414 dB/m at 976 nm and normal group velocity dispersion (GVD) of +0.071 ps^2/m at 1.04 μm. The SC-PBG fiber has the mode field diameter of 9 μm and exhibits anomalous GVD of -0.054 ps^2/m at 1.04 μm. Figure 2 shows the transmission band and dispersion of the SC-PBG fiber. The inset in Fig. 2 shows the microscope image of the fiber cross-section displaying 10 rings of Ge-doped rods around the undoped silica core. The transmission loss of the SC-PBG fiber was estimated from the measurement as 68.4 dB/km and the group birefringence as $\sim 10^{-5}$ at 1.04 μm. The 10% output coupler and the dichroic pump coupler were made of single-mode fiber with normal GVD of +0.023 ps^2/m and mode-field diameter of 6.4 μm. The round-trip dispersion of this cavity was estimated from measurements to be in the anomalous dispersion regime for wavelengths longer than 1040 nm. The mode size in the SC-PBG fiber is slightly larger than the diameter of the mode field in the core of a standard fiber. It is expected,

#69016 - $15.00 USD Received 16 March 2006; revised 24 April 2006; accepted 26 April 2006

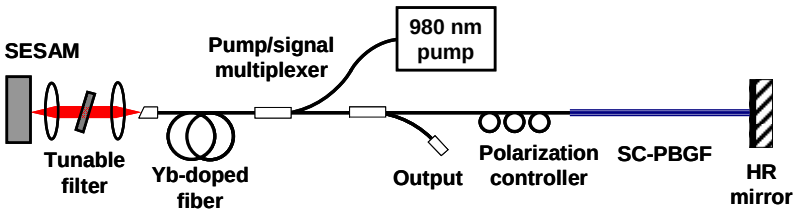

Fig. 1. Laser setup with SC-PBG fiber for cavity dispersion compensation. HR mirror – high reflectivity mirror.

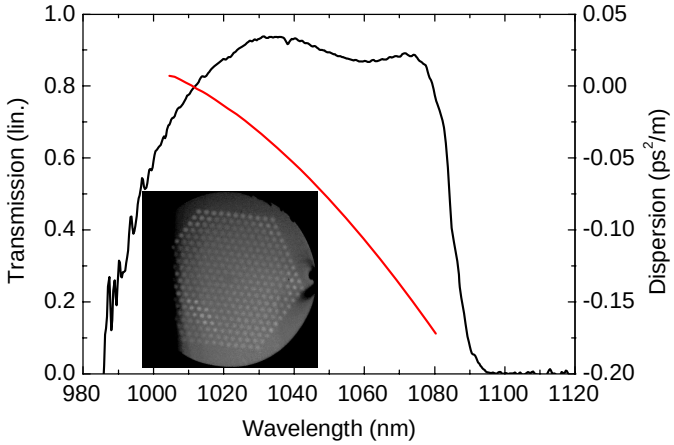

Fig. 2. Transmission (black curve) and dispersion (red curve) of the SC-PBG fiber used for dispersion compensation. The inset shows the cross-sectional view of the fiber.

therefore, that optical nonlinearity of the SC-PBG fiber would not dominate the total nonlinearity in the laser cavity. Despite some mode mismatch, the guided mode of the bandgap fiber fits quite well the mode of the normal fiber resulting in ~1 dB splice loss with standard fiber. The other end of the SC-PBG fiber was butt-coupled to a high reflective mirror in order to avoid further splice loss and any unwanted reflections from the fiber end.

3. Results

The laser was pumped with a single-mode grating-stabilized laser diode, which provided a power of 120 mW at 980 nm. An antireflection-coated aspheric lens with a focal length of 2.0 mm was used to focus the beam on the absorber mirror. Proper SESAM alignment resulted in self-starting mode-locking with a fundamental repetition rate of ~15 MHz. The laser delivered an average output power of ~2 mW corresponding to the pulse peak power of 250 W.

Although the SC-PBG fiber shows a good performance in GVD compensation, it was concluded that a major limitation to the pulse width and quality arises from the third-order dispersion (TOD) generated in the SC-PBG fiber used in this study. The TOD of the photonic bandgap fiber estimated from the measurements gives the value of 1.4 ps^3/km at 1.04 μm. The effect of the higher-order dispersion was further studied using tunable pulsed operation by inserting a birefringent filter at the Brewster angle into the air-segment of the cavity as shown in Fig. 1. Without the filter, the laser operates at ~1035 nm where the SC-PBG fiber has the transmission maximum, as seen in Fig. 2. Figure 3 shows the pulse spectra and intensity autocorrelations when the laser was tuned to different wavelengths. From Figs. 3(a)–

#69016 - $15.00 USD Received 16 March 2006; revised 24 April 2006; accepted 26 April 2006

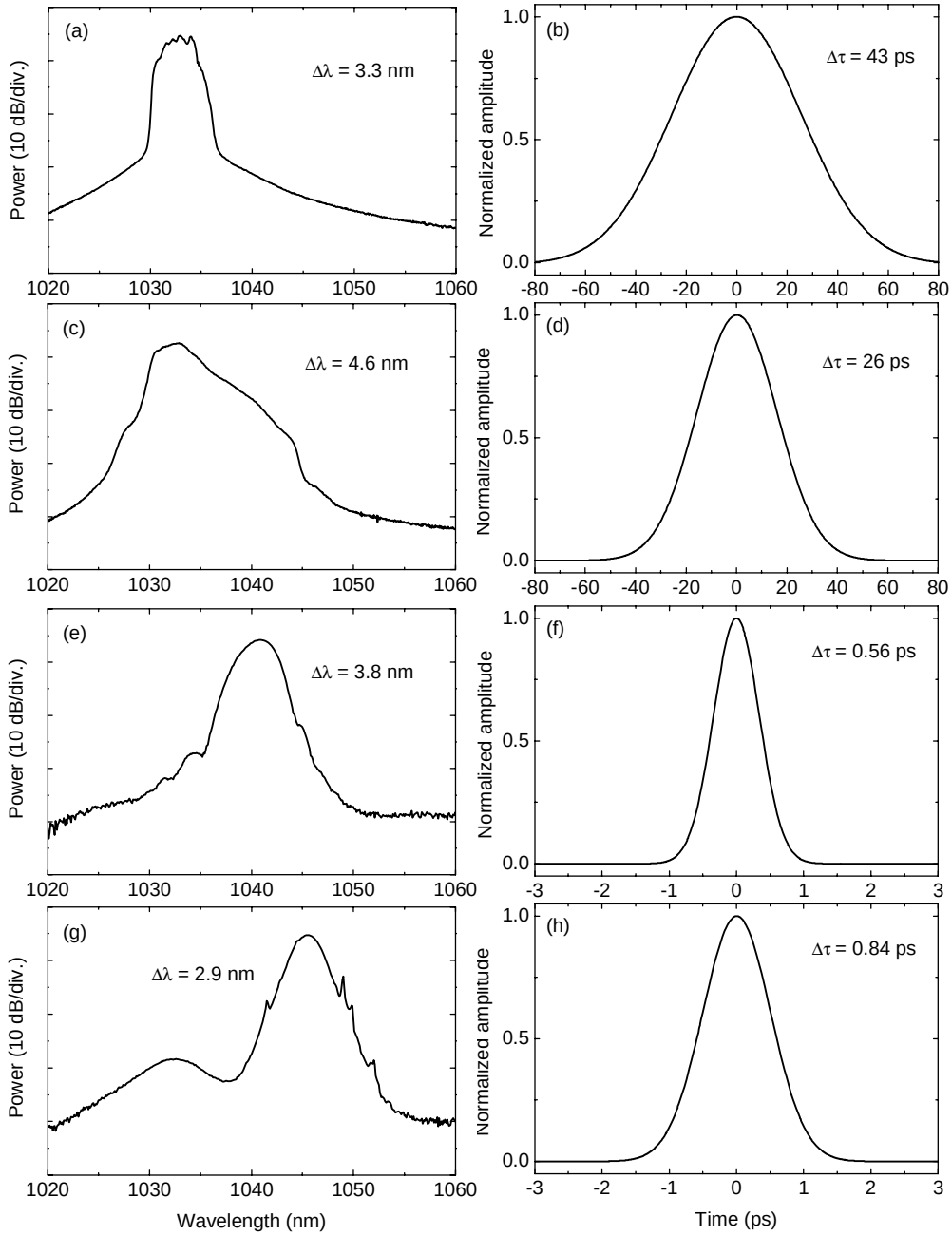

Fig. 3. The intensity autocorrelation traces (right) and corresponding spectra (left) obtained for tunable mode-locked operation. Plots (a)–(d) correspond to net normal cavity dispersion, (e)–(h) to total anomalous cavity dispersion.

#69016 - $15.00 USD Received 16 March 2006; revised 24 April 2006; accepted 26 April 2006

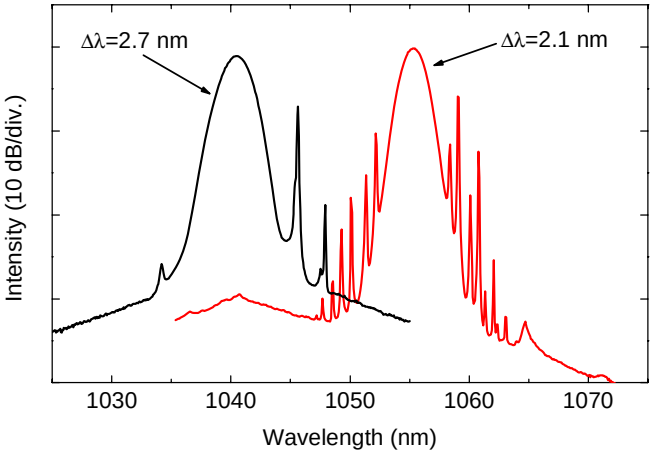

Fig. 4. Mode-locked pulse spectra obtained with 0.55-m long ytterbium fiber. The total cavity dispersion calculated from the soliton sidebands equals -0.13 ps^2 at 1040 nm and -0.52 ps^2 at 1055 nm.

(d), it is clear that owing to low value of anomalous dispersion generated by SC-PBG fiber at the short wavelengths (< 1035 nm), the laser operates with net normal cavity dispersion resulting in long pulses. This feature is expected from the dispersion curve shown in Fig. 2. In contrast, operation at longer wavelengths [Figs. 3(e)–3(h)] shows substantial soliton pulse compression indicating the total anomalous dispersion of the laser cavity.

Next, to further illustrate strong wavelength dependence of the SC-PBG fiber dispersion and, consequently, high value of TOD, the length of an ytterbium fiber was decreased down to 0.55 m. The spectral sidebands in the pulse spectra, shown in Fig. 4, give a clear signature of the soliton regime. The average cavity dispersion estimated from the soliton sidebands is -0.13 ps^2 at 1040 nm and -0.52 ps^2 at 1055 nm. The group-velocity dispersion derived from the spectral location of the sidebands agrees with total cavity GVD calculated from measured dispersion of the fibers comprised in the cavity.

In order to optimize the pulse duration generated by the laser, we changed both the length of the active fiber and the operation wavelength. The results of this study are summarized in Fig. 5. The shortest pulse we obtained by dispersion compensation with SC-PBG fiber has the width of 0.46 ps. With the spectral width of 4.6 nm, the time-bandwidth product becomes 0.59 remaining still above the transform-limited value. Since the laser comprises sections of fiber with both normal and anomalous dispersion, the pulse duration and chirp evolve gradually when pulse propagates inside the laser cavity. The nearly transform-limited pulse is expected to appear by placing the output coupler at the location within the cavity that corresponds to the highest pulse compression factor. The output fiber pigtail may also add certain chirp to the pulse. Although further pulse reduction is expected, it is obvious that third-order dispersion in the photonic bandgap fiber would eventually limit the dechirped pulse duration. These aspects remain a subject for future study. Also, we expect that the performance of this laser can be improved with advances in photonic bandgap structures.

#69016 - $15.00 USD Received 16 March 2006; revised 24 April 2006; accepted 26 April 2006

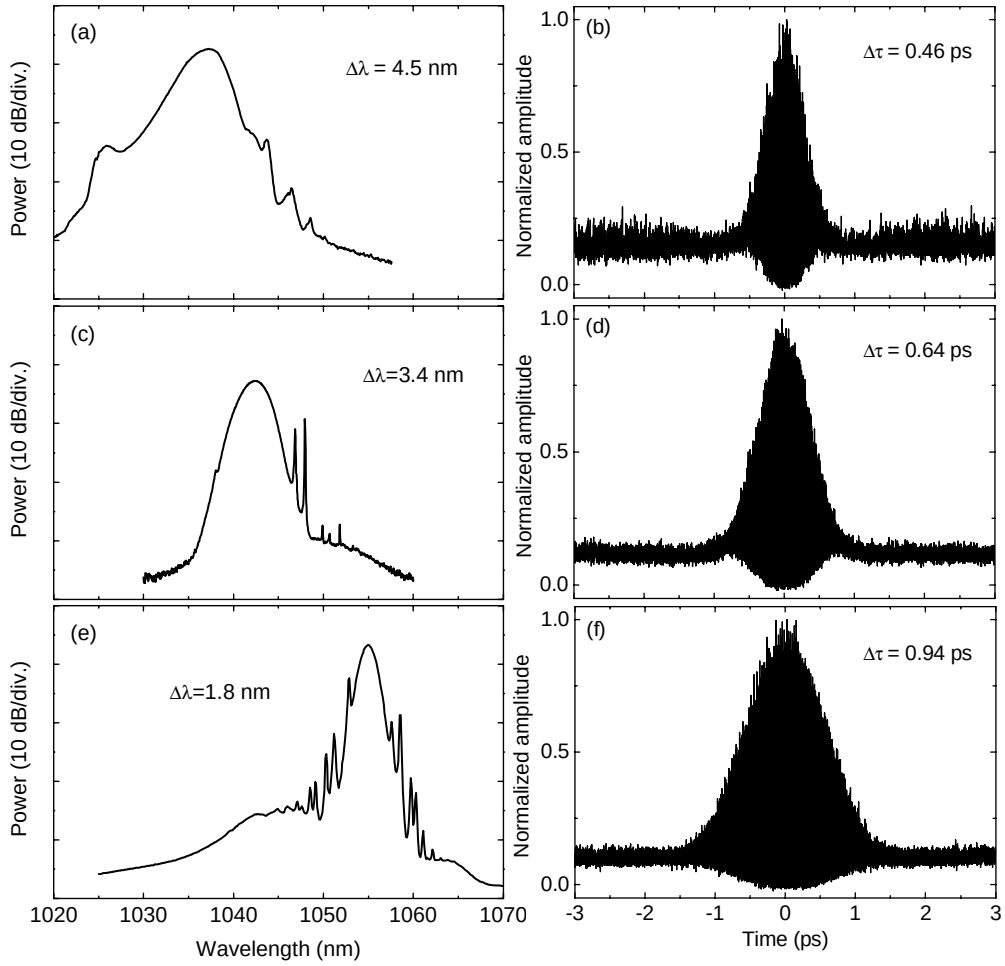

Fig. 5. Interferometric autocorrelations and spectra for cavities with different lengths of ytterbium-doped fiber: (a), (b) 1.15 m, (c), (d) 1.7 m and (e), (f) 1.7 m. Pulse durations and corresponding optical pulse bandwidths are shown.

4. Summary

We demonstrated an environmentally stable all-fiber soliton ytterbium laser using solid-core photonic bandgap fiber for dispersion compensation at 1 μm. The self-starting mode-locked operation of the subpicosecond soliton laser is achieved by the semiconductor saturable absorber. This approach may constitute an important step towards novel generation of ultrafast fiber oscillators.

Acknowledgments

The authors acknowledge the financial support of the Academy of Finland (project GEMINI) and EU-FP6 URANUS project. Photonic bandgap fiber was provided by Crystal Fibre A/S in frame of the EU project. We also acknowledge discussions with Claus Friis Pedersen from NKT Research.

#69016 - $15.00 USD Received 16 March 2006; revised 24 April 2006; accepted 26 April 2006

PUBLICATION 5

A. Isomäki and O. G. Okhotnikov, "Femtosecond soliton mode-locked laser based on ytterbium-doped photonic bandgap fiber", *Opt. Express*, Vol. 14, No. 20, pp. 9238–9243 (2006)

Femtosecond soliton mode-locked laser based on ytterbium-doped photonic bandgap fiber

A. Isomäki and O. G. Okhotnikov

Optoelectronics Research Centre, Tampere University of Technology,
P.O. Box 692, FIN-33101, Tampere, Finland
antti.isomaki@tut.fi

Abstract: We demonstrate a solid-core ytterbium-doped photonic bandgap fiber laser passively mode-locked with a semiconductor saturable absorber. Gain and anomalous dispersion simultaneously provided by the photonic crystal fiber allow for a compact subpicosecond soliton oscillator. We also discuss the effect of higher-order dispersion in photonic bandgap fiber on laser performance.

OCIS codes: (060.2340) Fiber optics components; (140.3510) Lasers, fiber; (260.2030) Dispersion; (320.7090) Ultrafast lasers

References and links

1. H. Lim, F. Ö. Ilday, and F. W. Wise, "Femtosecond ytterbium fiber laser with photonic crystal fiber for dispersion control," Opt. Express **10**, 1497-1502 (2002)
2. A. Isomäki and O. G. Okhotnikov, "All-fiber ytterbium soliton mode-locked laser with dispersion control by solid-core photonic bandgap fiber," Opt. Express **14**, 4368-4373 (2006)
3. J. C. Knight, "Photonic crystal fibres," Nature **424**, 847-851 (2003)
4. N. M. Litchinitser, A. K. Abeeluck, C. Headley, and B. J. Eggleton, "Antiresonant reflecting photonic crystal optical waveguides," Opt. Lett. **27**, 1592-1594 (2002)
5. F. Luan, A. K. George, T. D. Hedley, G. J. Pearce, D. M. Bird, J. C. Knight, and P. St. J. Russell, "All-solid photonic bandgap fiber," Opt. Lett. **29**, 2369-2371 (2004)
6. R. F. Cregan, J. C. Knight, P. St. J. Russell, and P. J. Roberts, "Distribution of spontaneous emission from an Er^{3+}-doped photonic crystal fiber," IEEE J. Lightwave. Technol. **17**, 2138-2141 (1999)
7. W. J. Wadworth, J. C. Knight, W. H. Reeves, P. St. J. Russell, and J. Arriaga, "Yb^{3+}-doped photonic crystal fibre laser," Electron. Lett. **36**, 1452-1454 (2000)
8. K. Furusawa, T. M. Monro, P. Petropoulos, and D.J. Richardson, "Modelocked laser based on ytterbium doped holey fibre," Electron. Lett. **37**, 560-561 (2001)
9. J. Limpert, T. Schreiber, S. Nolte, H. Zellmer, A. Tünnermann, R. Iliew, F. Lederer, J. Broeng, G. Vienne, A. Petersson, and C. Jakobsen, "High-power air-clad large-mode-area photonic crystal fiber laser," Opt. Express **11**, 818-823 (2003)
10. J. Limpert, A. Liem, M. Reich, T. Schreiber, S. Nolte, H. Zellmer, A. Tünnermann, J. Broeng, A. Petersson, and C. Jakobsen, "Low-nonlinearity single-transverse-mode ytterbium-doped photonic crystal fiber amplifier," Opt. Express **12**, 1313-1319 (2004)
11. M. Moenster, P. Glas, G. Steinmeyer, and R. Iliew, "Mode-locked Nd-doped microstructured fiber laser," Opt. Express **12**, 4523-4528 (2004)
12. M. Moenster, P. Glas, G. Steinmeyer, R. Iliew, N. Lebedev, R. Wedell, and M. Bretschneider, "Femtosecond Neodymium-doped microstructure fiber laser," Opt. Express **13**, 8671-8677 (2005)
13. D. G. Ouzounov, F. R. Ahmad, D. Müller, N. Venkataraman, M. T. Gallagher, M. G. Thomas, J. Silcox, K. W. Koch, and A. L. Gaeta, "Generation of megawatt optical solitons in hollow-core photonic band-gap fibers," Science **301**, 1702-1704 (2003)
14. J. Jasapara, T. H. Her, R. Bise, R. Windeler, and D. J. DiGiovanni, "Group-velocity dispersion measurements in a photonic bandgap fiber," J. Opt. Soc. Am. B **20**, 1611-1615 (2003)
15. C. Zhang, G. Kai, Z. Wang, T. Sun, C. Wang, Y. Liu, J. Liu, W. Zhang, S. Yuan, and X. Dong, "Design of tunable bandgap guidance in high-index filled microstructure fibers," J. Opt. Soc. Am. B **23**, 782-786 (2006)
16. A. Wang, A. K. George, and J. C. Knight, "Three-level neodymium fiber laser incorporating photonic bandgap fiber," Opt. Lett. **31**, 1388-1390 (2006)
17. R. Herda, A. Isomäki, and O. G. Okhotnikov, "Soliton sidebands in photonic bandgap fibre lasers," Electron. Lett. **42**, (2006)

#73421 - $15.00 USD Received 25 July 2006; revised 18 September 2006; accepted 18 September 2006

1. Introduction

To operate fiber lasers with λ≤1.3 μm in femtosecond pulse regime, normal dispersion of the laser cavity should be compensated by an appropriate cavity element with anomalous dispersion. Regular dispersion compensation based on diffraction gratings, however, violates an "all-fiber" nature of the laser. Recently, the dispersion compensators based on the photonic crystal fiber have been demonstrated resulting in compact all-fiber systems [1, 2]. Photonic crystal fibers with light guided by total internal reflection typically have a solid silica-based core surrounded by a silica-air photonic crystal cladding [3]. Anomalous dispersion in this type of crystal fibers, however, could be generated with rather small core diameters. Although, the high nonlinearity of these fibers is widely used in supercontinuum generation, their poor mode matching with standard fibers results in high loss when using them as an intracavity dispersion compensator. An alternative solution is based on photonic bandgap (PBG) fibers [3]. An all-solid PBG fiber [4, 5] made of a silica core and an array of higher index (e.g. Ge-doped) strands in the cladding has the advantage of a good mode matching with standard fibers. Furthermore, the all-solid structure exhibits no surface modes [5] and allows for high anomalous dispersion with low nonlinearity as compared with index guiding photonic crystal fibers. Another issue that makes these fibers particularly attractive for light emitting devices is the possibility to dope the silica core with rare-earth ions.

Er- and Yb-doped photonic crystal fibers first reported in [6] and [7] have later been used in different types of lasers [8, 9] and amplifiers [10]. More recently, Nd-doped photonic crystal fiber has been used as gain medium in a passively mode-locked fiber laser at 1.06 μm [11, 12].

In this Letter, we report on the first demonstration of a mode-locked laser using an ytterbium-doped photonic bandgap (Yb-PBG) fiber as a gain medium and a dispersion compensator. Since the dispersion compensation is provided by the gain fiber, simple and compact femtosecond laser architecture can be realized. This approach offers potentially higher repetition rates when compared with the fiber lasers using standard Yb-doped fiber and a separate PBG fiber for dispersion compensation. We show that using a semiconductor saturable absorber mirror together with the Yb-PBG fiber allows for self-starting femtosecond mode-locked laser with repetition rate above 100 MHz around 1-μm wavelength range.

2. Photonic bandgap fiber laser characteristics

The experimental setup of the mode-locked laser is illustrated in Fig. 1. The fiber cavity is comprised of 0.27 m of ytterbium-doped PBG fiber and 0.47 m of standard single mode fiber. The free end of the Yb-doped PBG fiber is butt-coupled directly to a saturable absorber mirror. The laser output is taken from a variable coupler composed of a polarizing beam splitter and a half-wave plate placed in the free space section of the cavity. Throughout the study, the output coupling was maximized by rotating the half-wave plate. Depending on the cavity parameters, the optimal value of the output coupling that allowed for stable mode-locked operation was ranged from 0.2 to 0.5. The laser was pumped with a single-mode grating-stabilized laser diode capable of delivering up to 300 mW of power at 980 nm.

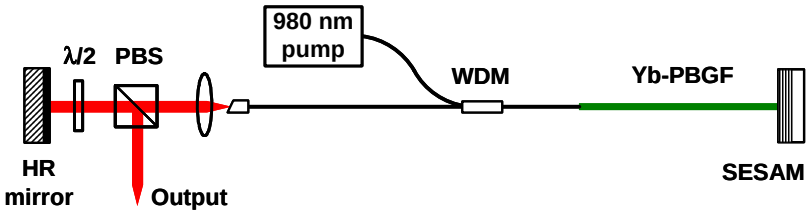

Fig. 1. Laser setup with Yb-PBG fiber. PBS: polarizing beam splitter, λ/2: half-wave plate, WDM: pump/signal multiplexer, HR mirror: high reflectivity mirror.

#73421 - $15.00 USD Received 25 July 2006; revised 18 September 2006; accepted 18 September 2006

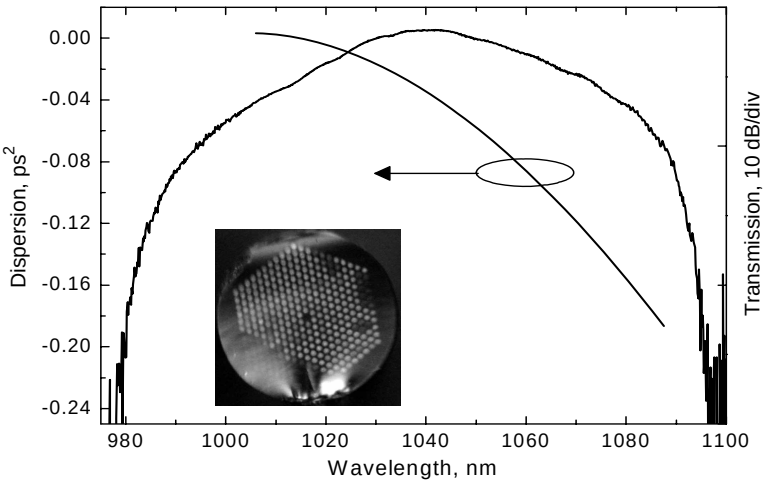

Fig. 2. Dispersion of the whole fiber cavity and the transmission spectrum of the 2nd order bandgap of the Yb-PBG fiber. The inset shows the cross-sectional view of the fiber

Figure 2 shows the 2nd order transmission band of the Yb-PBG fiber recorded using a white-light source. The bandgap ranges from 980 to 1100 nm covering both the pump wavelength and the laser transition of the Yb-doped fiber. Although the transmission band shape of the PBG fiber is to certain extent affected by the high level of Yb doping, it is evident that the pump wavelength is located close to the short-wavelength edge of the band. The pump radiation is, therefore, weakly guided that in turn may decrease the overall pump efficiency. With optimization of the band spectral positioning, an improvement in the output power would be expected.

The inset in Fig. 2 shows a microscope image of the PBG fiber cross-section displaying 10 rings of Ge-doped inclusions with the refractive index of ~1.465 in pure silica background. The fiber diameter is 200 μm and the periodic structure has the spacing of 8.3 μm. The core was formed by replacing one inclusion in the middle with Yb-doped silica rod having the refractive index close to that of pure silica. The core's numerical aperture is ~0.21 and it guides the fundamental mode with the field diameter of 9 μm. The mode size in the Yb-PBG fiber is slightly larger than the 6.4-μm mode diameter in the core of a standard fiber. It is expected, therefore, that optical nonlinearity of the Yb-PBG fiber would not dominate the total nonlinearity in the laser cavity. Owing to small mode mismatch between bandgap fiber and normal fiber, the splice loss was ~1 dB.

The measured round-trip group-velocity dispersion (GVD) of the laser cavity is seen in Fig 2. as well. The dichroic pump coupler made of standard single-mode fiber has a normal GVD of +0.024 ps^2/m, while the PBG fiber exhibits anomalous GVD of -0.075 ps^2/m at 1035 nm. Thus, the total cavity has an anomalous round-trip dispersion of -0.017 ps^2 at 1035 nm corresponding to the signal wavelength of the experiments.

Another important feature of the Yb-PBG fiber is the spectral position of the zero-GVD wavelength. The anomalous waveguide dispersion due to the resonant-like PBG structure tends to shift the zero-GVD towards the short-wavelength edge of the transmission band [13]. On the other hand, in case of an all-solid PBG fiber, the strong silica material dispersion at short wavelengths moves the zero-GVD to the opposite direction [5]. In case of the Yb-PBG fiber used here, the waveguide GVD is dominant over the material dispersion of silica at 1 μm wavelength range. We attribute this to the fact that the cutoff wavelength of the fundamental core mode is located at the band edge at 1094 nm. This gives rise to a rapid increase of dispersion at the long-wavelength edge and also shifts the zero-GVD to the short-wavelength side of the transmission band [14]. The effect is especially pronounced for the mode propagating in the secondary band instead of the fundamental one [15].

#73421 - $15.00 USD Received 25 July 2006; revised 18 September 2006; accepted 18 September 2006

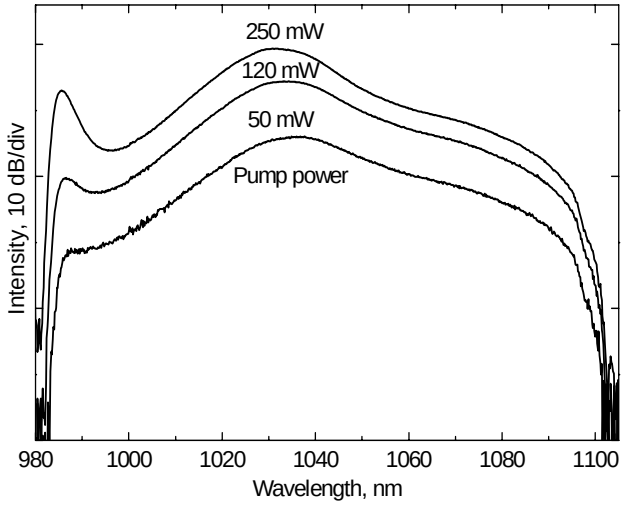

Fig. 3. Amplified spontaneous emission from the Yb-PBG fiber.

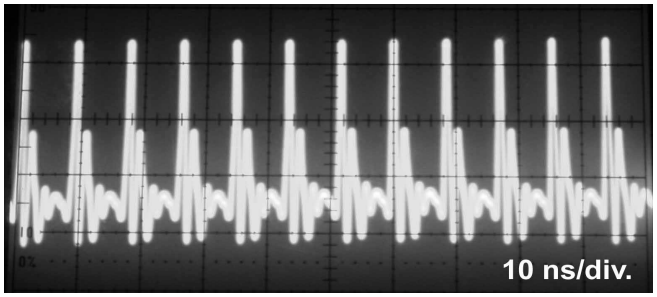

Fig. 4. Mode-locked pulse train (10 ns/div). The spikes at the end of the pulses are artifacts of detection electronics.

Figure 3 shows the spectrum of amplified spontaneous emission (ASE) from Yb-doped bandgap fiber for different pump powers. In these measurements, the lasing was avoided by blocking the laser mirrors. The figure illustrates that ASE spectrum matches closely the transmission band of the PBG fiber demonstrating an efficient filtering provided by the band spectral shape. This feature of the photonic bandgap structure was previously used to suppress undesired four-level transition in the Nd-doped fiber [16].

3. Mode-locked operation

The laser exhibits self-starting mode-locked operation emitting the pulse train at the fundamental repetition rate of 117.5 MHz, as shown in Fig. 4. An average power of 3 mW at the output corresponds to the pulse energy of 25.5 pJ. As it was mentioned above, this characteristic is expected to advance with improving the guiding of the pump radiation. Fig. 5 shows the optical spectrum of the pulse with a spectral width of 4.0 nm. The corresponding intensity autocorrelation is shown in the inset of Fig. 4. A sech^2-fit yields a pulse duration of 335 fs (FWHM), which gives a time-bandwidth product of 0.37 indicating a nearly transform limited pulse operation.

Although the Yb-PBG fiber shows a good performance in GVD compensation, it has significant dispersion of higher orders, particularly third-order dispersion (TOD). The TOD of the Yb-PBG fiber estimated from the measurements gives the value of 2.3 ps^3/km at 1.04 μm. As a result, the dispersion is changed significantly across pulse spectrum. This exceptionally

#73421 - $15.00 USD Received 25 July 2006; revised 18 September 2006; accepted 18 September 2006

large value of TOD was found to affect the shape of soliton pulse spectrum and may set an ultimate limit for pulsewidth generated from photonic bandgap fiber lasers. Namely, the spectral sidebands in the pulse spectrum show notable asymmetry. Typically, we observe 2-3 soliton sidebands in the long-wavelength tail of the spectrum which corresponds to higher anomalous dispersion regime, while sidebands were never recorded at the short-wavelength wing of the spectrum, as seen from Fig. 6. The spectra have been obtained by changing the length of the fibers with normal and anomalous GVD. The dispersion values shown in Fig. 6 are measured at 1035 nm corresponding to the central wavelength of the pulse spectra. The asymmetric sideband formation was found from numerical simulation to be due to a high value of TOD in PBG fiber [17]. Generally, these observations confirm a high immunity of the soliton pulses to higher order dispersion.

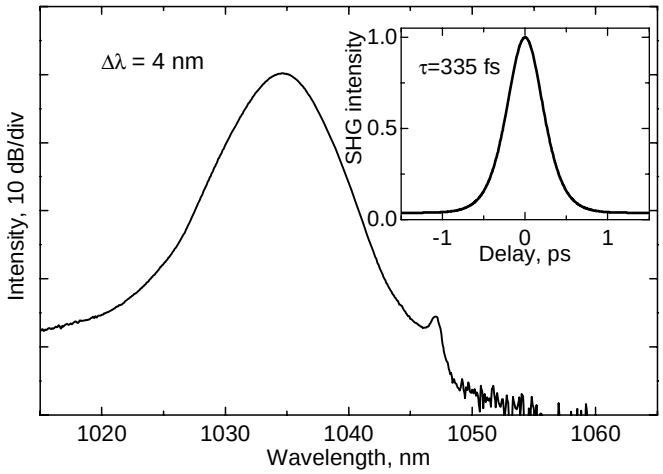

Fig. 5. Mode-locked pulse spectrum. Inset: measured intensity autocorrelation.

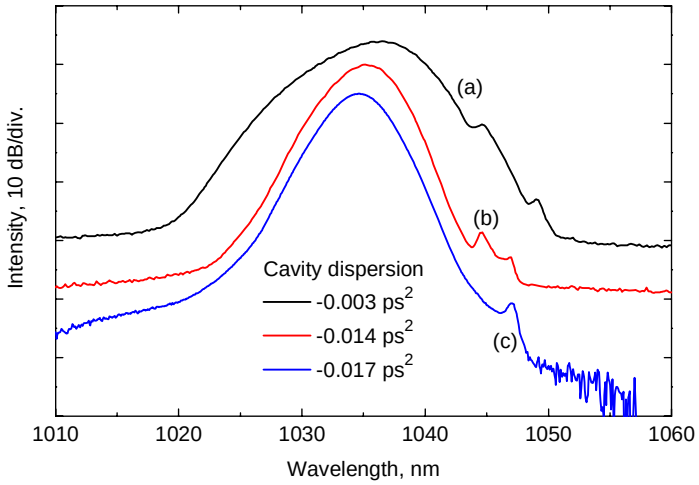

Fig. 6. Pulse spectra for different cavity dispersions. The lengths of the Yb-PBG fiber and the standard single mode fiber are (a) 0.35 m and 1.0 m, (b) 0.35 m and 0.8 m, (c) 0.27 m and 0.47 m, respectively. Some asymmetry in the soliton pulse spectra can be expected for different values of cavity dispersion, as discussed in the text. The difference in noise floor between the curves is due to variations in the sensitivity level of the optical spectrum analyzer. It should be noted that spectra are offset arbitrarily in respect of Y-axis for clarity.

#73421 - $15.00 USD Received 25 July 2006; revised 18 September 2006; accepted 18 September 2006

4. Conclusion

We have demonstrated an environmentally stable soliton laser using ytterbium-doped all-solid photonic bandgap fiber providing both gain and dispersion compensation at 1 μm. The self-starting subpicosecond mode-locked operation is achieved by the semiconductor saturable absorber. We believe that this approach represent the new generation of ultrafast fiber oscillators operating with repetition rates above 100 MHz.

Acknowledgments

The authors acknowledge the financial support of the Academy of Finland (project GEMINI) and EU-FP6 URANUS project. Yb-doped photonic bandgap fiber was provided by Crystal Fibre A/S in the frame of the EU project. We acknowledge useful discussions with Claus Friis Pedersen from NKT Research.

#73421 - $15.00 USD Received 25 July 2006; revised 18 September 2006; accepted 18 September 2006

Tampereen teknillinen yliopisto
PL 527
33101 Tampere

Tampere University of Technology
P.O. Box 527
FIN-33101 Tampere, Finland